A WEIGHTED OVERLAP-ADDITION APPROACH TO DECONVOLUTION OF THE INDUCTION LOG

By

KEITH ALAN TEAGUE

Bachelor of Science in
Electrical Engineering
Oklahoma State University
Stillwater, Oklahoma
1979

Master of Science
Oklahoma State University
Stillwater, Oklahoma
1980

Submitted to the Faculty of the Graduate College
of the Oklahoma State University
in partial fulfillment of the requirements
for the Degree of
DOCTOR OF PHILOSOPHY
May, 1984

A WEIGHTED OVERLAP-ADDITION APPROACH TO

DECONVOLUTION OF THE INDUCTION LOG

Thesis Approved:

Thesis Adviser

David J. Soldan

James R. Rowland

Gary J. Stewart

Norman N. Durham

Dean of the Graduate College

ACKNOWLEDGMENTS

I will always be indebted to my adviser, Rao Yarlagadda, whose encouragement and persistence have sustained my motivation and interest during my graduate study at Oklahoma State University. The suggestions and assistance he has provided have helped to make my work satisfying and enjoyable. The high academic and professional standards he has set for himself have been an example which I hope to be able to follow. I also appreciate the time and effort spent by the other three members of my committee: David Soldan, Gary Stewart, and James Rowland.

I also appreciate the care taken by those who helped prepare the manuscript. Charlene Fries, in particular, has been an enormous help. Finally, I am grateful for the financial assistance provided by the Society of Professional Well Log Analysts in the form of a Graduate Fellowship, and to the members of the Oklahoma State University Research Consortium for Enhancement of Well Log Data Via Signal Processing for their consultation and guidance.

TABLE OF CONTENTS

TABLE

LIST OF FIGURES

CHAPTER I

INTRODUCTION

The induction log is an electronic device which allows measurement of the electrical conductivity of the earth in a borehole. This information is useful in determining prospective areas of production in oil and gas exploration. The instrument is particularly valuable since it does not require physical contact with the borehole walls or fluids as some other instruments such as the Laterolog require. The induction log uses an electromagnetic field to allow measurement of conductivity deep inside the formation through which the borehole passes. The tool offers advantages over other methods of measuring formation conductivity but has limitations of its own which must be addressed. Correction of some of the errors introduced into data measured with the induction log due to the nonideal behavior of the induction log system response is addressed in this research.

Since publication of the first paper dealing with the induction log, improvements in the operation of the instrument have been sought [1, 2, 3, 4, 5]. One of the most important problems encountered with the induction log is related to its nonlinear behavior. When collecting data, the induction log is highly influenced by the conductivity of the rock formation in the vicinity of the tool. This is due to the fact that as the conductivity of the formation increases, the signal generated by the induction tool penetrates less deeply into the formation. This introduces

attenuation and phase shift of the received signal, which under ideal circumstances would be proportional to the formation conductivity. The attenuation and phase shift are often referred to as propagation effects or skin effect and are most evident when the tool is near areas of high conductivity. Another serious limitation is common to many data gathering instruments. This problem is one of poor high frequency response which causes the measured data to be a smoothed or low-pass filtered version of the actual data. Note that since induction log data are measured in the spatial rather than time domain, the terms frequency and spectrum as used in this dissertation refer to the coefficients of the Fourier transform representation of the signal. The transform domain representation has units of reciprocal distance rather than Hertz. The smoothed signal represents an apparent conductivity of the formation and is considered as the weighted effect of the volume of earth within the depth of investigation of the tool. Under certain assumptions, this effect may be modeled simply as a convolution of the tool system response with the formation. These two problems together distort the measured data to such an extent that many features may be concealed and conductivity values are likely to be incorrect. The vertical resolution, in particular, is seriously affected, leading to poor delineation of bed boundaries especially when considering thin beds and large contrasts in conductivity. The problem may thus be described as one of improving induction log data quality by increasing resolution of the tool to thin beds and improving the accuracy of apparent conductivity of thick beds. In addition, reduction of additive noise is also considered. The problem is a difficult one and, although one recent author [6, p. 9] has stated ". . . the resolution of resistivity logs cannot be improved in a meaningful

manner by any deconvolution technique," the approach which is the subject of this work will be shown to provide some useful results.

Solutions to the problem are twofold. The data smoothing of the induction log may be corrected through classic linear means if nonlinear behavior is neglected. This is possible if the conductivity of the data being measured is not too high. In this case the induction log system response may be considered to be non-time-varying, and any of several deconvolution schemes may be used if the "constant" system response is known. Unfortunately, the nonlinear behavior of the induction log may not usually be ignored since there is no control over the location of regions of high conductivity within the borehole. For this reason, the system response must be considered to be time-varying if the smoothing is to be corrected, since the actual system response will be constantly changing. If the problem is approached and successfully solved with a time-varying response, the nonlinear behavior may thus be at least partially corrected. Thus a deconvolution procedure must be developed which is accurate and stable, and which also will account for nonlinear effects present in the data. It is here where the real difficulty lies.

The system response of the induction log varies in a very complicated manner. Solution of the integral equations for the response of the induction log in an arbitrary formation requires the application of a finite element or finite difference model and an excessive amount of computation. A solution computed in this manner may not be unique. A complete solution to the problem is thus considered to be impractical except under certain limiting assumptions which severely restrict the scope of the problem. In fact, to perform deconvolution of the induction log

based upon the complete theory including nonlinear effects requires that one know the answer to the problem to solve the problem!

This dissertation describes a new approach to deconvolution of the induction log. In this application, deconvolution is used to mean the removal of the effects of the vertical component of the system response from the measured data. The goal of the deconvolution operation is to improve the induction log data quality by increasing the resolution of the tool and improving the accuracy of the measured apparent conductivity data. The new approach, referred to as weighted overlap-addition convolution or WOAC, is a segmented procedure utilizing overlapping windows in a manner similar to that of short-term analysis and synthesis which is often applied to speech and speech-like signals. This approach has not been applied to the inducation log problem before. This method is an attempt at linearizing the induction log deconvolution problem so as to provide a good linear approximation to the solution of a nonlinear problem. In this adaptive procedure the induction log data are processed using a segmented technique whereby the segments overlap and the system response is allowed to vary from segment to segment. In addition, each segment of data is weighted by the appropriate window function so that the effect of the varying system response is lessened away from the center of each segment, thus simulating a continuous time-varying system response. This new procedure is easily modified to use almost any convolution method such as Wiener filtering and its variations, constrained least squares filtering, Jansson's method, Kalman filtering, and many others. Additive noise is included in the model. It is believed that while not offering a complete and absolutely accurate solution to the problem, this new approach may produce a solution that is closer to the

desired result than other methods currently in use. In addition, under circumstances where the conductivity of the formation is low so that propagation effects are likely to be insignificant and a nonadaptive approach may be acceptable, the system response may be held constant and the number of overlapping segments may be reduced, thereby lessening the number of calculations that must be performed.

The induction log suffers from still other problems that this dissertation does not address. These include the effects on the system response due to eccentricity of the sonde in the borehole, moving the tool across boundaries between layers of low and high conductivity, and dip. The correction of errors introduced by these and other effects is quite involved as is the complete solution of the induction log deconvolution problem and is beyond the scope of this research.

Overview

Chapter II describes the induction log from an historical perspective and gives several theoretical representations for the induction log. Limitations and problems associated with practical application of the induction log are discussed along with some steps currently performed to improve the performance of the instrument. The original geometrical factor theory developed by Doll [7] to describe the induction log is presented and discussed. Maxwell's equations are introduced and are used in the contemporary theory of the induction log. A relationship between the geometrical theory and the contemporary theory is given.

Chapter III presents a linear system theory model for the induction log and other similar data acquisition instruments. Steps for implementing a linear convolutional model are described. A number of filtering

methods of practical value in deconvolution are presented and classified. Included in the discussion are Wiener filtering and several of its variations, constrained least squares filtering, deconvolution by successive approximation, L_1 filtering, Jansson's method, and Kalman filtering. Recursive median filtering is introduced as an effective postfilter. Finally, a weighted overlap-addition approach to deconvolution of the induction log is proposed as a partial solution to the deconvolution problem involving skin effect.

In Chapter IV, the weighted overlap-addition approach to deconvolution is fully developed and described in terms of short-term analysis and synthesis. Its use in an adaptive manner to partially account for some of the nonlinear effects encountered with the induction log is outlined. Application in a nonadaptive manner is also considered. Advantages and disadvantages of the procedure are discussed.

Chapter V discusses the actual implementation of WOAC to the induction log deconvolution problem. The cases with and without inclusion of nonlinear effects are addressed. The full implementation of WOAC as an approximate linear solution to the nonlinear deconvolution problem is described in detail. Problems associated with the calculation of the induction log vertical system response and the choice of parameters associated with WOAC are discussed.

Computer simulations of WOAC deconvolution of the induction log are included in Chapter VI. The generation of synthetic data with and without nonlinear effects is detailed. All examples include additive noise to more accurately simulate real data. An example of deconvolution of real induction log data is given. Numerous comparisons of the various methods and parameter choices with respect to performance are made and

analyzed. Spatial and spectral representations of error associated with the deconvolution are described. An application of recursive median filtering as a postfilter to remove amplified additive noise after deconvolution is also presented and shown to provide useful benefits.

Chapter VII provides a summary of the results of this research and presents motivation for further research. Suggested topics for future investigation are included as are goals of this research which were not met.

CHAPTER II

INDUCTION LOGGING

Well logging is an often used method in petroleum exploration for obtaining information about the subsurface. The induction log is one of many instruments available for measuring a variety of characteristics of formations through which a borehole passes. Often measured characteristics include information relating to porosity, permeability, spontaneous potential, and conductivity. In particular, the induction log provides information on the approximate conductivity of the subsurface. This information may be used to evaluate water and hydrocarbon saturations or for discrimination between water and hydrocarbon bearing formations.

Induction logging is accomplished by lowering a specialized electronic sonde into the borehole. The sonde contains the electronics necessary to generate the signals which allow measurement of formation conductivity. The sonde is suspended from the surface by a steel cable which encloses several conductors through which data are transmitted to the surface. The instrument consists of an insulating mandrel around which at least two, and probably more, coils are wound. Figure 1 illustrates schematically a two-coil induction sonde as described by Doll [7]. The coils are referred to as the transmitter and receiver, and, in sondes which have more than two coils, several coils may actually comprise the transmitter and receiver. For example, a common modern induction log, the 6FF40, has three transmitter and three receiver coils. The coils

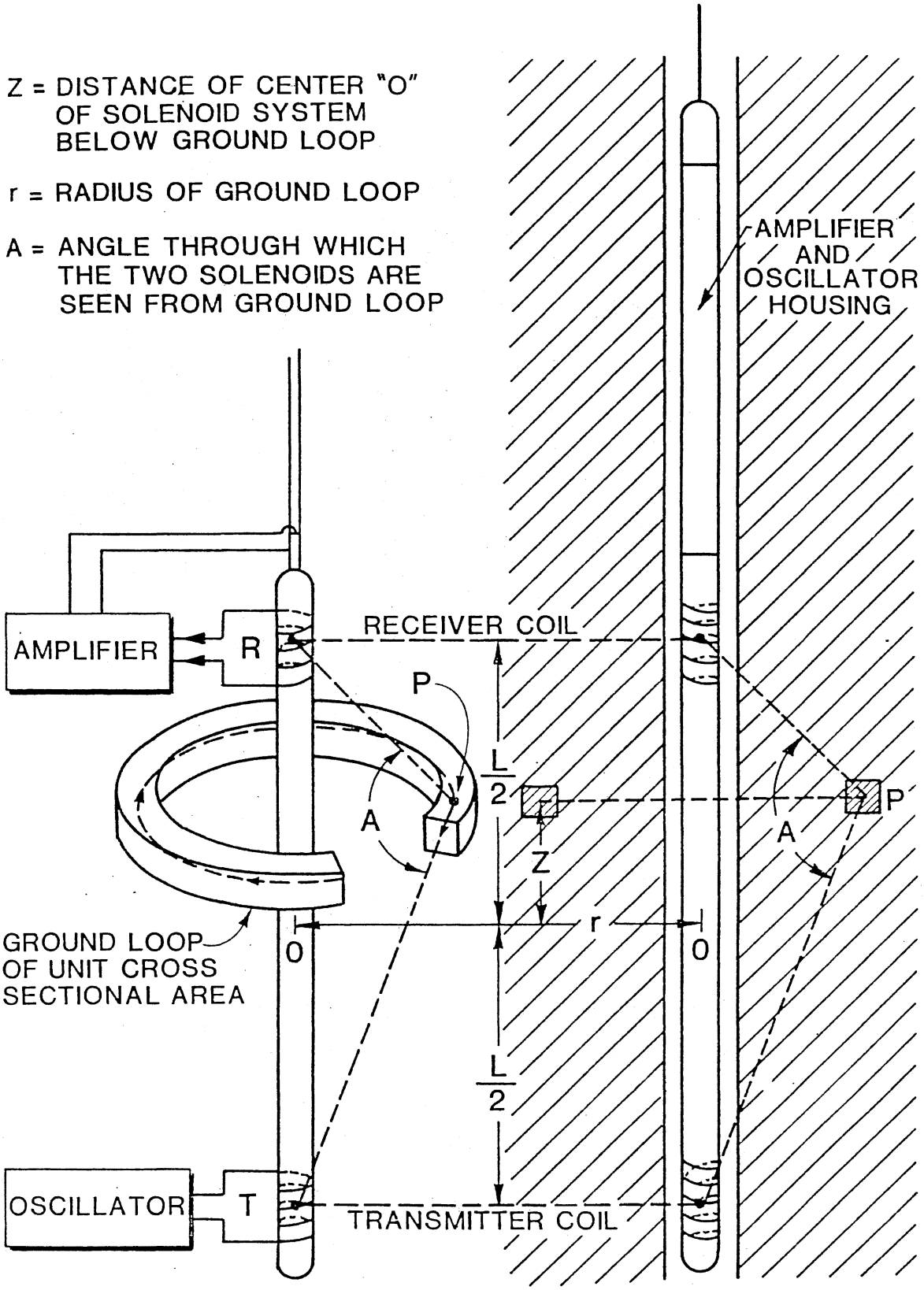

Figure 1. A Schematic Drawing of Apparatus Used in Induction Logging

are spaced a predetermined distance apart which determines the basic response characteristics of the tool. A constant amplitude alternating current at a frequency of approximately 20 KHz is passed through the transmitter coil. A magnetic field is thus generated in the vicinity of the sonde. This field excites the earth surrounding the borehole near the sonde, causing eddy currents to flow in the earth around the sonde. If the ground is assumed to be layered and homogeneous such that each layer is horizontal and there is symmetry of revolution about the borehole, the eddy currents can be assumed to flow through only one layer coaxially around the sonde. In other words, under these assumptions eddy currents do not have to cross boundaries between media of differing conductivities.

The eddy currents flowing around the borehole generate a secondary magnetic field proportional to the conductivity and position of each homogeneous layer. The receiver detects the secondary magnetic field while at the same time rejecting the mutual component generated directly by the transmitter. Ideally, the field induced in the receiver by the eddy currents should be proportional to the conductivity of the surrounding media since the transmitter current is of constant amplitude. In addition, the ideal sonde should measure conductivity of the formation directly adjacent to the center of the tool and far from the borehole wall to avoid effects due to invasion. Thus the ideal induction log response would be very sharp and deep. Of course, this is not the case, although multi-coil sondes do have sharper responses than older two-coil sondes. The response of the induction log has characteristics of a low-pass filter so it smoothes the data it is measuring.

Modern multi-coil instruments are focused so that the added coils direct and intensify the investigation characteristics of the sonde. Focused sondes have an actual investigation characteristic such that the volume of investigation is shaped like a cylinder with a minimum radius of about 10 inches and a maximum radius of about 250 inches. The conductivity measured by the sonde may thus be considered to be a weighted sum of values due to the contribution of each layer of earth to the total signal generated in the receiver. The signal produced by the tool as the sonde is moved up the borehole is sent up the cable to the surface where it is usually filtered and stored. Samples are usually taken every six inches and are plotted to form an induction log which is a chart that represents the apparent conductivity profile of the earth through which the borehole passes.

Presented in the following two sections are several representations of the induction log theory. Described first is the original geometrical factor theory for the induction log presented by Doll [7] followed by two variations of the contemporary induction log theory. The information presented in these sections is not intended to be exhaustive but to serve as background information for the deconvolution procedure which will be described in Chapter IV. Complete information and theoretical derivations may be found in the References.

Doll Theory

The earliest work on the induction log as we know it today was performed by Doll and published in his now famous 1949 paper [7]. In his work, he described the induction log in terms of the spatial configuration of the sonde and the surrounding media under the layered media

assumptions made earlier. This theory is easy to understand and apply but fails to account for nonlinear effects introduced by interaction of the electromagnetic fields with media of high conductivity. Indeed, the Doll theory of the induction log fails to make any reference at all to electromagnetic field theory.

Induction logging was first applied to dry boreholes or those filled with oil base mud which has low conductivity compared to the surrounding media. Doll theorized that if the media were excited with an alternating electromagnetic field, a secondary magnetic field would be generated by eddy currents flowing through the formation. This field would be in proportion to the conductivity of the surrounding formation and could be detected by a receiver coil mounted on the logging tool. This is still the basis for all induction log theory today.

Doll defined a unit ground loop as a horizontal loop of homogeneous ground having circular shape with its center on the axis of the borehole and whose cross section was a small square of unit area (see Figure 1). If the media were layered, horizontal, and homogeneous, the measured conductivity would be the sum of the signals generated by all the layers in proximity to the tool. The contribution of a volume of medium to the total received signal would thus be a function of the cross section of the region, of some particular geometrical factor which is determined by the position of the region with respect to the sonde, and of the conductivity of the region. It must be assumed that the dimensions of the coils are small when compared with the diameter of any ground loop whose influence we wish to determine and that one ground loop does not influence another at the frequencies of interest. These assumptions allow the signals from different regions to be considered separately. As will be

seen later, these assumptions are not always good since there are effects which have not been considered but that may be significant. These effects are nonlinear and are characterized by phase shift and attenuation of the electromagnetic field as it is propagated through the formation, resulting in a change in the received signal from the ideal. The nonlinearity will be considered when the induction log is modeled using electromagnetic field theory.

The Doll geometrical factor theory may now be described. The following variables and corresponding definitions will apply:

E = total signal at the receiver

e = part of E contributed by a unit ground loop

r = radius from the tool center

z = altitude from the tool center

C = conductivity of the unit ground loop

K = apparatus constant

f = frequency of excitation

L = spacing between transmitter and receiver

I = intensity of the transmitter coil current

g = unit geometrical factor

A[T] = cross-sectional area of the transmitter coil

A[R] = cross-sectional area of the receiver coil

C[A] = conductivity of a region A

G[A] = geometrical factor of a region A.

Of the total signal received, the portion contributed by one unit ground loop of radius, r, and distance, z, with respect to the sonde center may be given as

$$e = KgC \tag{2.1}$$

where C is the conductivity of the current loop, g is a geometrical factor to be defined later, and K is a tool constant given by

$$K = \frac{16\pi^2 f^2 A[T] A[R] I}{L} \tag{2.2}$$

The geometrical factor is determined completely by the spatial arrangement of the unit ground loop with respect to the coils. The Doll unit geometrical factor, g, may be written as a function of r and z as

$$g(r,z) = \frac{L}{2} \frac{r^3}{[r^2 + (\frac{L}{2} - z)^2]^{3/2} [r^2 + (\frac{L}{2} + z)^2]^{3/2}} \tag{2.3}$$

The unit geometrical factor given by Equation (2.3) is a dimensionless quantity that when integrated over all r and z is unity.

Based upon the relationships given above, the received signal, E, may be found by summing all the contributions over all r and z as

$$E = K \int\int gC \, drdz \tag{2.4}$$

Recall that both the conductivity and unit geometrical factor in Equation (2.4) are functions of position. If, as was assumed earlier, the media may be assumed to be layered, homogeneous, and horizontal, Equation (2.4) may be written in terms of the signal components from each discrete volume of earth:

$$E = K[C[A] \int\int_A gdrdz + C[B] \int\int_B gdrdz + \ldots] \tag{2.5}$$

where the components are contributions from regions A, B, C, etc., with corresponding conductivities C[A], C[B], C[C], etc. The apparent conductivity, C_a, measured by the induction log is given as the ratio, E/K. The intregrated geometrical factors contained in Equation (2.5) may be

thought of as weights which are a measure of what fraction of the received signal is due to a particular region. Thus the logging operation may be represented as a convolution. An important point to note is that even though a particular region has a small geometrical factor, it may produce a large contribution to the total received signal if its conductivity is large. Thus a highly conductive region distant from the tool may affect the apparent conductivity significantly. And, if the bed being measured is thin compared to other nearby beds or if beds of higher conductivity are nearby, the apparent conductivity measured by the sonde may differ significantly from that of the bed under investigation. The Doll geometrical factor theory tends to weight conductive regions distant from the tool far too heavily. This effect can be easily explained when the electromagnetic field theory is taken into account.

The Doll geometrical factor may be separated into a vertical component and a radial component of response which may be considered independently. The vertical component describes how the induction log responds to a thin horizontal bed, and the radial component describes how the induction log responds to a thin cylindrical bed. The vertical and radial investigation characteristics may be found by integrating Equation (2.3) over all r or z, respectively. The integration leads to expressions for the radial and vertical components of the ideal response which are represented graphically in Figures 2 and 3, respectively.

Although the results presented here are for a two-coil induction logging instrument, they may also be extended to focused sondes with more coils. The response is then the sum of the contributions to the received signal due to the individual coil pair combinations. Addition of the proper coils will produce a response that is both deeper and narrower,

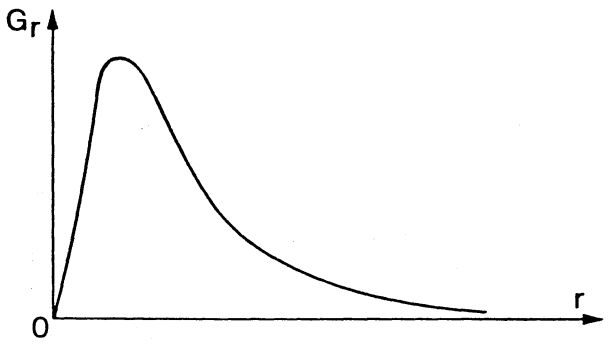

Figure 2. A Radial Investigation Characteristic for the Induction Log

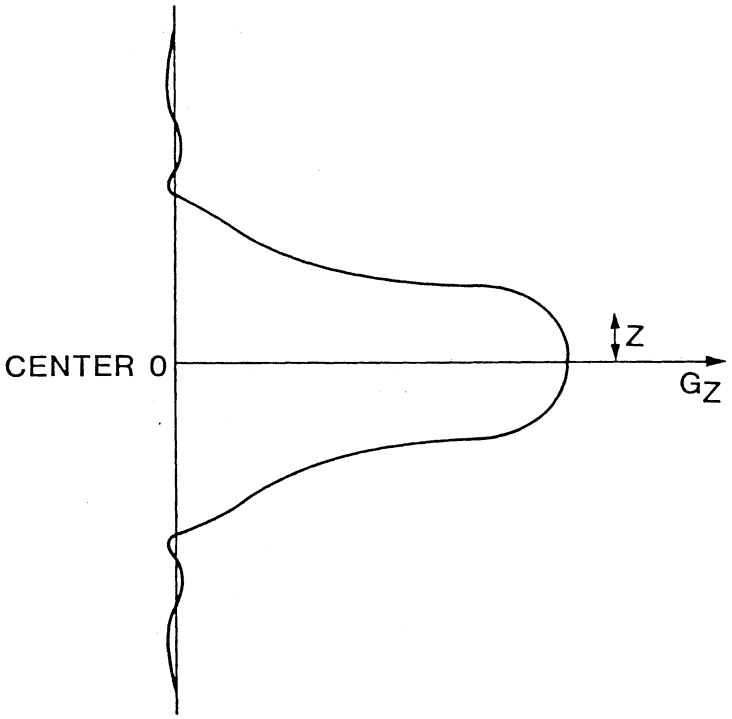

Figure 3. A Vertical Investigation Characteristic for the Induction Log

and which results in a more accurate determination of conductivity and resolution of bed boundaries. Thus it is possible to design induction sondes which can more closely approximate the ideal response. This does not solve the problem; it only lessens its severity.

The Doll geometrical factor theory is not satisfactory for describing the response of a real sonde in highly conductive formations. It does, however, provide a relatively simple mechanism for understanding the basic operating principles of the induction log. The geometrical factor theory is of value in analyzing the performance of the induction log and for calculating formation conductivities. Included in the next section is the modern theory for the induction log. This contemporary interpretation accurately describes the nonlinear behavior of the induction log by accounting for the interaction of electromagnetic fields with conductive regions.

Complete Induction Log Theory

The geometrical factor theory of Doll presented in the previous section makes many simplifying assumptions so as to remain relatively easy to understand. The most important of these assumptions is ignoring properties of electromagnetic field theory which describe the operation of the induction log. When an electromagnetic field penetrates a conductor, eddy currents are produced inside the conductor. The eddy currents contribute a magnetic field of their own which affects to some extent the original field generated by the transmitter. In addition, ohmic losses cause a portion of the power in the eddy currents to be dissipated. These two effects help reduce the field within the conductor, resulting in more current flowing along the outside of the conductor than inside and

also causing a phase shift of the secondary magnetic field. The attenuation and phase shift of the electromagnetic field as it propagates through a conductor is often referred to as skin effect. The term is often used to refer to all the effects of coupling between the primary and secondary fields in areas of high formation conductivity.

Several recent papers [1, 2, 8, 9, 10, 11] have re-examined the original induction log theory developed by Doll. A brief summary of some of the work by Moran and Kunz [8] and Thadani and Hall [9] will be presented in the following sections. In each case the original induction log theory has been redeveloped or expanded with the aid of electromagnetic field theory so that the previously neglected nonlinear effects could be included in the analysis. Although the analysis proceeds through fundamentally different theoretical concepts, it has been shown that the geometrical factor theory may be obtained as well from this model under certain simplifying assumptions [9].

Maxwell's equations for the electromagnetic field [12] are given by Equations (2.6) and (2.7) below:

$$\nabla \times \bar{E} = \frac{\partial \bar{B}}{\partial t} = 0 \qquad \nabla \cdot \bar{D} = \bar{q} \tag{2.6}$$

$$\nabla \times \bar{H} - \frac{\partial \bar{D}}{\partial t} = \bar{J} \qquad \nabla \cdot \bar{B} = 0 \tag{2.7}$$

where the variables are defined as follows:

$\bar{E}$ = electric field strength;

$\bar{B}$ = magnetic flux density;

$\bar{H}$ = magnetic field strength;

$\bar{D}$ = electric flux density;

$\bar{J}$ = current density;

q = volume charge density; and

∇ = vector del operator.

The previously given assumptions of symmetry as well as the assumptions in Equation (2.8) below are made:

$$\bar{B} = \mu\bar{H} \qquad \bar{D} = \varepsilon\bar{E} \qquad \bar{J} = \sigma\bar{E} \tag{2.8}$$

The expressions in Equation (2.8) are valid in regions not containing sources and the magnetic permeability, μ, the dielectric constant, ε, and the electrical conductivity, σ, are constant throughout each region. The source is assumed to be an idealized point dipole and all field quantities are assumed to be complex. Maxwell's equations become

$$\nabla x\bar{E} = i\omega\mu\bar{H} = 0 \qquad \nabla\cdot\bar{E} = q/\varepsilon \tag{2.9}$$

$$\nabla x\bar{H} - (\sigma - i\omega\varepsilon)\bar{E} = \bar{J}_s \qquad \nabla\cdot\bar{H} = 0 \tag{2.10}$$

where $\bar{J}_s$ corresponds to the source current and σ is proportional to the conduction current. The term, $\omega\varepsilon$, may be considered to be very small compared to σ, so Equation (2.10) may be written as

$$\nabla x\bar{H} - \sigma\bar{E} = \bar{J}_s \tag{2.11}$$

The measure of conductivity has been shown to exhibit some dependence on the frequency of investigation [13]; however, field experiments have demonstrated that any variation in conductivity as a result of a change in frequency is small [14]. As a result, the theoretical value of conductivity is considered to be the same as that measured with a direct current source. Figure 4 illustrates the cylindrical coordinate system of Reference [8] that is used to describe the variation of the electromagnetic fields. The equations finally become

$$\nabla x\bar{E} - i\omega\mu\bar{H} = 0 \qquad \nabla\cdot\bar{E} = 0 \tag{2.12}$$

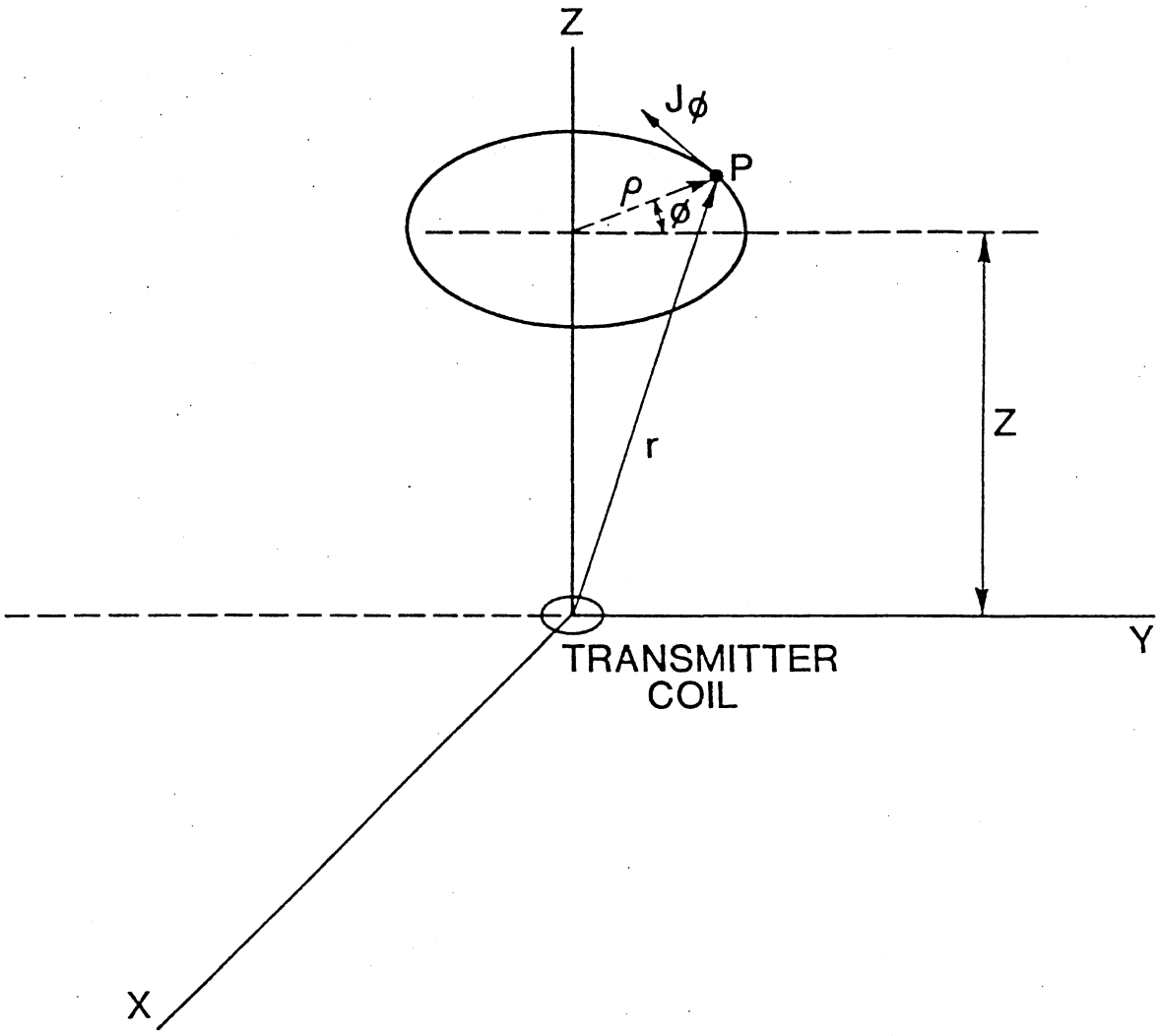

Figure 4. The Cylindrical Coordinate System Used by Moran and Kunz [8]

$$\nabla x\bar{H} - \sigma\bar{E} = \bar{J}_s \qquad \nabla\cdot\bar{H} = 0 \tag{2.13}$$

which may be solved easily only under certain limiting assumptions.

If a homogeneous medium is assumed in addition to the symmetry assumptions made earlier, a scalar solution to the vector potential is given by Equation (2.14) below [8]:

$$A_\phi(\rho,z) = \int_{v'} J_{s_\phi}(\rho',z') \cos(\phi - \phi') \frac{e^{ikr^*}}{r^*} dv' \tag{2.14}$$

where

$$r^* = \{(z-z')^2 + \rho^2 + \rho'^2 - 2\rho\rho' \cos(\phi - \phi')\}^{1/2} \tag{2.15}$$

$$k^2 = i\omega\mu\sigma \tag{2.16}$$

By including the appropriate boundary conditions for continuity of E, A, and H, Equation (2.14) may be simplified:

$$A_\phi = \frac{T\ I\ (\pi a^2)}{4\pi} \frac{\rho}{r^3}(1 - ikr)e^{ikr} \tag{2.17}$$

where

T = number of turns on the transmitter;

a = radius of the transmitter coil; and

I = current in the transmitter coil.

The voltage induced in the receiver coil of a two-coil induction tool in a homogeneous medium may be calculated using Equations (2.17) and (2.18) to give Equation (2.19):

$$E_\phi = i\omega\mu A_\phi \tag{2.18}$$

$$V = \frac{2TR\ (\pi a^2)^2}{4\pi} Ii\omega\mu\ (1 - ikL) \frac{e^{iKL}}{L^3} \tag{2.19}$$

where R is the number of terms on the receiver coil.

Equation (2.19) contains a component that is in phase with the transmitter current as well as an out-of-phase component. The out-of-phase component, which is due to the mutual coupling between the transmitter and the receiver, is referred to as V_x and is given in Equation (2.20).

$$V_x = k\sigma \frac{\delta^2}{L^2} \left(1 - \frac{2}{3}\frac{L^3}{\delta^3} + \ldots\right) \tag{2.20}$$

This component must be rejected by the electronics in the sonde. The in-phase component, which is the signal that is desired to measure, may be expressed as in Equation (2.21):

$$-V_r = k\sigma \left(1 - \frac{2}{3}\frac{L}{\delta} + \ldots\right) \tag{2.21}$$

where

$$K = \frac{(\omega\mu)^2 \ (\pi a^2)^2 \ TRI}{4\pi L} \tag{2.22}$$

and

$$\delta = \left[\frac{2}{\mu\omega\sigma}\right]^{1/2} \tag{2.23}$$

The expression given by Equation (2.23) is called the skin depth and is a measure of the order of magnitude of the penetration depth of the electromagnetic field in a conductor. If the frequency is approximately 20 KHz, the skin depth may be found to be about 140 inches for a formation with conductivity of one mho/meter [8]. The apparent conductivity of the formation may be found as

$$\sigma_a = \frac{-V_r}{K} \approx \sigma\left(1 - \frac{2}{3}\frac{L}{\delta}\right) \tag{2.24}$$

where the higher order terms have been neglected.

The rather brief development outlined above for the complete induction log theory of Moran and Kunz [8] is only shown here for an infinite homogeneous medium and a simple tool. Although the results are given only for a two-coil sonde, Moran and Kunz indicate how the theory may be easily extended to multi-coil sondes. Solution of the partial differential equations above in more complicated formations is a complex problem best performed using finite difference or finite element techniques. Graphs are often provided to aid in approximating the solution in other formations or when invasion is present.

Thadani and Hall [9] have performed a slightly different derivation from the one just outlined. Beginning with Maxwell's equations and using the coordinate system of Figure 5, it has been shown that the apparent conductivity may be computed to be as given below in Equation (2.25):

$$\sigma_a = \int\int \sigma(\rho',z')\, g\,(\rho',z')\, d\rho'\, dz' \tag{2.25}$$

where

$$g(\rho',z') = \frac{4\pi L}{(\pi\, a_T^2\, \pi\, a_R)\ TI2}\, \rho'\, A_{\phi R}\,(\rho',z') \int \frac{\cos(\phi - \phi')}{r_2^3}\, d\phi \tag{2.26}$$

where A[T] is the area of the transmitter coil and A[R] is the area of the receiver coil. Equation (2.26) above is defined to be the propagated geometric factor which may be compared to the Doll geometric factor of Equation (2.3). The propagated geometric factor accounts for propagation effects and may thus be used in the general case. As in the previous

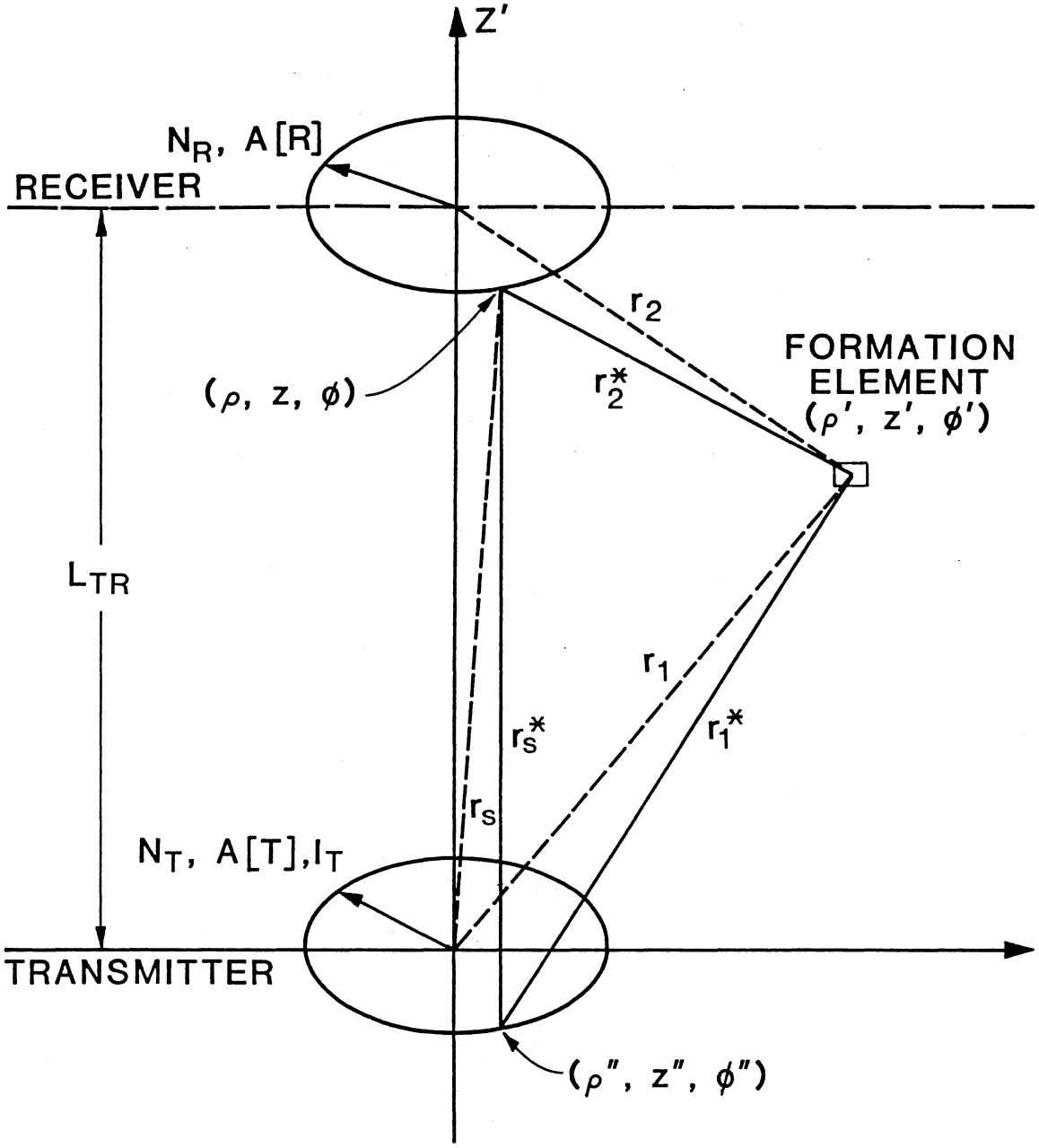

Figure 5. The Cylindrical Coordinate System Used by Thadani and Hall [9]

development, evaluation of the equations is not always easy. Equations (2.25) and (2.26) may be used to develop a unified technique for computing propagated geometric factors. Thadani and Hall have shown that for any formation geometry possessing cylindrical symmetry, the propagated geometric factor at each point may be determined by computing the vector potential, A_ϕ, at the point using Equation (2.17) as given by Moran and Kunz and then applying Equation (2.26). Equation (2.25) may then be used to sum the contribution of each differential formation element to compute the apparent conductivity. Thadani and Hall have suggested that solutions may be found analytically for simple formation geometries and numerically for more complex geometries.

A relationship between the propagated geometric factor and the Doll geometric factor is given by Equation (2.27):

$$g_p(\rho',z') \approx g(\rho',z')\,\mathrm{Re}\,\{(1 - ikr_1)e^{ikr_1}\} \tag{2.27}$$

Using the coordinate system of Figure 5, the Doll geometric factor may be written as

$$g(\rho',z') = \frac{L}{2}\frac{\rho'^3}{r_1^3\, r_2^3} \tag{2.28}$$

Thus the propagated geometric factor is identical to the Doll theory when the medium exhibits low conductivity. For higher conductivity the propagated geometric factor differs from that predicted by Doll due to attenuation and phase shift. The comments regarding the complexity of the solution given by Moran and Kunz also apply to that just presented.

Although the induction log response may be calculated for an infinite homogeneous region or for a fairly simple nonhomogeneous region,

calculation of the response in general is impractical. It is for this reason, if nothing else, that the deconvolution problem is most often approached without correction for skin effect. Indeed, if the conductivity of the formation being measured is low enough, skin effect will be insignificant. Research dealing with other new methods of describing the induction log and its nonlinear response is still being published. Perhaps in the not too distant future, a truly practical representation for the complete solution will be found. For the time being, the complete problem seems much too difficult to solve exactly and an approximate solution seems most reasonable.

Problems and Practices

As detailed in the preceding sections, the induction log suffers from nonideal behavior that may become troublesome, particularly when highly conductive beds are present in the proximity of the sonde. Correction of these problems has taken various forms, usually with very simple procedures. Often, some of the problems are ignored completely. A reliable deconvolution procedure would provide at least partial simultaneous correction for some of the errors associated with the induction log.

Although neglected in the earlier discussion, errors will be introduced if the borehole fluids or the invaded zone has significantly higher conductivity than the deep uninvaded formation which the induction log is attempting to measure or if the area of investigation has a bed of higher conductivity on one or both sides. In both cases the induction log is likely to weight the more conductive areas too heavily and produce erroneous results, since the eddy currents tend to circulate through the more conductive regions. The resistivity of horizontal beds adjacent to the

bed of interest is referred to as shoulder bed resistivity. It is current practice in the industry to apply a very simple deconvolution filter with three nonzero weights to partially correct for the effect of adjacent beds.

The induction log is better at measuring higher conductivities than lower ones, due to noise and basic inaccuracy in the instrument. Since the measurement is one of conductivity, an error that may be a very small fraction of the apparent value at high conductivity can be a large fraction at low conductivity. The induction log is considered most accurate when measuring conductivities greater than about 0.005 mho/meter [15].

Most induction logs have a correction factor applied to provide some adjustment for propagation effects. This correction is performed by multiplying the conductivity signal from the induction sonde by a scaling factor which is computed for each data point. This results in the data being scaled to what it would be if the measurement were made in an infinite homogeneous medium. The nonlinear process of selectively scaling the data is often referred to as boosting. Boosting is necessary because the induction log system response decreases in magnitude as the conductivity of the formation being measured increases. This effect also causes a decrease in the depth of investigation of the tool.

The two techniques mentioned above for reducing the errors due to shoulder beds and propagation effects are very simple approaches to correction of a complex problem. The deconvolution filter applied to correct for shoulder beds can hardly be considered effective in removing the distortion introduced by the smoothing action of the induction log. In a similar manner, boosting may be considered to be a simple-minded effort for magnitude correction. Both of these problems are due directly

to changes which occur in the induction log system response due to changes in formation conductivity. A proper deconvolution procedure would seem to be the appropriate choice to partially correct these problems more effectively.

Goals of Deconvolution

As detailed above, the induction log suffers from two rather severe problems: low resolution and nonlinear response. Both of these problems are inherent in the design of the tool. Although various corrections have been applied to reduce the errors introduced by the induction log and tool design has been greatly improved with the addition of focused tools with deep investigation characteristics, much is left undone. Since the induction log smoothes the data it collects, its operation may be described as a low-pass process. If the smoothing could be removed, the bed resolution could be greatly improved. The induction log also exhibits a varying amount of gain as the conductivity of the formation under investigation changes. If this gain change could be eliminated, the accuracy of the data could be made much higher. All of these effects comprise errors that occur due to changes in the induction log system response attributable to its nonlinear behavior. All of these errors may be at least partially corrected through deconvolution using a properly calculated linear approximation to the time-varying inverse system response. The problems to be addressed throughout the remainder of this dissertation deal with the development and implementation of an appropriate deconvolution procedure which can be applied to adequately correct for at least some of this nonlinear behavior.

CHAPTER III

DECONVOLUTION

Any linear time-invariant system may be modeled as a convolution of the input signal with the system response which describes the system. Equation (3.1) illustrates this process, where x is the input data to the system, h is the system response, and y is the output of the system.

$$y = x * h \tag{3.1}$$

The convolution operation may also be defined in the Fourier transform domain as given in Equation (3.2). Lower case letters will be used to represent variables in the time or spatial domain and upper case letters will be used to represent variables in the Fourier transform domain.

$$Y = XH \tag{3.2}$$

This definition represents identically the operation given above in the time or spatial domain. To more accurately approximate real data, an additive noise term, η, may be added, resulting in Equations (3.3) and (3.4) which correspond to Equations (3.1) and (3.2), respectively.

$$y = x * h + \eta \tag{3.3}$$

$$Y = XH + N \tag{3.4}$$

Figure 6 presents the forward operation including additive noise in block diagram form. One may consider the linear system representation given in Equation (3.2) above to be a linear approximation to the operation of

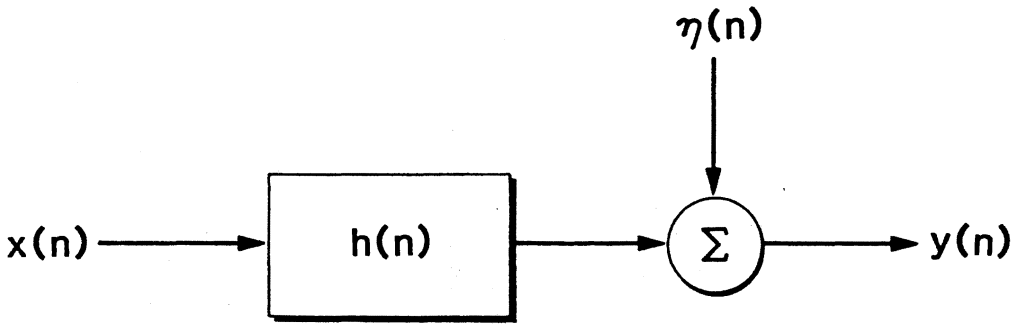

Figure 6. A Block Diagram Representation for Linear Filtering With Additive Noise

the induction log if x is the actual conductivity data, h is the vertical component of the system response, and y is the apparent conductivity measured by the sonde.

An inverse operation to Equation (3.1) may be specified as given in Equation (3.5), although the inverse may not exist everywhere.

$$x = y * h^{-1} \tag{3.5}$$

This representation is often referred to as inverse filtering. Equation (3.5) may also be represented in the Fourier transform domain as given in Equation (3.6):

$$X = \frac{Y}{H} \tag{3.6}$$

The inverse operation is generally referred to as deconvolution since it is the inverse of the forward convolution operation given above.

If the system response, h, is considered to be linear, time-invariant, symmetric, and low-pass, then the forward convolution operation given above may be considered to be a simple smoothing operation. This process results in features in the input data being spread and smeared. Features which are thin or of high contrast are attenuated and detail is lost. All data gathering instruments may suffer from this problem to varying degrees due to limited high frequency response. If some of the nonideal effects introduced by an instrument's system response may be removed or canceled, the quality of the data may be improved. Deconvolution is the process by which this correction may be attempted. The objective of deconvolution is thus to estimate an original signal x, given a distorted signal y and some information and assumptions about the system response h. Generally, the estimate of the original signal will be calculated to minimize a previously chosen performance measure. The

deconvolution operation can be expected to produce an improvement in sharpness as well as in accuracy. Ideally, deconvolution should restore the smoothed data to its original form; however, the presence of additive noise and modeling errors will limit the performance of any deconvolution technique. This is due primarily to the fact that under the assumptions presented earlier for the system response, the deconvolution process is a high-pass operation which results in the amplification of high frequency information in the convolved data. The presence of additive noise and terms near zero in the system response exacerbate the problem of excessive noise amplification. In addition, numerical errors introduced during calculations and lack of convergence of transformed sequences at discontinuities further limit performance and introduce additional noise.

Even considering the problems briefly mentioned above, deconvolution is common practice in many applications dealing with data acquisition. In particular, techniques of deconvolution have been successfully applied to certain problems in well logging [16], image processing [17], optics [18, 19, 20], absorption spectroscopy [21], and seismic processing [22]. The techniques involved include both linear and nonlinear methods in one and two dimensions. Deconvolution is applied to sharpen edges and improve resolution, remove blur and distortion in images, detect and improve the resolution of spectral lines, and remove ghosts and echoes.

Deconvolution Methods

A variety of common methods exist for performing deconvolution. These include, but are not limited to, inverse filtering, Wiener filtering and its variations, constrained least squares filtering, Kalman

filtering, L_1 filtering, successive approximation deconvolution, and Jansson's method. In addition, techniques are available for calculating approximate deconvolution filters which may be applied in a manner similar to inverse filtering without some of the limitations of inverse filtering. There are many possible combinations of filtering techniques that make use of the methods mentioned above; however, only the methods above will be described in detail. The simplest approach to deconvolution is inverse filtering and it will be presented first.

Inverse Filtering

Inverse filtering [17] is an elementary unconstrained method for performing deconvolution. In particular, if the system model is given as in Equation (3.1), then an inverse operation may be easily described as given above in Equations (3.5) and (3.6), where the representations are in the time or spatial domain and the Fourier transform domain, respectively. The deconvolved signal, x, may be recovered from Equation (3.6) by taking an inverse Fourier transform to give

$$\hat{x} = F^{-1}\left[\frac{Y}{H}\right] \approx F^{-1}[X] \tag{3.7}$$

Since the deconvolution operation may be described as a division in the Fourier transform domain, it is easy to see that if there is a zero in the spectrum of the system response, a division by zero will result and the inverse filter will not exist. Inverse filtering is not derived to account for additive noise which means that any noise present in the data will result in further errors being introduced by the deconvolution. These two limitations usually result in inverse filtering being unstable unless the spectrum of the system response is nonzero and known exactly,

and the signal is noise free. Otherwise, noise present in the signal will often be amplified due to division by a number near zero so that the result includes more noise than signal. In the presence of noise, the expression for the recovered signal given in Equation (3.7) above becomes

$$\hat{x} = F^{-1}\left[\frac{Y}{H} + \frac{n}{H}\right] \approx F^{-1}\left[X + \frac{n}{H}\right] \tag{3.8}$$

where the noise term may dominate the deconvolution process if the coefficients of the transform of the inverse filter become very small. Only rarely is inverse filtering a practical method for deconvolution.

Some actions may be taken to limit the effects described above. Assuming the operation is to be performed in the Fourier transform domain, a small constant may be added to the system response to increase the size of the values near zero in the transform domain system response. This will prevent division by zero and reduce the amplification of noise. The effect of this modification is quite similar to Weiner filtering. If only a few coefficients in the inverse filter response are very small, they may sometimes be neglected when performing the deconvolution, without adversely affecting the deconvolved result. Rather than performing inverse filtering with the complete original system response, another option is to retain and apply only the coefficients which occur prior to the first zero in the inverse system response spectrum. This has the effect of deconvolving with an approximation to the original system response. Other techniques are also possible, but these are three of the common ones. In any event, the inverse filter usually must have some modification made to it before it can be applied with any success in any practical situation. Other methods of deconvolution are likely to offer a

much higher probability of success than inverse filtering, so inverse filtering will not be considered further.

Wiener Filtering

Weiner filtering [17] is a statistically optimum deconvolution method which minimizes the least squares error criterion

$$||y - h\hat{x}||^2 = ||n||^2 \tag{3.9}$$

where the variables are as defined before. Wiener filtering is thus optimal in an average sense. The Wiener filter may be defined in the Fourier transform domain as

$$\hat{X} = \left[\frac{|H|^2}{H(|H|^2 + \gamma\, S_n/S_f)}\right] Y \tag{3.10}$$

where S_n is the noise power spectral density, S_x is the power spectral density of the original data, and γ is a parameter which must be calculated to satisfy the constraint given in Equation (3.9). When γ is variable, this form of the Wiener filter is often referred to as the parametric Wiener filter. It is interesting to note that if the noise power spectral density is zero, which is a result of there being no noise present in the data, then the Wiener filter may be reduced to the inverse filter discussed earlier. The form of the Wiener filter given in Equation (3.10) is rarely applicable for deconvolution problems such as the one addressed by this research since the two power spectral density functions are almost never known a priori or easily estimated. However, if the spectral densities may be reliably estimated, Wiener filtering may provide results of high quality.

A second form of the Wiener filter may be written if γ is set to unity. This filter is usually referred to simply as the Wiener filter. If, in addition, the power spectral densities are not known, the Wiener filter may be written as given in Equation (3.11)

$$\hat{X} = \left[\frac{|H|^2}{H(|H|^2 + K)} \right] Y \tag{3.11}$$

where K is a constant related by the expression

$$K = \frac{S_n}{S_f} \tag{3.12}$$

The Wiener filter now minimizes the error criterion given below:

$$E[(x - \hat{x})^2] \tag{3.13}$$

It is this form of the Wiener filter which is most often applied since the power spectral densities are rarely known. Even if little is known about the spectral densities, K may be approximated such that the noise in the deconvolved data is not of an excessive amplitude due to the deconvolution process. In effect, the extent of the restoration may be controlled by proper selection of K. Experience has shown that K may often be chosen to be approximately equal to or up to about an order of magnitude greater than the noise variance. Wiener filtering often produces results that are better than those obtained with the other methods described here while requiring a relatively small number of calculations.

Variations on Wiener filtering referred to as soft suppression [23], power subtraction [24], and magnitude subtraction [24] may also be applied to perform deconvolution. The primary difference between Wiener filtering and these methods is the extent of the deconvolution which is

performed as the signal-to-noise ratio varies. With these methods, the deconvolution filter is presented as a function of the short-term signal-to-noise spectral density ratio estimate [25] which may be calculated. More information may be found in the References.

Constrained Least Squares Filtering

Constrained least squares filtering differs from Wiener filtering in that instead of being optimal in an average sense, it is optimal for each signal deconvolved [17]. This procedure requires information regarding the noise mean and variance, two parameters which may often be estimated or measured. Constrained least squares filtering is derived based on two error criteria. The first is a smoothness criterion whereby the second derivative of the signal is minimized using an approximation to the second derivative operator. As before with Wiener filtering, the least squares criterion given in Equation (3.9) is also minimized by the proper choice of the parameter γ. Equation (3.14) below is a common Fourier transform domain representation of the constrained least squares filtering method

$$\hat{X} = \left[\frac{|H|^2}{H(|H|^2 + \gamma|P|^2)} \right] \tag{3.14}$$

where the variable P approximates the second derivative and the other variables are as previously defined.

The parameter γ may be computed iteratively. If a residual vector of length M is defined as

$$r = y - h\hat{x} \tag{3.15}$$

where the residual is a monotonically increasing function of γ, then it

is required that γ be adjusted until the residual is within certain specified error bounds given by

$$||r||^2 = ||n||^2 \pm A \tag{3.16}$$

where

$$||n||^2 = (M - 1)\ [\sigma_\eta^2 + \bar{\eta}^2] \tag{3.17}$$

The parameter A defines the allowable error, σ^2 is the variance of the noise, and $\bar{\eta}$ is the mean of the noise. The algorithm may be implemented as follows:

1. Select an initial value for γ and estimate Equation (3.17).
2. Compute the deconvolution Equation (3.14).
3. Calculate Equations (3.15) and (3.16).
4. Adjust γ.
5. Test for satisfaction of error bounds.
6. If error bounds are not met, then go to step 2.

When the error bounds are satisfied, the deconvolution is correct within the error established by Equation (3.16). The results obtained with constrained least squares filtering may be very good, although the computational requirements are substantially greater than with Wiener filtering.

Kalman Filtering

Kalman filtering [26, 27] is a technique for signal estimation based upon the state-variable representation of a system. Although this method is often derived to represent a forward operation, it may also be derived to perform deconvolution. It is assumed that the measurement process is the output of a linear system driven by white noise plus an additive

noise term to simulate observation in the presence of measurement noise. The Kalman filter has been shown to provide the best solution possible based upon mean square error and several other criteria if the process and noise are Gaussian. If not, the Kalman filter still represents the optimum linear system solution.

Synthesis of the Kalman filter requires construction of the appropriate state-variable model for the message process. Once the model is constructed, the Kalman filter is completely specified except for the filter gain. Obtaining the parameters which describe how the system behaves and the statistics which describe the noise is necessary to implement the Kalman filter. The identification of the required parameters and statistics may often limit the performance obtainable with Kalman filtering. The identification problem is often addressed separately from the filtering problem and may be very difficult to solve. The parameters and statistics will be assumed known for the case considered here.

The Kalman filter is derived to operate on the measured data, represented by Equation (3.18) below, and to statistically minimize the error between the desired signal and the predicted signal output from the filter

$$z(k) = x(k) + v(k) \tag{3.18}$$

where the random process $z(k)$ is the observed signal, $x(k)$ is the desired signal, and $v(k)$ is noise. Equation (3.18) may be rewritten to include vector valued processes and the possibility that the desired process is distorted in some way prior to measurement. In particular, the distortion may be considered to be a convolution.

$$z(k) = y(k) + v(k) = H(k)\, x(k) + v(k) \tag{3.19}$$

Linear system theory may be applied to rewrite Equation (3.19) in state-variable form as

$$x(k+1) = F(k)\ x(k) + G(k)\ u(k) + fm \tag{3.20a}$$

$$y(k) = H(k)\ x(k) + v(k) \tag{3.20b}$$

where m is the mean of the observed data. In Equation (3.20), the message model is generated by the random process, u(k). Both u(k) and v(k) are generally assumed to be zero-mean random processes with correlation functions as given in Equation (3.21):

$$\phi_u = E[u(k)\ u(j)^T] = Q(k)\ \delta(k-j) \qquad \phi_{uv} = 0 \tag{3.21a}$$

$$\phi_v = E[v(k)\ v(j)^T] = R(k)\ \delta(k-j) \qquad \phi_{uz} = 0 \tag{3.21b}$$

These parameters must be properly estimated to ensure satisfactory performance. The Kalman filter equations may be represented [28] as

$$x(k+1) = K(k)\ z(k) + F(k)\ \hat{x}(k) - K(k)\ H(k)\ \hat{x}(k) \tag{3.22}$$

$$K(k) = P(k)\ H^T(k)\ R^{-1}(k) \tag{3.23}$$

$$P(k) = E[\tilde{x}(k)\ \tilde{x}^T(k)] \tag{3.24}$$

$$\tilde{x}(k) = \hat{x}(k) - x(k) \tag{3.25}$$

$$\begin{aligned} P(k+1) = {} & F(k)\ P(k) + P(k)\ F^T(k) \\ & - P(k)\ H^T(k)\ R^{-1}(k)\ H(k)\ P(k) \\ & + G(k)\ Q(k)\ G^T(k) \end{aligned} \tag{3.26}$$

An inverse Kalman filter may also be represented based upon the block diagram of Figure 7. If the relationship between the input and the output of the system is known, the system may be modeled as

$$x_1(k+1) = A_1(k)\ x_1(k) + G_1(k)\ s(k) \tag{3.27a}$$

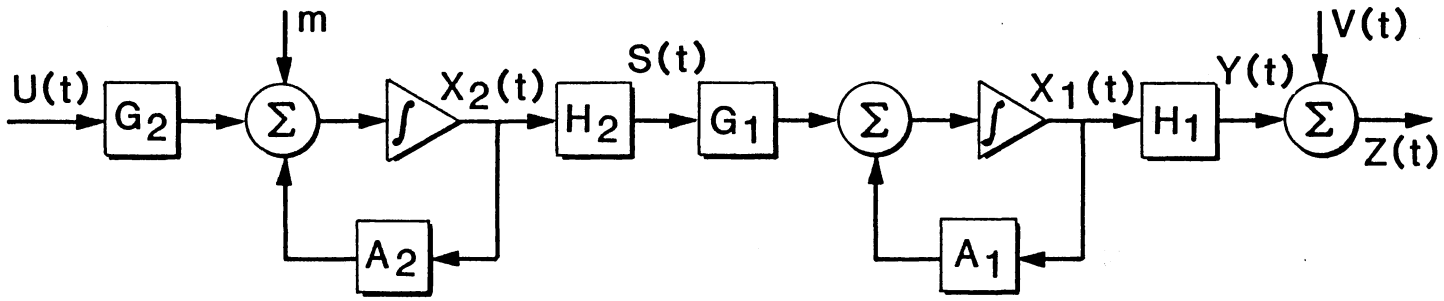

Figure 7. The System Model for Kalman Filtering

$$z(k) = y(k) + v(k) = H_1(k)\, x_1(k) + v(k) \tag{3.27b}$$

where z(k) is the measured signal plus noise, s(k) is the desired signal, and x(k) contains lagged values of s(k). Equations relating the desired signal to a white noise generating process may be written as

$$x_2(k+1) = A_2(k)\, x_2(k) + G_2(k)\, u(k) + f_2 m \tag{3.28a}$$

$$s(k) = H_2(k)\, x_2(k) + u(k) \tag{3.28b}$$

where m represents the mean of the desired signal. The equations above may be combined to give the desired state-variable formulation of Equation (3.29)

$$x(k+1) = F(k)\, x(k) + G(k)\, u(k) + fm \tag{3.29a}$$

$$z(k) = H(k)\, x(k) + v(k) \tag{3.29b}$$

where F(k) and G(k) are assumed known as before. If this formulation represents the induction log, then z(k) represents the apparent conductivity plus noise, and $H_1(k)$ contains the induction log system response.

Equation (3.28) may be modeled as an ARMA process of specified order and non-zero mean, where an ARMA process is one whose transfer function may be represented as the ratio of two polynomials. The statistics which describe the conductivity process, the order of the ARMA model, and the coefficients of the ARMA model may be estimated from the data to be processed. The ARMA model may be described as the transfer function

$$H(z) = \frac{1 + \sum_{i=1}^{j} h_i\, z^{-i}}{1 + \sum_{i=1}^{j} a_i\, z^{-i}} \tag{3.30}$$

with u(k) the driving noise source and s(k) the output conductivity sequence. Thus,

$$1 + \sum_{i=1}^{j} h_i z^{-i} = (1 + \sum_{i=1}^{j} a_i z^{-i}) s(z) \tag{3.31}$$

If s(z) is represented as

$$s(z) = s_o + s_1 z^{-1} + s_2 z^{-2} + s_3 z^{-3} + \ldots \tag{3.32}$$

then the system of Equation (3.31) may be solved by a method such as least squares since s(k) is the known data. The model order must have been previously estimated. Graupe [29] addresses the problems associated with system identification and model order selection. The problem of system identification was not considered in this research.

The full state-variable representation may be completed with

$$F = \begin{bmatrix} A_1 & G_1 H_2 \\ 0 & A_2 \end{bmatrix} \qquad H = \begin{bmatrix} H_1 \vdots H_2 \end{bmatrix}$$

$$G = \begin{bmatrix} G_1 \\ \cdots \\ G_2 \end{bmatrix} \qquad x = \begin{bmatrix} x_1 \\ \cdots \\ x_2 \end{bmatrix} \qquad f = \begin{bmatrix} 0 \\ \cdots \\ f_2 \end{bmatrix} \tag{3.33}$$

where A_2 and G_2 depend upon solution of the ARMA transfer function model. The Kalman filter to solve Equation (3.29) may now be formed in the same manner as represented in Equations (3.22) through (3.26). The initial conditions for the filter and the necessary system parameters must be supplied. The solution to the deconvolution problem is observed as part of the vector, x(k). The prediction will lag the input due to the length of the filter since the input data are processed sequentially, point by point.

Actual solution of the Kalman filter equations may be performed using a variety of techniques for solving difference equations. The implementation used to produce the results included in Chapter VI was a Chandrasekhar-type recursive algorithm [30]. Much information, in addition to the references already given, on the formulation and solution of the Kalman filtering problem is available in the literature [31, 32, 33].

L_1 Filtering

Many common filters are based upon the minimization of a least squares, or L_2, error criterion. Examples include Wiener filtering and constrained least squares filtering. Although least squares methods are widely used, there are many other choices which may be made as to minimization of an error criterion. One of these which has not usually been applied to well log data is the least absolute deviation, or L_1, error criterion. This nonlinear method has been applied in such diverse fields of study as economics, solution of differential equations, and deconvolution of seismic data.

Consider the convolution of Equation (3.34),

$$y_n = x_n * a_n \tag{3.34}$$

which may be written in matrix notation as Equation (3.35)

$$\underline{y} = X\,\underline{a} \tag{3.35}$$

where a and y are vectors of dimension M and Q, respectively. Given the forward filter or system response represented by the matrix X and the measured data represented by the vector y, the goal of L_p deconvolution is to recover the unknown actual data represented by the vector a with

$$\underline{a} = (X^T X)^{-1} X^T \underline{y} \tag{3.36}$$

where the length of the filter response included in X is N. In particular, one is to find an a to minimize the error criterion

$$E_p = \sum_{n=1}^{Q} |(y_n - x_n * a_n)|^p \qquad Q = N + M - 1 \tag{3.37}$$

where p = 2 corresponds to the least squares error criterion and p = 1 corresponds to the least absolute deviation criterion. The values of p between one and two correspond to other error criteria which are between the extremes of L_1 and L_2, respectively. The parameter p determines the tradeoff between de-emphasizing and emphasizing aberrant data. That is to say, the L_1 method is least sensitive to aberrant data and L_2 is most sensitive [34]. Another way to state this is to say that L_1 is robust since a few large errors in the data will not cause large errors in the output. The output of an L_1 procedure will predict the actual data more often than will an L_2 method. Also, the residual vector of an L_1 process will contain more zeros than will the L_2 vector.

Several algorithms are available for solving the L_1 deconvolution problem. These include linear programming [35], iterative reweighted least squares [36], and residual steepest descent algorithms [37]. The algorithm used in this research to apply L_1 was an implementation of iterative reweighted least squares as described in Reference [34]. This approach iterates toward the L_1 solution after starting from the well known least squares solution. At each iteration, the residuals from the previous iteration are weighted and a new least squares problem is solved using the weighted residuals from the previous step. Equation (3.38) represents the algorithm for solving Equation (3.35) based upon the L_1

error criterion rewritten in Equation (3.39). Thus, the solution is

$$\underline{a}(k+1) = (X^T W(k) X)^{-1} X^T W(k) \underline{y} \tag{3.38}$$

where W(k), a diagonal matrix, is calculated from the chosen residual vector, namely

$$r(k) = \underline{y} - X \underline{a}(k) \tag{3.39}$$

so that

$$W_i(k) = |r(k)|^{p-2} \qquad 1 \leq p \leq 2 \tag{3.40}$$

Equation (3.40) is calculated from Equation (3.39) using the relations given below [34]. Let

$$\rho(x) = |x|^p \tag{3.41}$$

Then the error vector for order p becomes

$$E_p = \sum_{n=1}^{Q} \rho(y_n - x_n * \underline{a}_n) \tag{3.42}$$

Taking derivatives with respect to a_i gives

$$0 = \sum_{n=1}^{Q} \rho'(\underline{y} - x * \underline{a})\, x_{n-i} \tag{3.43}$$

which may be written as

$$0 = \sum_{n=1}^{Q} \left[\frac{\rho'(r_n(k))}{r_n(k)}\right] (y_n - x_n * a_n) x_{n-i} \tag{3.44}$$

An expression for the diagonal entries in the matrix W may be written

$$(W(k))_{ii} = W_i(k) = \frac{\rho'(r_i(k))}{r_i(k)} \tag{3.45}$$

which leads to Equation (3.40) as desired. An upper limit is usually placed on values produced by Equation (3.40) so that $W(k)_i$ can be kept from getting very large. Thus the individual values of the entries in W will be large when the signal is predicted accurately and small otherwise. Accurate predictions are therefore weighted more heavily while less accurate predictions will be de-emphasized. Since noise is random and unpredictable, it will receive the smallest weights as the process proceeds toward a solution.

Equations (3.38) through (3.40) above may be rewritten using circulant matrix theory so that they may be solved using Fourier transforms to improve the computational efficiency [34]. Even so, the L_1 solution is computationally complex so that it requires a very large amount of time to solve problems of reasonable size. It has also been noted that L_1 solutions may not always be unique and the predictive filters may not be stable in general [34]; however, the largest problem with L_1 deconvolution is the enormous amount of time required to produce a solution.

Deconvolution by Successive Approximation

Several similar successive approximation techniques for deconvolution have been described in the literature. Most references involve deconvolution of spectral lines [18, 19, 20], although the most recent is presented with geophysical applications in mind [38]. The goal of successive approximation deconvolution is to transform the solution of the deconvolution problem into an iterative process which employs only smoothing, the mathematical inverse of deconvolution as it is normally defined and a much better behaved operation. This is the approach first taken by Van Cittert [18] and later modified by Jansson and others to include

a relaxation parameter. The modified procedure, referred to as Jansson's method, is described in the next section. The primary advantage of an iterative algorithm such as this one is that the deconvolution process may be observed at each iteration and stopped before noise present in the data is amplified excessively. Another point that may be an advantage in some applications is that all calculations may be performed in either the spatial or Fourier transform domain, as desired. Disadvantages associated with this type of iterative procedure include difficulty in determining convergence, bed splitting, and over-correction.

The successive approximation deconvolution procedure may be described as given in Equation (3.46), where the variables are as previously defined and the subscripts denote the ith approximation to the original data.

$$\hat{x}_i = \hat{x}_{i-1} + (y - \hat{x}_{i-1} * h) \tag{3.46}$$

Note that the zeroth approximation is just the signal to be deconvolved, y. At each succeeding iteration an updated approximation is computed.

A Fourier transform domain representation may be written as Equation (3.47):

$$\hat{X}_i = (I - H)\hat{X}_{i-1} + Y \tag{3.47}$$

where I is the identity matrix. Equation (3.47) may be solved at the kth iteration and expressed as Equation (3.48):

$$\hat{X}_k = Y \sum_{j=o}^{k} (I - H)^j = Y \Big/ \left[\frac{H}{1 - (1 - H)^{k+1}} \right] \tag{3.48}$$

The denominator may be interpreted as an effective filter response function for H after k iterations. Note that this becomes inverse filtering

as K approaches infinity, provided that H is not very small. If H is very small, Equation (3.48) may be expressed as Equation (3.49):

$$\hat{X}_k \approx \frac{Y}{(k+1)^{-1}} \tag{3.49}$$

Thus although when H is very small and inverse filtering would divide by H with unpredictable results, successive approximation divides by the linear term given in Equation (3.49) above. This implies that the high frequency components of the deconvolved signal increase linearly with the number of iterations.

At first glance it would seem that this linear increase in noise with iteration would limit the number of iterations that may be applied and the resolution that can be obtained. Wertheim [20] has shown that this need not be the case. After a sufficiently large number of iterations have been performed, the correction applied in Equation (3.46) consists almost entirely of noise. The approximated noise may be subtracted from the data so that the noise that has been accumulating throughout the process may be partially removed. After k iterations the noise correction will be as given in Equation (3.50):

$$\hat{x} = x_k - k[y - x_k * h] \tag{3.50}$$

Represented in the Fourier transform domain, Equation (3.50) may be written as Equation (3.51):

$$\hat{X} = Y\left[\frac{1 - (1-H)^{k+1} - kH\,(1-H)^{k+1}}{H}\right] \tag{3.51}$$

This indicates that successive approximation may be performed more efficiently than might otherwise be imagined. It also gives a procedure for

calculating an inverse filter using Equation (3.48) or Equation (3.51) if a correction for accumulated noise is desired.

The successive approximation approach is useful for deconvolving data. Unfortunately, when the noise content is increased, the method may not perform reliably. Although a correction for noise is possible and appears attractive, its use may leave some doubt as to the validity of the deconvolved data [20]. The method is most useful when the additive noise content of the signal to be deconvolved is low. It may also be difficult to accurately determine the rate of convergence and the extent of convolution for successive approximation deconvolution. Jansson's method, an iterative deconvolution technique that some believe to be better than successive approximation [21], is described in the next section.

Jansson's Method

Jansson's method [19] is a nonlinear deconvolution algorithm derived from a successive approximation method first described by Van Cittert. Jansson's method in one dimension is fully described in a monograph by Blass and Halsey [21] and in two dimensions in a paper by Frieden [18] which also discusses Van Cittert's method. This method is an iterative procedure that produces at each iteration an estimate of the actual data. It is nonlinear since a relaxation parameter, dependent on the amplitude of the data point being processed, is applied at each point. It can be implemented in either the spatial domain or the Fourier transform domain. The algorithm is rather specialized in that it is typically constrained to data ranging between zero and one. These constraints are easy to meet, however, since the data may be normalized and the normalizing

constant saved so that the true amplitudes may be restored after the deconvolution.

Jansson's method is given in Equation (3.52), where the variables are as previously defined, the subscripts denote the ith approximation to the original data, and A(y) is a relaxation parameter:

$$\hat{x}_i = \hat{x}_{i-1} + A(y)\ [y - \hat{x}_{i-1} * h] \tag{3.52}$$

As noted earlier, the relaxation parameter is dependent on the value of the data point being processed. In general, A(y) is defined similarly to Figure 8. Its value falls off to zero at each extreme of the range of data values. In this manner the constraints necessary to Jansson's algorithm are built into the relaxation parameter. The correction applied by the relaxation parameter is thus only partial when A(y) is less than unity. Since negative values may be generated in the deconvolved data with this procedure, they are normally set equal to zero or a very small positive value at the end of each iteration when they occur. One family of expressions for A(y) which has been applied with some success is given in Equation (3.53):

$$A(y) = A_{max}\ [\hat{x}_{i-1}\ (1 - \hat{x}_{i-1})^k] \tag{3.53}$$

where A_{max} is a constant which affects the convergence step size and k is a constant usually set to unity. A_{max} is most often chosen to be less than about 4.0. Defining A_{max} to be large will result in faster convergence but may also introduce instability into the algorithm.

The data dependence introduced by the relaxation parameter is what sometimes enables Jansson's algorithm to perform better than other methods for some types of data. It is the data dependence, however, which

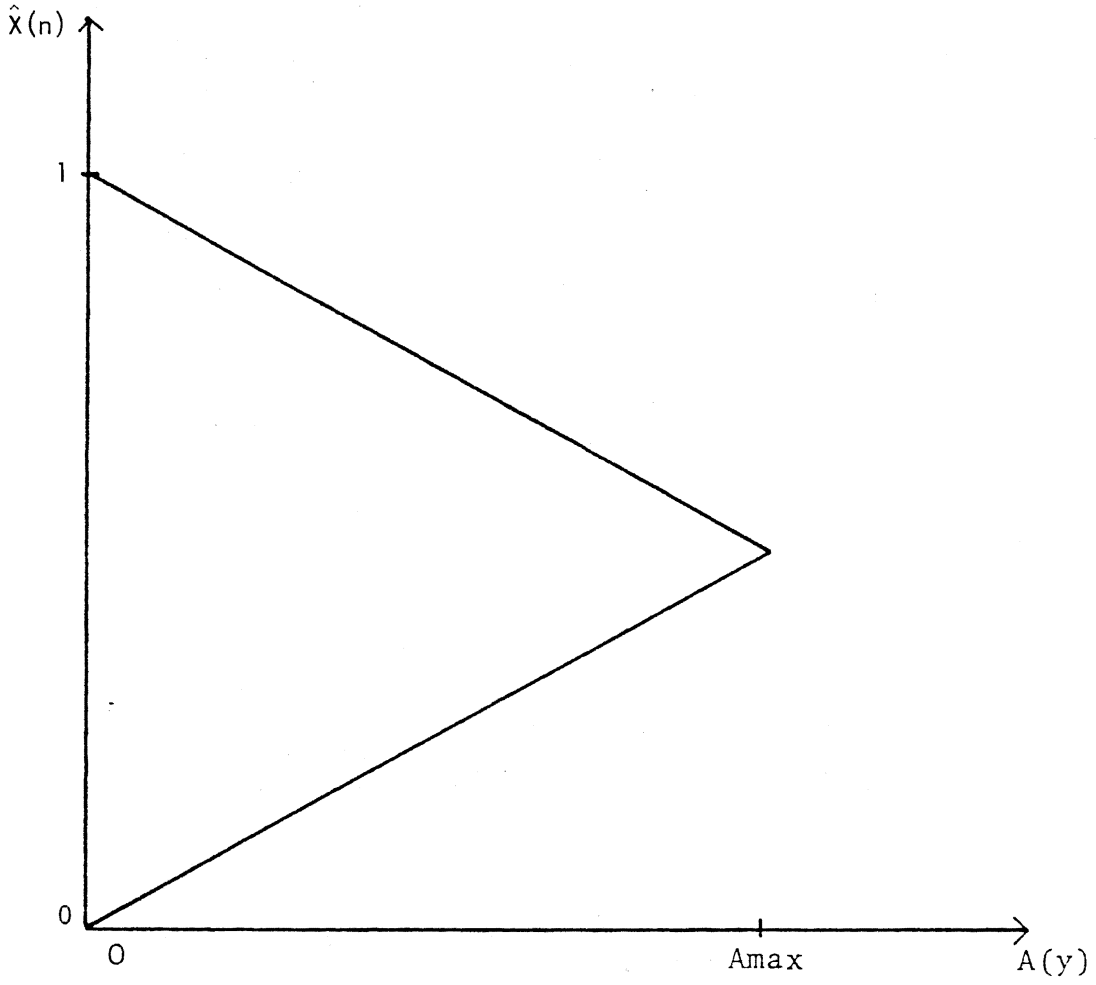

Figure 8. A Relaxation Parameter, A(y), for Jansson's Method

makes it very difficult to describe exactly how Jansson's method functions. The references give reasonable accounts regarding the algorithm's general performance. They have also shown that the method approaches, in the limit and given certain assumptions and constraints, the inverse filtering estimate.

It is interesting to note that, within certain constraints, the signal being deconvolved may be smoothed during the iterative process using a median filter or other low-pass filter with the result being faster convergence and fewer spurious features attributable to amplified additive noise. Since smoothing and deconvolution work against each other, smoothing must be used very carefully to ensure that desired features are not degraded unnecessarily in the process. Jansson's method is noise tolerant in that the signal will be restored to a greater extent than will additive noise be amplified. Results obtained using Jansson's method to deconvolve induction log data resemble those obtained with successive approximation and have not been as good as those obtained using other methods.

Median filtering, a nonlinear low-pass filtering procedure, may also be used in general to reduce amplified noise if the operation is performed following deconvolution. This postfiltering operation may be performed in conjunction with any of the methods above. Recursive median filtering, in particular, has been shown to provide useful results without adversely affecting the data. The examples of Chapter VI include results produced with postfiltering by repeated application of recursive median filtering.

Goals for Deconvolution of the Induction Log

At this point it is illustrative to restate the goals which are desirable if the induction log deconvolution problem is to be successfully approached. The induction log is a nonlinear device which operates as a low-pass filter whose system response is dependent upon the conductivity of the data it is measuring. In particular, the gain of the tool decreases as the conductivity of the formation under investigation increases since the generated electromagnetic field will not penetrate as deeply into a conductor. The gain change is due to the area under the system response curve changing and also to portions of it becoming negative as the conductivity increases. Thus the relative gain of the tool changes, as does the spectral response of the tool. Other effects are also present but these two are important ones which this research will address.

Successful solution of the induction log deconvolution problem must include the correction of much of the smoothing which the instrument imposes upon the measured data. This goal can be most easily achieved by deconvolution of the data with the induction log system response if the response may be considered non-time-varying. Since the system response is not really fixed, the deconvolution must also account at least partially for variations in the system response. This can be achieved if the deconvolution problem is approached as the nonlinear problem it is but with a linearized solution. In particular, if the deconvolution filter can be varied in a manner that will approximate the manner in which the real response varies due to changes in average conductivity, an approximate solution can be obtained. The induction log deconvolution problem may thus be considered to be two separate problems: a basic deconvolution problem and partial correction of the nonlinear distortion due to

skin effect. A deconvolution procedure will be considered successful, then, if it can significantly correct for the smoothing introduced by the poor high frequency response of the induction log as well as for the nonlinear variations introduced by changes in the average formation conductivity. As was mentioned in Chapter I, the terms frequency and spectrum are not intended to imply a relationship to time when used to describe the induction log. The induction log measures conductivity with respect to distance so the coefficients of the Fourier transform of the induction log are actually in units of reciprocal distance. Frequency and spectrum are convenient, if not absolutely accurate, terms which will be used throughout this dissertation, however, to describe the induction log response.

The statements above suggest a solution where the deconvolution filter is allowed to change occasionally as the deconvolution progresses. It follows that the deconvolution filter should be allowed to change quickly enough so as to follow rapid changes in average formation conductivity. This goal can best be achieved if a segmented approach to deconvolution is applied so that the deconvolution filter may be selected to best match the data in the segment being processed while remaining fixed over the segment. The nonlinear problem may thus be modeled as a sum of overlapping linear convolutions allowing the system response to be constant during each convolution but changed as required from one segment to the next. The technique of short-term analysis and synthesis which combined overlap-addition convolution with a spectral modification of overlapping windowed data segments will be developed in the next chapter and will be shown to provide a satisfactory solution to this difficult problem. The approach will be referred to as weighted overlap-addition convolution, or WOAC.

CHAPTER IV

WEIGHTED OVERLAP-ADDITION CONVOLUTION

Weighted overlap-addition convolution (WOAC) is a convolution procedure based upon overlap-addition convolution [39] as well as on techniques of short-term analysis and synthesis often applied in the processing of speech and other quasi-stationary signals [40]. These techniques have been well described in the signal processing literature and elsewhere. Overlap-addition convolution, an efficient convolution technique, offers numerous advantages over the familiar "brute-force" techniques often applied in both the spatial and Fourier transform domain. Among these advantages are the data may be processed in relatively short segments so that only a small portion of a possibly infinitely long signal needs to be available at one time, Fourier transforms may be used to efficiently perform the actual convolution, and the procedure has been well documented in the literature. In addition, numerous methods of deconvolution such as Wiener filtering and its variations, constrained least squares filtering, successive approximation, L_1 filtering, Kalman filtering, Jansson's method, and others may be easily implemented with this procedure. The weighted procedure, WOAC, is a modified version of overlap-addition convolution offering improved performance when deconvolution is the goal. Although WOAC is primarily intended to perform deconvolution, it can easily be used for convolution as well. Throughout the discussion which follows, deconvolution is generally assumed; however, any

other filtering process which may be modeled as a convolution could be performed.

It is useful to describe what is generally meant by overlap-addition convolution since it will be used to develop WOAC. The first step in performing overlap-addition convolution is to split the data to be convolved into sequential segments as illustrated in Equation (4.1)

$$x_k(n) = \begin{cases} x(n)\ w(n), & kL \le n \le (k+1)L - 1 \\ 0 \quad , & \text{otherwise} \end{cases} \tag{4.1}$$

where $x(n)$ is the original data and $w(n)$ is a properly chosen window function that selects which portion of the data will comprise each segment. The window function is normally chosen to be a rectangular window for overlap-addition convolution since the operation is usually low-pass. This will not be the case when deconvolution is performed with WOAC since low spectral leakage is very important. When these segments are properly summed, the original data may be recovered as shown in Equation (4.2):

$$x(n) = \sum_k x_k(n) \tag{4.2}$$

The segments given by Equation (4.1) may be convolved one by one with the desired filter as shown in Equation (4.3) to produce convolved segments:

$$y_k(n) = x_k(n) * h(n) \tag{4.3}$$

If $x_k(n)$ is of length L and $h(n)$ is of length M, then the result of each convolution will be $L + M - 1$ points in length. The convolved segments may then be properly combined by overlapping and adding to produce the result given in Equation (4.4) which is equivalent to the convolution specified in Equation (4.5):

$$y(n) = \sum_k y_k(n) \tag{4.4}$$

$$y(n) = x(n) * h(n) \tag{4.5}$$

The equations above are the starting point for building the weighted convolution procedure referred to previously as WOAC.

Overlap-addition convolution as given above may be modified to approximate a nonlinear system such as the induction log whose system response function varies for one reason or another. For example, if one supposes that the system response of an instrument varies in some manner, the operation of the instrument may be approximated using overlap-addition convolution if the system response function, h(n), is varied from segment to segment in a manner similar to the actual variation. In this case, Equations (4.3) and (4.4) would become Equations (4.6) and (4.7), respectively,

$$\hat{y}_k(n) = x_k(n) * h_j(n) \tag{4.6}$$

$$y(n) \approx \sum_k \hat{y}_k(n) \tag{4.7}$$

where the subscript on h(n) denotes a particular variation of the system response. As before, the operation described here is assumed to be low-pass, and the segmenting is performed with a rectangular window function.

In both of the descriptions of overlap-addition convolution given above, the forward convolution operation was assumed. If in Equations (4.3), (4.5), and (4.6) the filter response function, h(n), is replaced with an appropriately calculated deconvolution filter, $h^{-1}(n)$, the deconvolution process may be shown. This is an extreme simplification of the description for WOAC since a major problem exists if the deconvolution description is formulated in this manner. A rectangular window

function is not appropriate for a high-pass operation due to excessive spectral leakage. However, if a window function other than a rectangular window is applied so that spectral leakage is reduced, its shape will be imposed periodically upon the deconvolved result. Overlapping windows may be used to remedy this problem. Rather than segmenting the data sequentially with segments following one another, the segments may be formed in such a manner that they overlap each other in some specified fashion. The use of overlapping windows is well known in signal processing. If the overlap is specified properly, the effect of multiplying the data by the window function will vanish, leaving only a small residual error, when the segments are summed. The application of overlapping windows in combination with overlap-addition convolution leads directly to short-term analysis and synthesis and the representation for WOAC.

Short-term analysis and synthesis is not a new technique and the theory that describes it is basic to representing a slowly time-varying signal such as the induction log. This technique has not, however, been used to describe induction log data or to perform deconvolution on it. Short-term analysis and synthesis is performed by analyzing the short-term spectra of the signal, modifying each spectrum as desired, and reconstructing the processed signal from its modified short-term spectra [41]. The analysis step involves computing the short-term Fourier transform of each data segment so that the specified spectral modification may be performed. The modification step may be any desired operation on the short-term spectra, but here it will be considered to be a multiplication of each spectrum with a spectrum derived from the desired deconvolution filter. Reconstruction is performed by taking the inverse

Fourier transform of each modified short-term spectrum to produce a processed (deconvolved) segment and properly summing it with the other processed segments to produce the complete result. Although short-term analysis and synthesis will be developed and described primarily in the Fourier transform domain, it may also be considered in the spatial domain if the transform domain multiplications are replaced by the appropriate convolutions. Although it is generally simpler to discuss WOAC using a transform domain representation, in some cases the particular deconvolution method chosen cannot be easily written in the transform domain. In these cases, there will be no choice except to implement WOAC using a spatial representation.

Let the data to be processed be given by $x(n)$, where the data length is long and may be infinite. The short-term Fourier transform of the signal may be defined to be

$$X_m(e^{jw_p}) = \sum_{i=mR-L+1}^{mR} x(i)\, w(mR - i)\, e^{-jw_p i} \tag{4.8}$$

where $w(n)$ is an appropriate window function which weights the input signal and determines which portion of the input is to be analyzed [42]. Now, $w(n)$ is specifically required to be a symmetric low-pass analysis window function of length L. The constant, R, in Equation (4.8) is determined by the desired number of overlaps in any analysis segment and is called the decimation rate. It has been shown that under certain conditions the original signal, $x(n)$, may be recovered within some small error by taking the inverse Fourier transform of each segment and overlap-adding the results [43]. The reconstructed signal, $x(n)$, may be given as in Equation (4.9)

$$\hat{x}(n) = \sum_m \sum_p X_m (e^{jw_p}) e^{jw_p n} \tag{4.9}$$

where the summation is over all m overlapping segments with corresponding short-term Fourier transforms. If the window is sufficiently sampled, Equation (4.9) may be simplified to give Equation (4.10)

$$\hat{x}(n) = \frac{R}{W(e^{jo})} \sum_m x_{mR}(n) \tag{4.10}$$

where $x_{mR}(n)$ is the resulting set of inverse transformed and overlapped segments. The equality given in Equation (4.10) will be satisfied only if the decimation rate is unity. In other cases, a small error due to the overlapping and added windows will be introduced. This error will usually be insignificant for small values of R, but depends on the relation below being satisfied [42]:

$$\frac{R}{W(e^{jo})} \sum_m w(mR - n) = 1 \tag{4.11}$$

Assuming the Kaiser window is chosen as the analysis window and the decimation rate is greater than about 8,0, the Kaiser window design parameter should be chosen properly to minimize error due to overlapping windows [44]. With a properly designed window the error introduced due to the overlap-addition will be very small.

A modification to the short-term Fourier transform may be included in the description for short-term analysis and synthesis presented above. If x(n) is again the data to be processed, where a filtering operation will now be performed on the short-term spectra, then the reconstructed signal is given in Equation (4.12),

$$\hat{y}(n) = \sum_m \sum_p X_m(e^{jw_p}) \, H(e^{jw_p}) \, e^{jw_p n} \tag{4.12}$$

where y(n) is the reconstructed and filtered signal and $H(e^{jw_p})$ is the filter function to apply. It has been shown that Equation (4.12) may be rewritten to give Equation (4.13) which is an expression for the filtered result [43]:

$$\hat{y}(n) = \frac{R}{W(e^{jo})} \, x(n) * h(n) \tag{4.13}$$

If x(n) is a sequence of induction log data and h(n) is a non-time-varying deconvolution filter for the induction log, Equation (4.13) may be considered to represent deconvolved induction log data. In a manner similar to Equation (4.12), a time-varying filter may be applied if $H(e^{jw_p})$ Is allowed to vary in some specified way as introduced earlier in Equation (4.6). If $H_k(e^{jw_p})$ is a discretely time-varying deconvolution filter for the induction log, the reconstructed signal may be represented by Equation (4.14):

$$\hat{y}(n) = \sum_m \sum_p X_m(e^{jw_p}) \, H_k(e^{jw_p}) \, e^{jw_p n} \tag{4.14}$$

As with Equation (4.13) above, it has been shown that the reconstructed signal given in Equation (4.14) may be rewritten in the form of Equation (4.15)

$$\hat{y}(n) = \frac{R}{W(e^{jo})} \sum_q x(n-q) \, \hat{h}(n-q,q) \tag{4.15}$$

where

$$\hat{h}(n-q,q) = \hat{h}(m,q) = \sum_r h_r(q) \, w(rR - m) \tag{4.16}$$

Equation (4.16) may be interpreted to be, for the qth value, the convolution of $h_r(q)$ with w(r). This implies that each coefficient in the time response due to the time-varying modification is smoothed by the window. Thus the modification is bandlimited by the window, but the procedure of Equation (4.15) acts as a true convolution of the deconvolution filter on the input [40, 43]. The result is to smooth and spread the effect of the deconvolution filters into the reconstructed signal. In some other adaptive convolution procedures, an instantaneous change in the filter coefficients may result in a discontinuity in the output; this is not possible with WOAC due to the overlapping windows.

Equations (4.12) and (4.14) describe the WOAC procedure in the frequency domain for a fixed deconvolution filter and a time-varying filter, respectively. Equation (4.12) may be used when WOAC is to be applied nonadaptively, and Equation (4.14) may be used when adaptive filtering is desired. Thus the procedure for WOAC may be described in terms of overlap-addition convolution with the inclusion of an analysis window, w(n), and overlapping segments separated by R points in the short-term transform of the signal. The choice of R is determined by the particular window being used and will be discussed in the next chapter. WOAC is a useful and relatively robust procedure for implementing various filtering methods of deconvolution.

CHAPTER V

IMPLEMENTATION OF WOAC

The successful application of WOAC depends heavily upon proper formulation of the procedure for the data to be deconvolved. This is particularly true when deconvolution, a high-pass operation, is the goal, but may be important to a lesser degree if a low-pass filtering operation is to be performed. Among the factors which must be carefully considered are proper selection of the analysis/synthesis window, selection of window length, calculation of the deconvolution filter to be applied, and choice of the actual deconvolution technique or techniques to use internal to WOAC. Weakness in any one of these areas can produce poor or unusable results. Deconvolution is basically an ill-posed problem since minor changes in the measured log will likely produce large fluctuations in the high frequency components of the log due to the inverse response strongly amplifying high frequency information. Thus, it cannot be emphasized too strongly that extraneous high frequency information (i.e. noise and discontinuities) in the data being processed must be controlled. At the same time, information about the sharp discontinuities in the lithology should be preserved. WOAC is designed to allow the segmented processing of data using techniques of short-term analysis and synthesis while reducing many undesirable effects which would likely be present if a less robust segmented approach were used. Certain problems such as Gibb's phenomena are unavoidable regardless of the deconvolution

procedure which is used. However, selection of an appropriate window and R, the decimation rate, will help in reducing the size of the ripples. The goal of WOAC is to derive the benefits associated with short-term processing while minimizing the many problems often associated with deconvolution.

Window Selection

Window choice is perhaps the most important decision that must be made before the WOAC procedure may be applied since it, more than any other factor, influences the appearance, quality, and reliability of the deconvolved data. The window used to segment the data must have high sidelobe attenuation to reduce spectral leakage. Spectral leakage introduces errors from various sources which may cause severe distortion of the result. The amplification of extraneous high frequency information may become particularly troublesome, causing nonexistent features to appear in the deconvolved data. This not only reduces the overall signal to noise ratio of the deconvolved data but also makes questionable the reliability of the result. Since one rarely knows the exact answer to the deconvolution of real data even after deconvolution, any process which introduces further uncertainty is highly undesirable. It is thus very important that the procedure produce a reliable estimate of true conductivity from the apparent conductivity data which is available.

The analysis window must be of finite length and must taper smoothly to zero at each end so that unnecessary discontinuities are not introduced at the window edges. The Hamming window, a commonly used window in similar applications of short-term analysis and synthesis, is an inappropriate choice for this procedure since its value at the window

edges is approximately eight percent of its peak value. It is, of course, inevitable that there will be discontinuities in the data being processed. It is also inevitable that discontinuities will have an adverse effect on the process since a Fourier series cannot converge there. The problems associated with a discontinuity are, however, generally controllable if a proper window can be chosen.

The family of windows generally called Kaiser windows [45] has very good attenuation of its sidelobes and offers good performance. The Kaiser window optimizes the narrowness of the window and the main lobe of the window spectrum. Furthermore, these windows are symmetric, another desirable characteristic. They also offer the convenience of allowing specification of window width and minimum spectral sidelobe attenuation through the selection of the window parameter, beta. For example, selecting a beta of 8.5 will produce a maximum sidelobe level down more than 60 dB compared to the amplitude of the central lobe. Useful values of beta range approximately from 6 to 20. At the lower end of this range performance is limited by maximum sidelobe level while at the upper end the central lobe of the window spectrum becomes excessively wide, allowing excessive amplification of high frequency information.

The spatial domain window width is also important since it affects how the data segment is weighted before deconvolution is performed. With beta chosen as 8.0, the window width, defined as the number of points between the points of inflection, is approximately 36% of the total window length. Figure 9 illustrates the relationship between the fractional point of inflection versus beta for the Kaiser window. Notice that the greatest decrease in the window width, represented by the fractional point of inflection, occurs for low values of beta. A narrow window

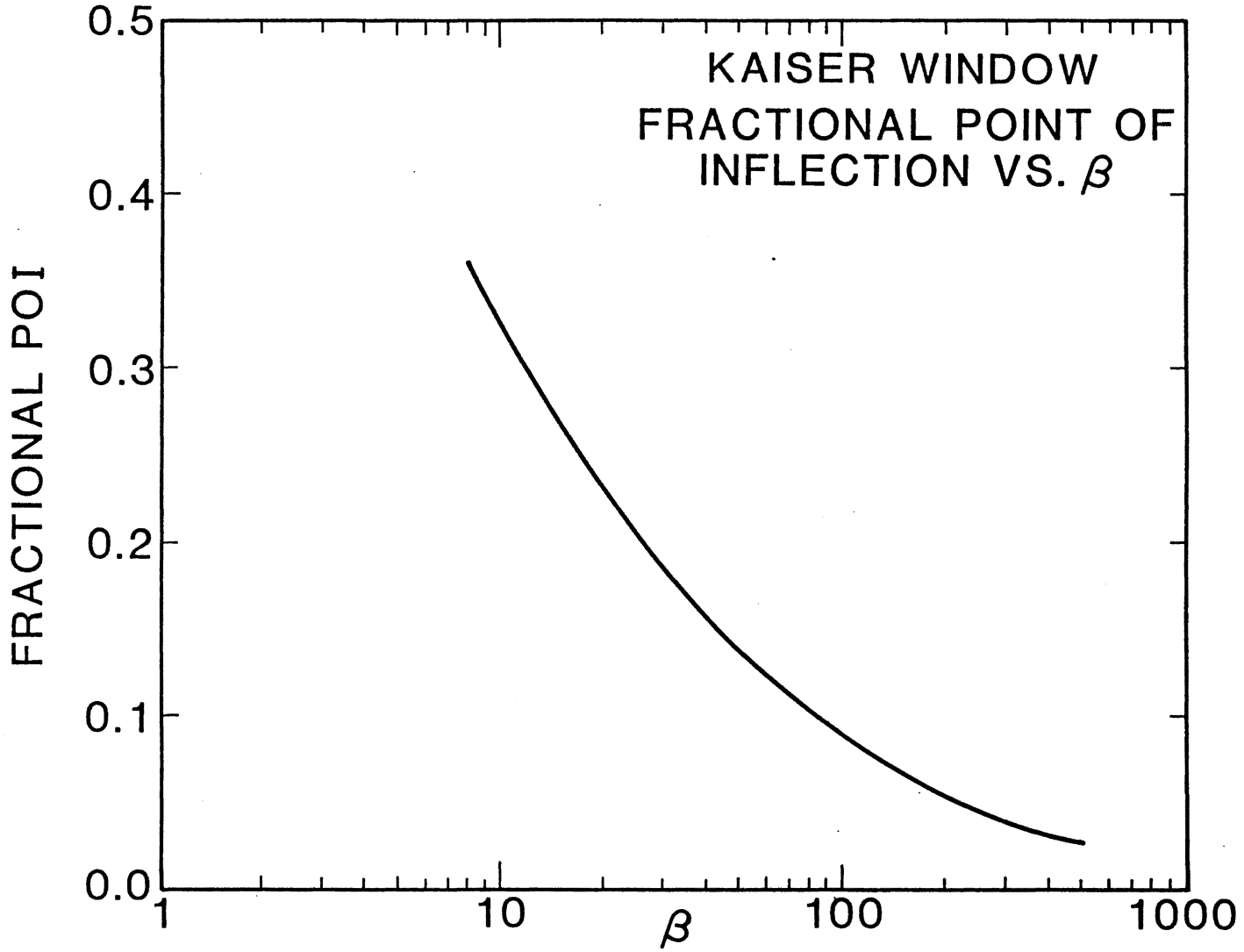

Figure 9. Kaiser Window Performance: Fractional Point of Inflection Versus Beta

width is desirable since it tends to isolate one segment from the next; however, one must consider the relationship between window width, the spectral characteristics of the window, and the performance of WOAC. Narrow window width is desirable since, in the adaptive implementation of WOAC, it allows the effect of each selected deconvolution filter to be more pronounced. Increasing beta causes the window width and the amplitude of the spectral sidelobes to decrease, and the central spectral lobe width to increase. Thus, although increasing beta decreases spectral leakage, the main lobe width increases allowing more amplification of noise. This is the reason for the useful range of beta given above. Figure 10 is a plot of absolute peak to peak error present in the deconvolved result due to an arbitrary single discontinuity present in the data versus beta. The segment length used with WOAC was 256, the filter length was 127, the decimation rate was unity, and Wiener filtering was the filtering method. The peak to peak error is a measure of the maximum ripple content of the deconvolved result associated with a discontinuity. The absolute magnitude of the error is meaningless, but the relationship between the error and beta is important. Notice that the peak to peak error increases slowly for small values of beta, but begins to grow quite rapidly as beta increases beyond approximately 20.

Thus, there is a compromise between having a narrow window width and having superior performance in the presence of real data which includes noise. The narrow window is desirable since it allows a particular deconvolution filter to be emphasized over a smaller number of points so that the effect of changing the filter is more isolated. However, at some value of beta the noise and ripples introduced by possible discontinuities and additive noise will become a significant portion of the

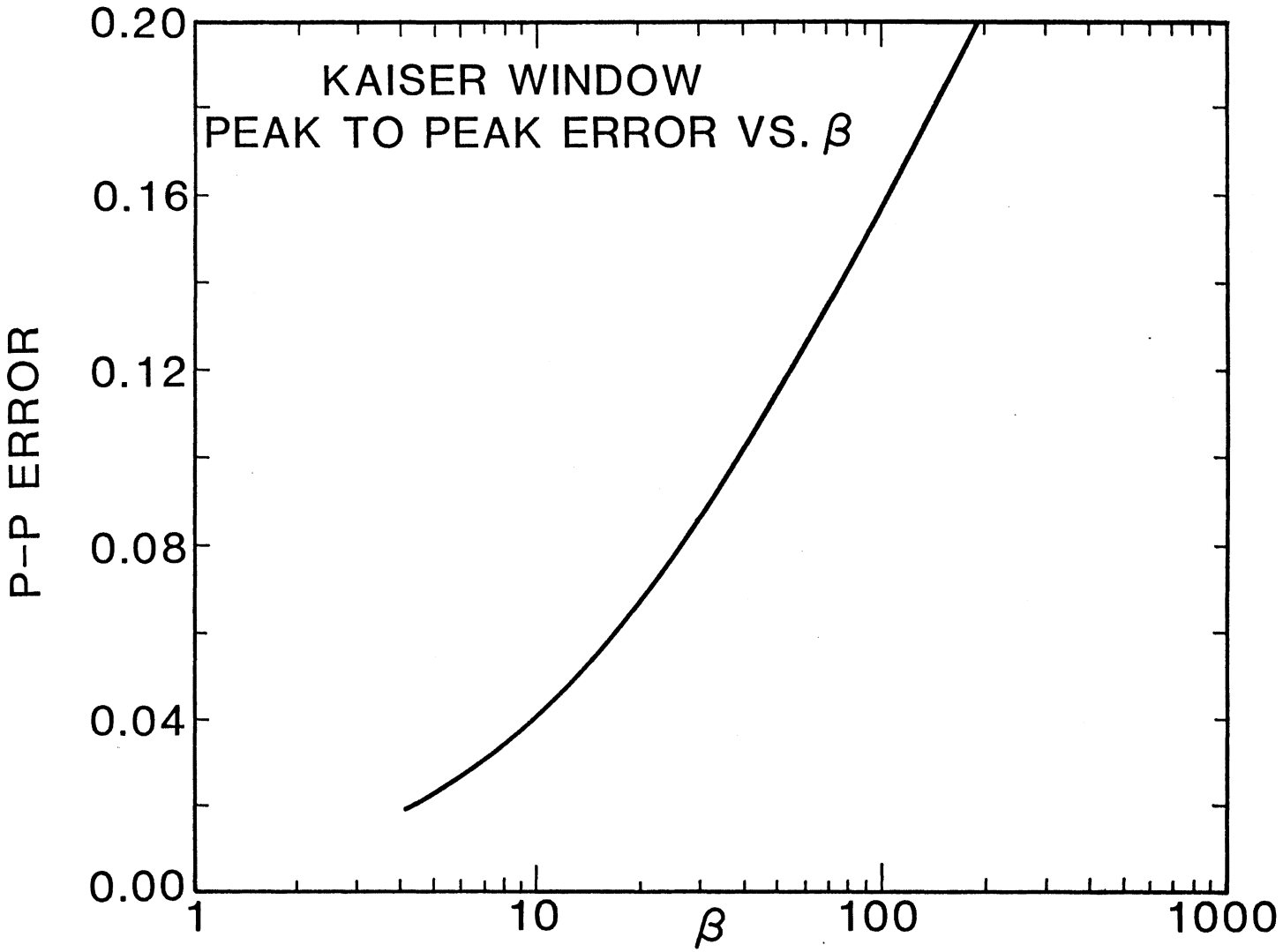

Figure 10. Kaiser Window Performance: Peak-to-Peak Error Versus Beta

signal contributed by the segment being processed. This effect will cause performance to be gradually degraded with increasing beta. A conservative choice of beta will provide suitable sidelobe attenuation while still producing a relatively narrow window width and satisfactory performance. Of several types of windows that have been used to produce sample results, the Kaiser window gave consistently superior performance, although other windows with similar characteristics are likely to produce similar results.

Selection of Decimation Rate

The choice of the decimation rate, R, is also related to the choice of beta. The decimation rate specifies the number of points between the beginning of adjacent overlapping segments, and thus the number of overlaps at each point in the data. For example, a decimation rate of unity means that a new segment will begin at every point so that the number of overlaps at any point will be equal to the segment length. The decimation rate must be chosen for the analysis window being used so that when the overlapping windows are summed together, the result approximates a constant amplitude. Only if the decimation rate is unity will error introduced due to overlapping windows be zero. For other values, some small error will be introduced, although this error may be minimized by the proper choice of beta [42]. When the decimation rate is not unity the error may be characterized as a periodic variation of small amplitude which will be apparent in the summed windows. The decimation rate is typically specified as a fraction of the window width and depends on the type of window. For example, if beta is chosen to be 8.0 and the segment length is 128, the decimation rate may be calculated to be about 23 [42].

This is to say that there should be no more than about 23 points between the start of adjacent windows with beta chosen above. Values between one and eight are often chosen and will produce similar results if the segment length is adequate. Generally, only if the decimation rate is large will the error due to the overlapping windows be significant. The primary advantage of a decimation rate very near unity, other than error due to overlapping windows which approaches zero, is that the deconvolution filter may be changed more rapidly to account for gross changes in conductivity and more accurately approximate the actual induction log response. If the data does not vary rapidly, or if a single deconvolution filter is to be applied throughout the data, a larger decimation rate may be justified since some of the advantages of a low decimation rate are not required. Calculation time may thus be reduced with little loss of accuracy.

Numerical Error

Also of interest is the error introduced by finite precision arithmetic on a digital computer. On a typical computer there are only about seven digits of precision. If the decimation rate is unity and the segment length is M, there will be M additions to form each point in the deconvolved result plus the operations required to perform the convolution on each segment. This latter number may be quite large if the segment length is long or if spatial domain convolution is performed instead of Fast Fourier transforms. Thus, there may be numerical errors due to the large number of operations. Increasing the decimation rate will help to reduce the error by decreasing the number of additions to form each point. Unfortunately if the decimation rate is increased too much, error

due to the overlapping windows will be introduced.

Selection of the Deconvolution Filter

Proper choice of the deconvolution filter is also of importance. Since this research is not concerned primarily with modeling the induction log, it must be assumed that a reasonably good model for the induction log vertical response exists and is available. As indicated earlier, the ultimate accuracy of this method and others depends upon the quality of the system response model used to perform the deconvolution. If one does not understand the convolution process, the corresponding deconvolution process becomes considerably more involved. Fortunately, the deconvolution problem does not seem to be terribly sensitive to small perturbations in the system model, although all modeling errors will be transferred to the result. Computer simulations using truncated vertical response functions of differing lengths have shown only a small error. The error between a long vertical response function of length 127 and the same response truncated to 31 points has been measured in terms of the difference between the area under the curves as well as in terms of absolute error. In both cases an error of less than 1% was observed. The area under the truncated curve is approximately 0.6% greater than with the original function. The absolute sum of the coefficients of the truncated response is about 0.9% less than with the original function. The majority of the error introduced during deconvolution with WOAC is the result of a shift in the average level of the deconvolved signal due to the slight difference in gain noted between the truncated filter and the original filter. An induction log response of 31 points appears to be adequate to model the tool response. Assuming a six inch sampling

interval, a 31 point response represents a response which extends seven and one-half feet above and below the tool. Slightly more accurate results have been obtained using a 63 point or a 127 point response at the expense of increased computation.

In the case of a non-time-varying system response, the errors associated with the system model will be relatively easy to follow. When a suite of system response characteristics is used with the adaptive implementation, the actual effect of the errors in the model used to generate the several deconvolution filters will be much more difficult to predict. In either case, since an overlap-addition approach is being used, errors and noise introduced by discontinuities in the data will be spread over the length of the convolution for the segment containing the discontinuity. This may be advantageous since the often large error which may be encountered at a discontinuity is distributed over the entire convolution length producing a smaller error at any given point. This characteristic does have one unfortunate consequence. Since the processing proceeds sequentially from segment to segment and overlap-addition convolution is performed, the errors due to a discontinuity will usually be spread in the direction the processing is moving and not uniformly around the discontinuity. Thus errors will not usually remain centered around a discontinuity, but will be spread forward in the spatial domain since the length of each deconvolved segment is greater than the original segment length in most cases. It is possible that this characteristic may not be acceptable in some applications. However, this is one compromise which must be made in order to implement deconvolution using this segmented approach.

Choice of Segment Length

There is one more important item to note regarding the actual implementation of WOAC. The segment length must be chosen properly to avoid aliasing problems. The segment length chosen in the deconvolution process must be at least twice the length of the deconvolution filter to assure adequate sampling for the short-term spectrum. This ensures that the effects of the original convolution can be adequately represented in the Fourier transform domain. If the segment length is L and the filter length is M, the length of each convolution performed must be at least L+M-1 points. This also applies to Kalman filtering and L_1 filtering except that at least L+M-1 points are required to produce each result of length L. It is often desirable to increase the segment length still further to produce better results. Although the theoretical lower bound on the segment length is twice the filter length, performance may continue to increase significantly until the segment length is four times to as much as eight times the filter length. Performance may be compared based upon signal to noise ratio. A measure of signal to noise ratio (SNR) may be defined as

$$SNR = \frac{E[x^2(n)]}{E[e^2(n)]} = \frac{\sum_n x^2(n)}{\sum_n (x(n)-\hat{y}(n))^2} \tag{5.1}$$

where x(n) represents the desired signal and e(n) represents the error which is the difference between the desired signal and the processed signal. Signal to noise ratio is often expressed in dB units as

$$SNR(dB) = 10 \log_{10} (SNR) \tag{5.2}$$

Figure 11, a plot of SNR versus segment length, illustrates how performance based on SNR increases as segment length increases for Wiener filtering. A 31 point filter response was used and 2 mmho standard deviation additive white Gaussian noise was present in the data being deconvolved. No recursive median filter was applied as a postfilter. Note the rapid degradation in performance as the segment length approaches the theoretical minimum at approximately 64 points. Conversely, the performance appears to approach an asymptote at approximately 47 dB as the segment length increases. Referring to Figure 11 it can be seen that most of the improvement has occurred when the segment length is 128, and performance ceases to increase by the time the segment length reaches 192 points or about six times the filter length. As will be demonstrated later, the basic shape of this plot does not change as the amount of additive noise is changed although the relative level of performance is a function of the additive noise.

Application of WOAC to the Induction Log Problem

The discussion up to this point has revolved around the development and use of WOAC in a general sense. The particular application of WOAC to deconvolution of the induction log is the principal goal of this research. As has been briefly mentioned earlier, several of the advantages of this weighted and segmented approach allow deconvolution to partially account for nonlinear effects present in the data if these effects can be approximated with a piecewise linear model. Especially useful are the ability to process the data in small segments using a fixed vertical response characteristic over each segment and the ability to overlap these segments during reconstruction so that any change in

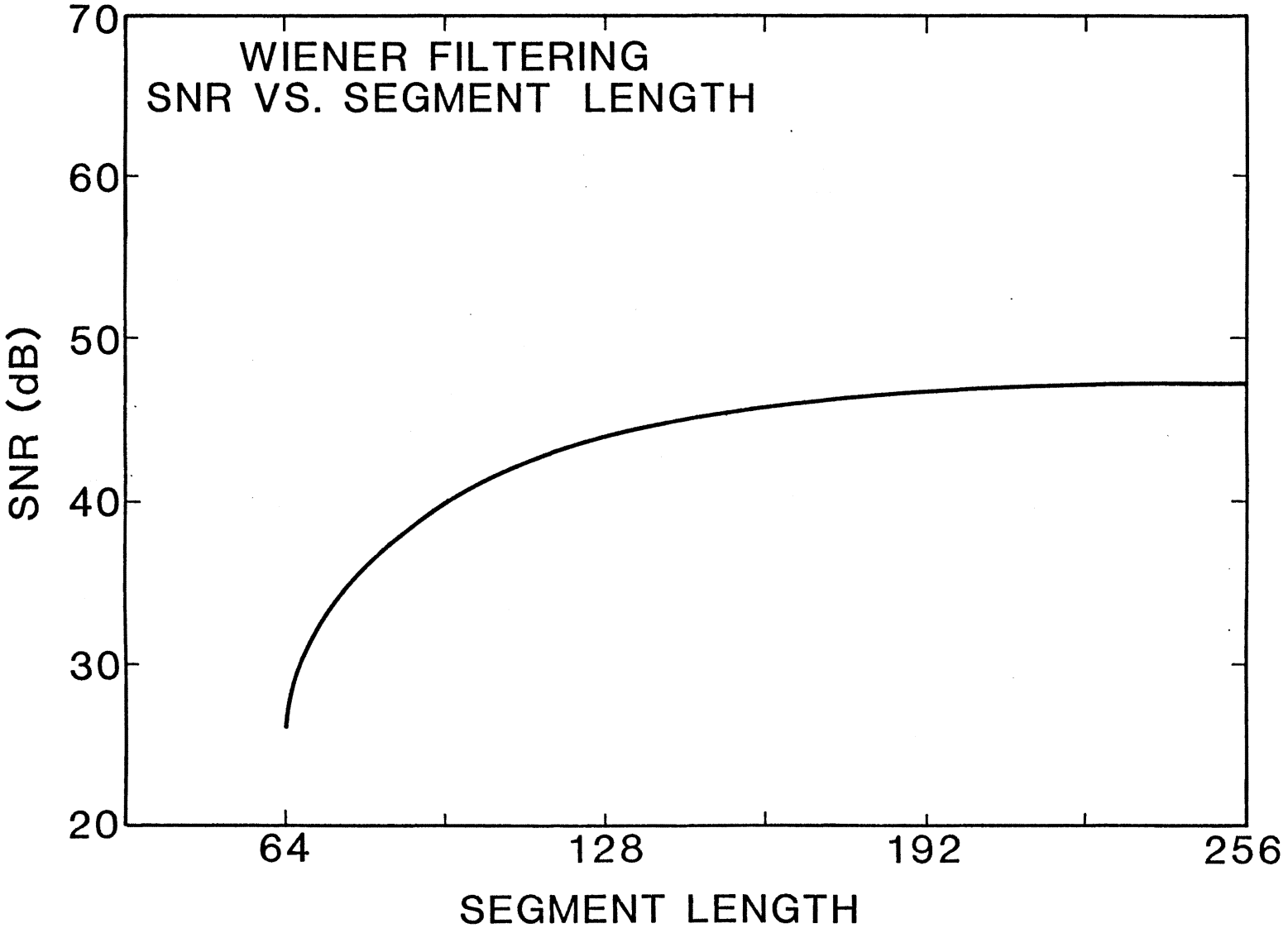

Figure 11. Wiener Filter Peformance: SNR Versus Segment Length

the vertical response is averaged into the result. These features, in particular, contribute to the usefulness of this procedure.

Two general cases exist which influence deconvolution of the induction log. If the induction log data is of relatively low conductivity, less than about 0.5 mho/meter, then the primary advantages of WOAC are reduced or lost. In this case, the induction log response does not vary significantly due to changes in the formation conductivity so the adaptive aspect of WOAC is of little use. There is some disagreement in the industry as to where the nonlinear effects become important to model. Many researchers consider the induction log to exhibit little nonlinear distortion due to skin effect when the conductivity is below the 1.0 to 0.2 mho/meter range. Unless it is necessary to process low conductivity data in small segments because of limited computer resources, the use of overlapping segments is inappropriate due to the number of calculations involved when compared to the level of benefits derived. Obviously, it may be impossible to process the entire data set at once. If computer resources are a limiting factor, then it may be appropriate to perform WOAC with a fixed response function, although the decimation rate probably should be raised as high as error will allow to decrease processing time. In the future, it may be possible to design special purpose hardware based upon WOAC so that real-time or near-real-time processing may be performed. In that case, WOAC would certainly offer advantages even if the response function were fixed.

The other case occurs when the data to be processed does contain areas of conductivity higher than that specified above. In this case it may be beneficial to partially account for the nonlinear distortion introduced due to skin effect. This correction may only be obtained if

the adaptive implementation of WOAC is applied. The adaptive application of WOAC involves the calculation of a suite of approximate vertical response characteristics which have been calculated to represent the actual induction log vertical response under certain conditions. The size of the suite normally used in this implementation is five, although higher accuracy could be achieved if a greater number were used. One method of constructing the suite of filter responses is to calculate each response for an infinite, homogenous region of specified conductivity using the integral equations given previously to describe the induction log in a homogeneous region. A response calculated in this manner can in some way approximate the actual induction log response when the instrument is located in a formation of the same average conductivity as that specified. Several responses may be calculated using this procedure so that a range of average conductivity values is approximated. As the data is being processed by WOAC, a measure of average conductivity for each segment may be computed. In particular, the average conductivity may be calculated from the apparent conductivity values near the center of the segment under analysis. Based upon this measure, the appropriate response may be chosen from the suite of previously calculated response functions. The selected response may then be applied to perform the actual deconvolution using the desired deconvolution method.

The calculation of the suite of response functions and the choice of the particular response function to apply for each segment are not well defined. It seems possible that a set of optimized choices could be made regarding these decisions; however, in the implementation which produced the results included in the next chapter no special procedure was used. The suite of vertical responses was calculated based upon an

arbitrary choice of conductivities for the infinite regions. The vertical responses may be found by solving Equation (2.17) numerically and fixing the conductivity. The conductivities were simply chosen to cover the range of values expected in normal operation, except that the responses were weighted toward the higher conductivity regions since these responses change faster. Also, since the system response becomes virtually constant once the formation conductivity decreases below about 0.1 mho/meter, system response functions for very low conductivities were not included. Further research to optimize the choice of vertical response functions might prove valuable for improving performance.

CHAPTER VI

APPLICATION OF WOAC TO DECONVOLUTION OF THE INDUCTION LOG

Using the information presented in the previous chapters, it is not too difficult to implement WOAC for a particular data sequence. This chapter contains examples of deconvolution performed on induction log data using WOAC with Wiener filtering, constrained least squares filtering, Kalman filtering, Jansson's method, L_1 filtering, and successive approximation. The implementation follows the suggestions and guidelines presented in the previous chapter. Several types of induction log data are deconvolved. These include two examples of ideal synthetic induction log data without skin effect, a segment of real induction log data, and a segment of synthetic induction log data with skin effect. Deconvolution is performed with the first two types of data using WOAC nonadaptively, while the last type is deconvolved using WOAC applied in an adaptive fashion. The synthetic data includes additive zero-mean, Gaussian white noise. Examples are provided with a range of noise variances to demonstrate the performance of WOAC in the presence of realistic amounts of noise. Performance is also demonstrated with respect to segment length and filter parameters, wherever possible.

The data sequences used in the examples which follow were generated by several sources. The ideal synthetic data without skin effect was generated using a simple convolutional model for the induction log. An

ideal formation consisting of two very wide beds with a relatively narrow bed in between was chosen. The side beds were assigned a conductivity an order of magnitude greater than the center bed so that the smoothing effects of the induction log would be emphasized by the large contrast between the beds. The data was properly sampled so as to minimize the effect of the discontinuity existing at each bed boundary of the center bed. The ideal data was tapered at each end of the sequence to attenuate any noise due to the discontinuities which exist there. The taper was applied using a cosine taper (Tukey) window covering the first and last 16 points of the data. The ideal data was convolved with the vertical response of the induction log calculated for an arbitrary conductivity to simulate the actual logging operation. The gain of the vertical response was normalized to unity for simplicity when skin effect was not considered. The vertical response for the forward operation was calculated with length 127 to reduce numerical errors which might be introduced by a truncated version of the response. A response of this length represents one which extends for about 32 feet above and below the center of the instrument. The response of the tool is essentially zero at these extremes. Zero-mean Gaussian white noise was added to the convolved log so as to simulate additive noise which may corrupt real data. Not modeled is noise which may be present due to cable stretch, tool eccentricity, non-uniform sampling, etc. The noise was generated by a pseudorandom number generator using either the Box-Muller transformation [46] or the central limit theorem. Examples were run using additive noise with standard deviations between 0.05 mmho/meter and 10 mmho/meter. A standard deviation of about 1 mmho/meter is considered "typical" for induction log data. This basic procedure was used to form the synthetic

data described below.

Two slightly different ideal formations were used to generate the ideal synthetic data without skin effect. The first was chosen to have a center bed of 20 samples thickness, and the second was chosen to have a center bed of 4 samples thickness. These represent beds of 10 feet and 2 feet thickness, respectively. The center bed in the former example was wide enough so as not to be badly distorted by the convolution. The center bed in the latter example was so narrow as to be severely distorted both in magnitude and width. These two sets of synthetic data will be referred to as case I and case II, respectively, in the examples which follow. The data have lengths of 322 points and 306 points, respectively. Figures 12a-c and 13a-c show the original data, the convolved data with additive noise, and the absolute error due to the convolution for case I and case II, respectively. The error introduced by convolution of the original data with the induction log vertical response was found to produce a SNR of 29.6 dB for case I and 20.8 dB for case II. These two ratios will provide a base for comparison of the filtering methods applied to these two cases.

The second data which was available was a segment of synthetic induction log data calculated including skin effect. The data was generated with a finite difference or finite element model and contributed by ARCO Oil and Gas Company. The tool model was again a 6FF40-type based upon, but not identical to, the Schlumberger model for the tool. Complete information describing this data was not available so the deconvolution filter applied in the examples can only be considered a rough approximation to the original tool response which generated the data. In addition, the data as received was of insufficient length to allow

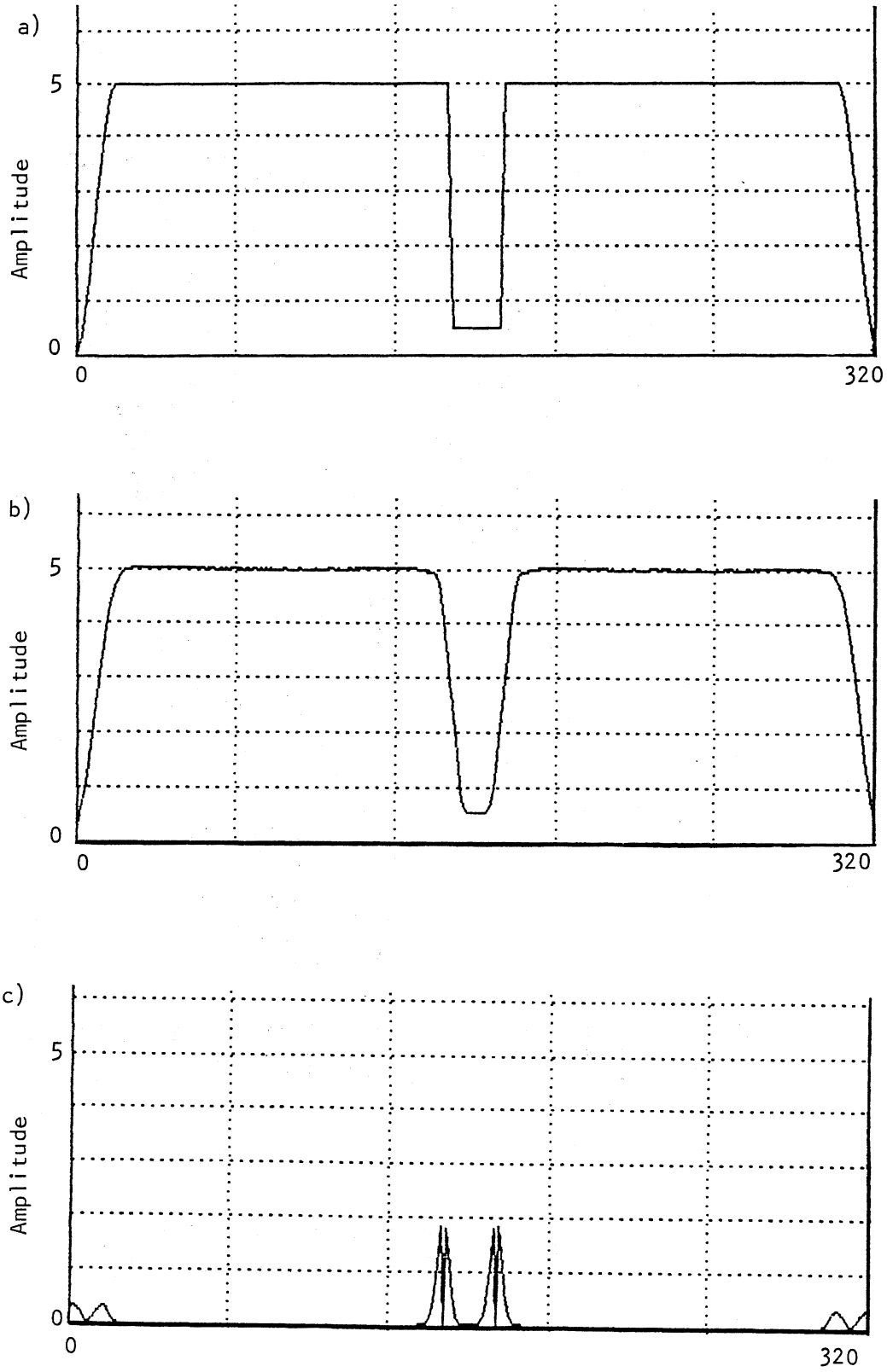

Figure 12. The Data of Case I. a) Original Data, b) Convolved Data, c) Absolute Error

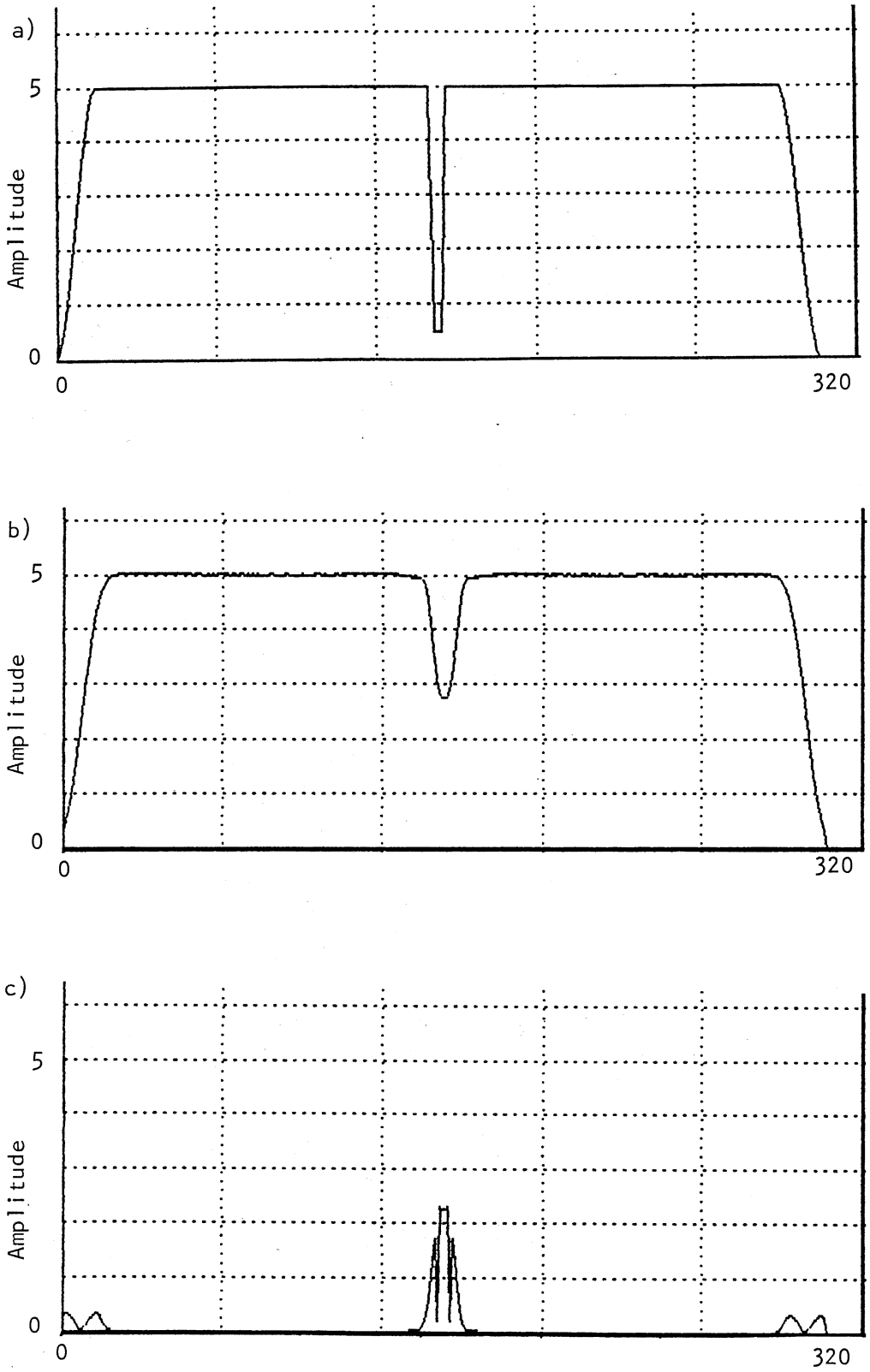

Figure 13. The Data of Case II. a) Original Data, b) Convolved Data, c) Absolute Error

adequate assessment of the performance of WOAC at the segment lengths required. The data was extended to almost four times its original length by padding the endpoints and reflecting and adding the padded sequence to itself. This resulted in a length of 402 points, representing about 201 feet of data. Proper sampling was used at the discontinuities to reduce errors. Noise of 1 mmho/meter standard deviation was added to the data to simulate real data. Figures 14a-c show the ideal data, the data generated including skin effect and additive noise, and the absolute error due to the convolution. The SNR of the synthetic data with skin effect was calculated to be 19.1 dB, which is the figure to be used for later comparison.

A segment of real induction log data contributed by Mobil Corporation was also used to study deconvolution. As with the previous data, the real data was tapered at each end for 16 points to reduce the end effects. Since the data was actually generated by a 6FF40-type induction instrument no noise was added. The real data as used in the examples is shown in Figure 15. This data was used primarily to show undesirable effects that might be introduced by WOAC during deconvolution of nonideal data either due to noise present in the data or modeling errors.

Several vertical response characteristics were calculated for use in the examples. A total of five were calculated for use in the adaptive case and one was chosen from the group for the nonadaptive cases. Each vertical response was calculated numerically for an infinite homogeneous region of specified conductivity. Shown in Figure 16 is the suite of five vertical responses calculated for homogeneous regions of 5, 2, 1, 0.5, and 0.2 mho/meter conductivity, from left to right. These responses were calculated with length 31 in contrast to the long filter used to

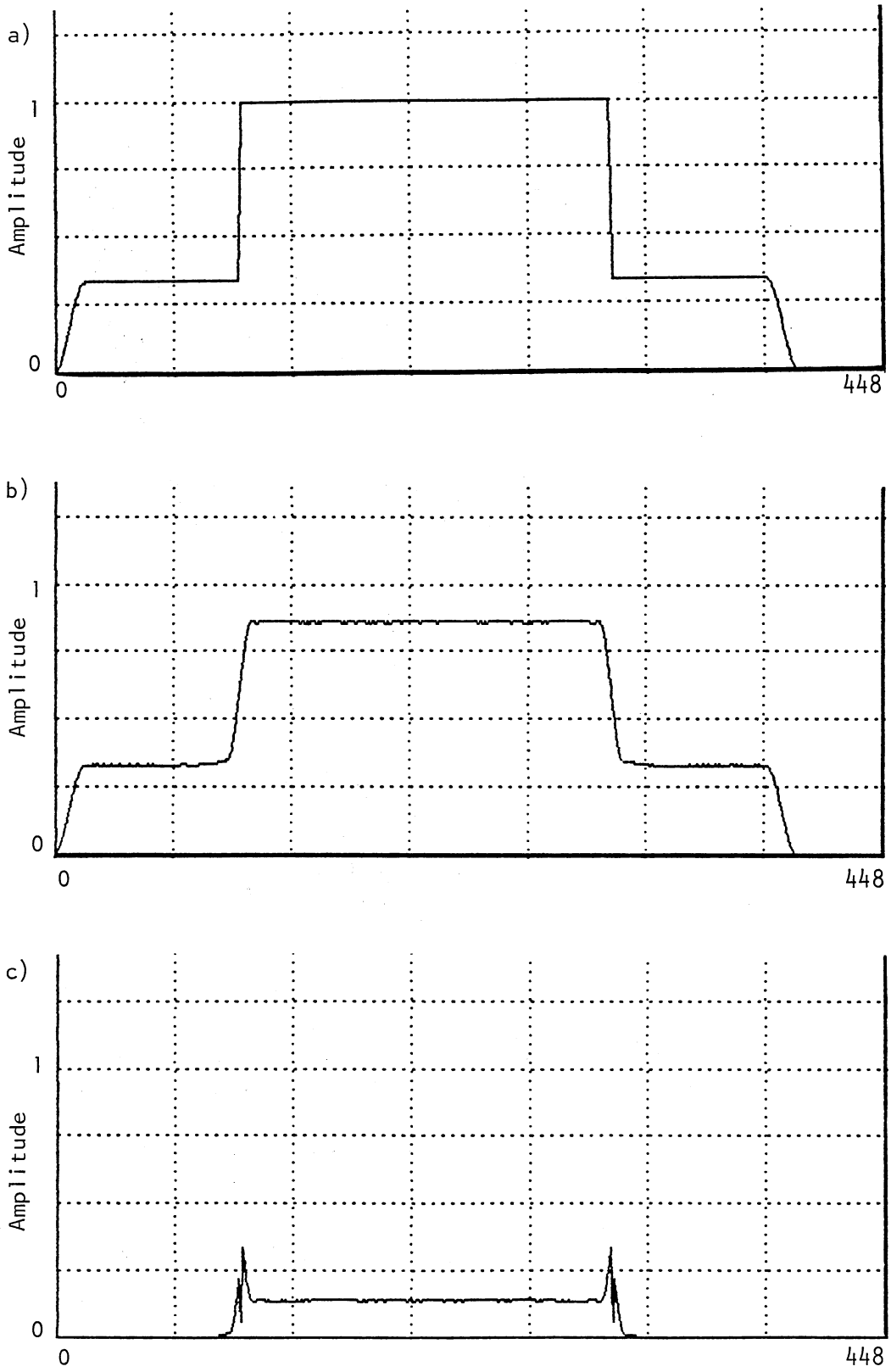

Figure 14. Synthetic Data With Skin Effect. a) Original Data, b) Convolved Data, c) Absolute Error

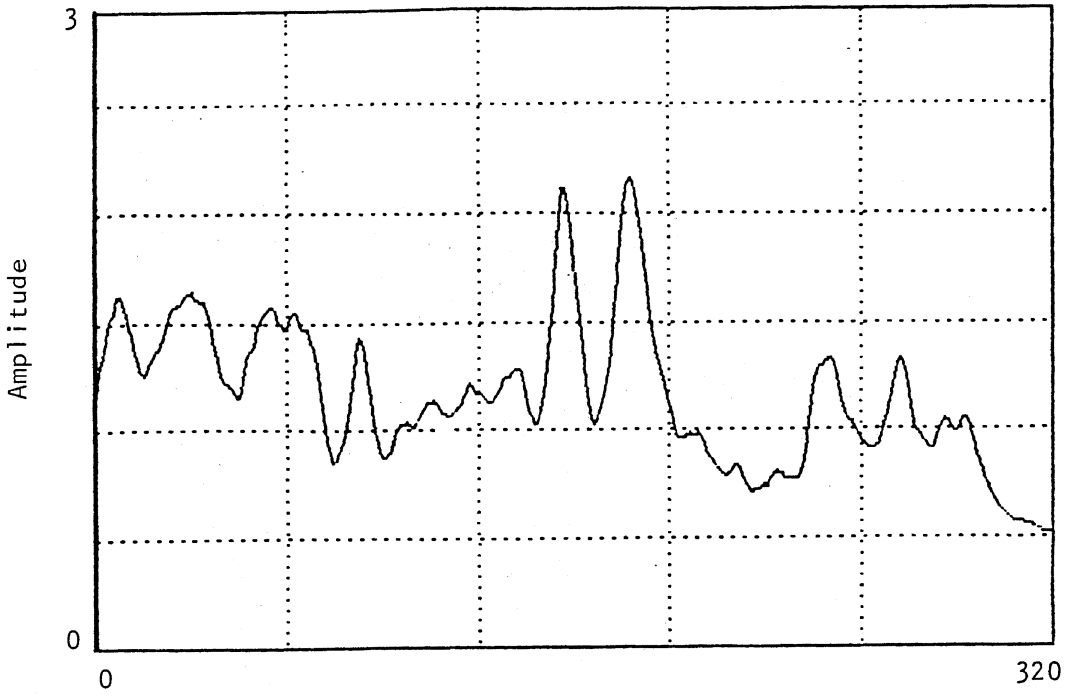

Figure 15. A Segment of Real Data

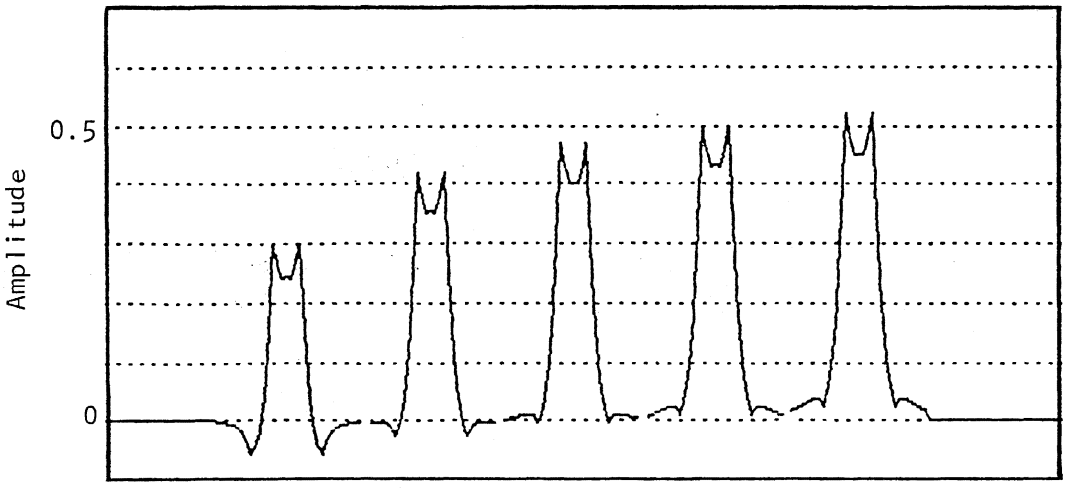

Figure 16. A Suite of Five 6FF40 Vertical Response Characteristics Calculated for Conductivities of 5.0, 2.0, 1.0, 0.5, and 0.2 mho/Meter

generate the ideal synthetic data described earlier. This was done since the exact vertical response will rarely be known and truncation effects are inevitable. The center response function, generated for 1 mho/meter conductivity, was applied when skin effect was not considered.

Some of the nonlinear effects present in the induction log are clearly evident in the suite of responses in Figure 16. It is interesting to note the manner in which the vertical response changes due to a change in gross formation conductivity. The spatial response of the induction log can be seen to change both in general shape and area under the curve. This implies that the spectral response of the filter will change as will the gain. Figures 17 and 18, respectively representing the vertical response spectra calculated for conductivities of 5 mho/meter and 0.2 mho/meter, illustrate the spectral changes which occur as conductivity varies. Although the general shape of the two spectra is similar, there are numerous differences, particularly in magnitude, between them. It should be noted here that not all nonlinear dependencies are modeled by the vertical responses shown. In particular, the response is forced to remain symmetric which is not necessarily the case with a real device.

An interesting aspect of short-term analysis and synthesis is the effect on the short-term spectrum of passing a discontinuity through the analysis window. Figure 19a-b shows a windowed data segment and its Fourier spectrum. The arbitrary segment of continuous data has length 128 and was windowed by a Kaiser window with beta equal to 8.0. The data in this case was constant so the spectrum is just the spectrum of the Kaiser window. Figure 20a-b shows a windowed data segment and its Fourier spectrum except that the segment has a small discontinuity inserted

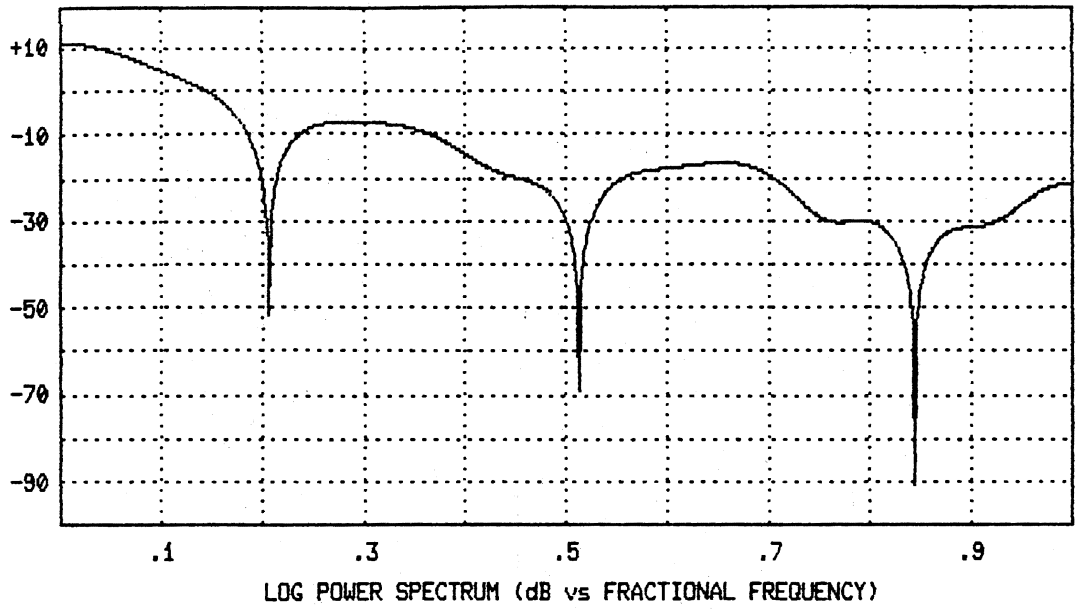

Figure 17. Spectrum of the Vertical Response Calculated for 5.0 mho/Meter Conductivity

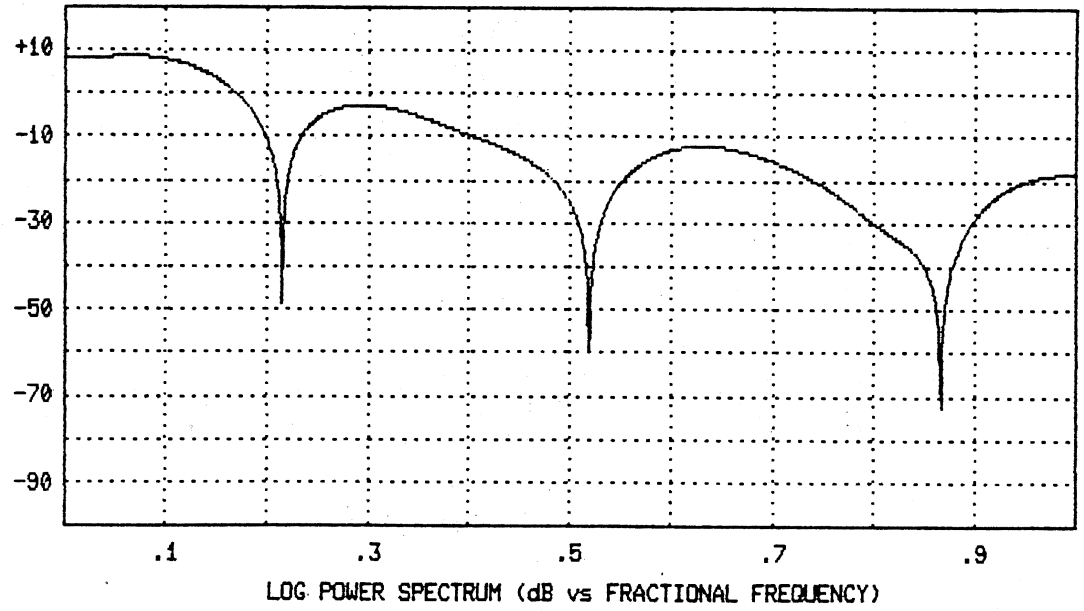

Figure 18. Spectrum of the Vertical Response Calculated for 0.2 mho/Meter Conductivity

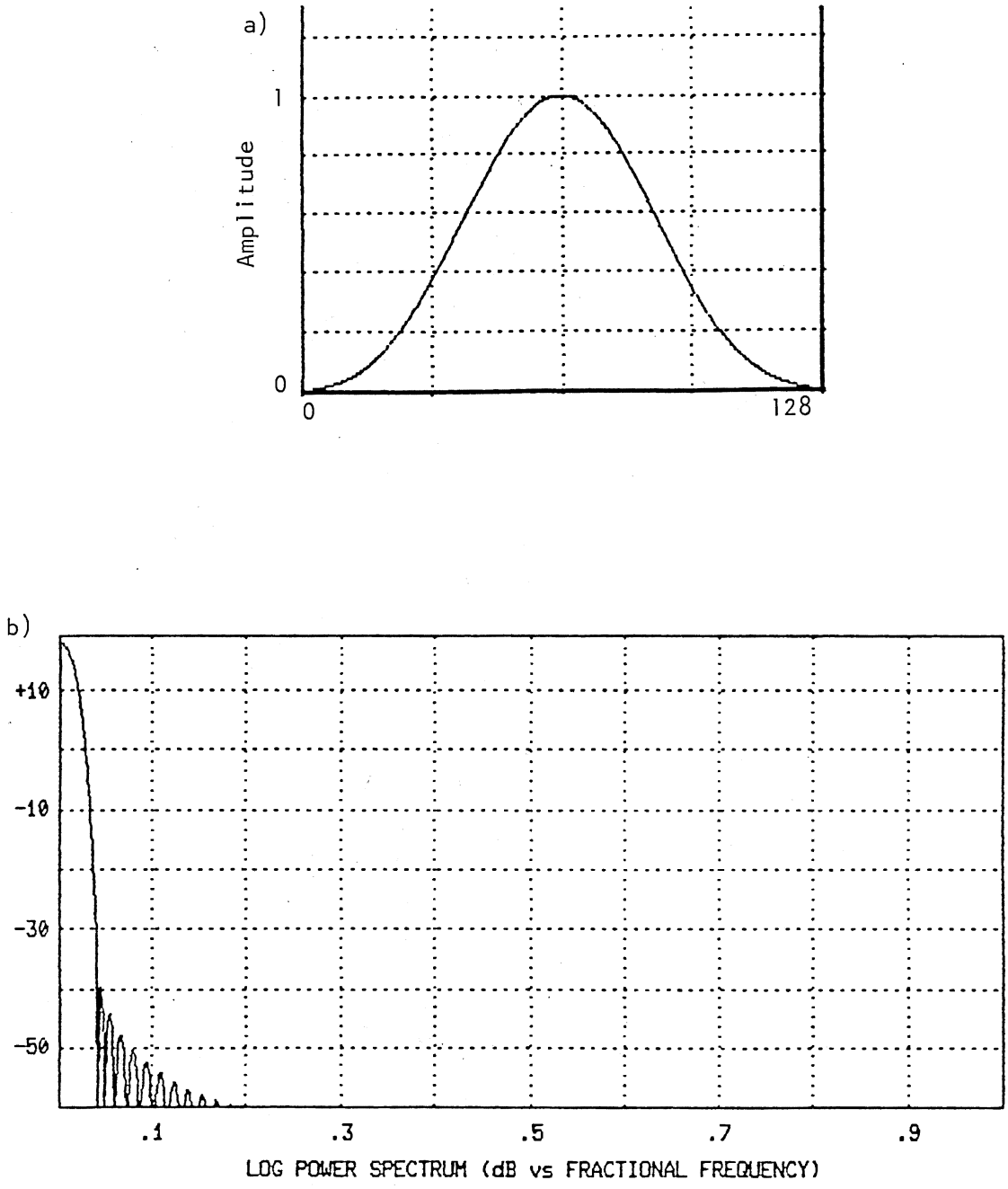

Figure 19. A Windowed Constant Amplitude Data Segment. a) The Data Segment, b) The Spectrum of the Segment

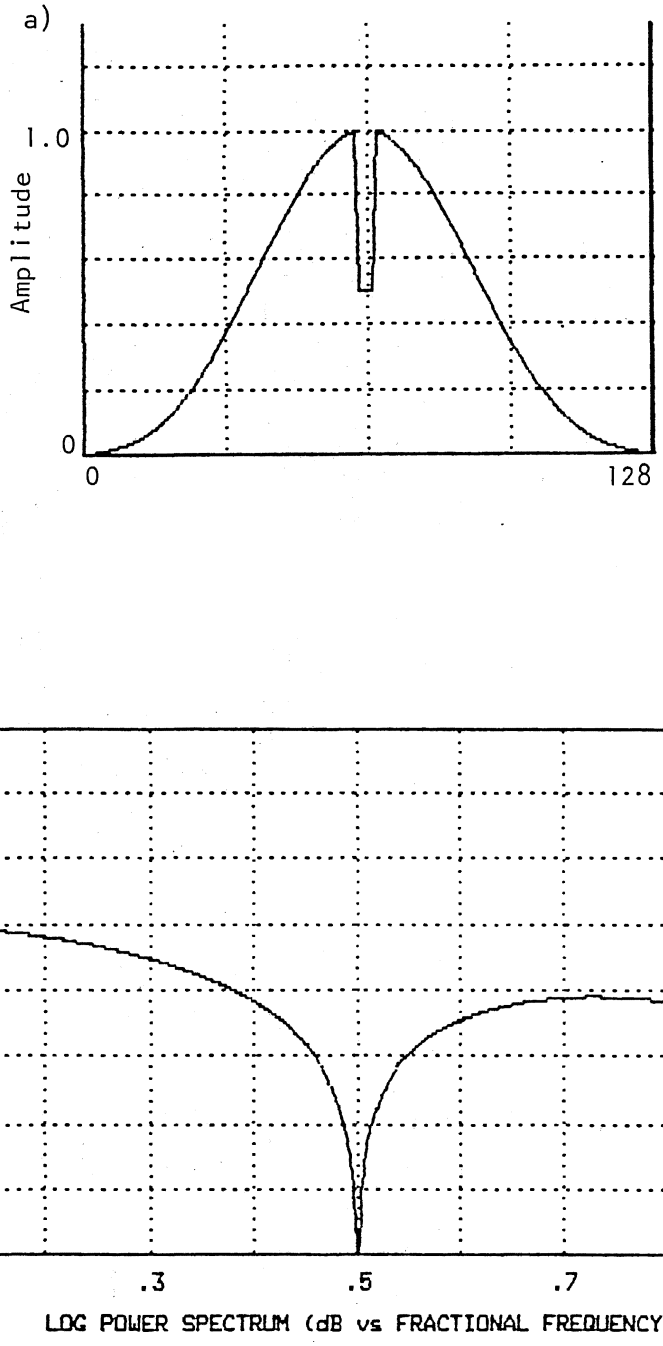

Figure 20. A Windowed Discontinuous Data Segment. a) The Data Segment, b) The Spectrum of the Segment

near its center. This could be considered to be a worst case condition for locating a discontinuity in a segment since, due to the windowing, the discontinuity is emphasized when it is located near the center of the segment. If convolution is being performed, no problem will exist since the high frequency information will be smoothed by the low-pass system response. On the other hand if deconvolution is being performed, the added high frequency information will be amplified by the deconvolution filter response. It is this process which produces the increased noise and ripples near discontinuities when deconvolution is performed with WOAC. If the discontinuity is replaced by a less severe variation in the smoothness of the data, there will be less high frequency information present in the spectrum and the problem will be less severe. This is the case normally encountered. The windowing operation deemphasizes less smooth sections of data as these areas move away from the center of the window. This lessens the distortion that would otherwise be introduced if the window were wider or had less sidelobe attenuation.

Presented in the following sections are results obtained with WOAC and the various filtering methods described earlier. Not all the methods are applied to all the test data due to obvious limitations associated with some of the methods. All the methods previously described are used with WOAC to deconvolve the two cases not including skin effect. Only Wiener filtering and constrained least squares are applied adaptively to the data including skin effect due either to poor performance or excessive calculations by the other methods. These two methods adequately illustrate the performance of WOAC applied adaptively. In all of the cases illustrated below, results are also presented with postfiltering using a 3 point or a 5 point recursive median filter to attenuate ampli-

fied noise. After the results have been presented for each of the methods, the individual results will be compared and summarized.

Wiener Filtering

Wiener filtering is one of the easiest and also one of the most effective deconvolution methods applied here. The implementation of WOAC with Wiener filtering is made assuming the ratio, K, of the noise to signal power spectral density is a constant as defined in Equations (3.11) and (3.12). The ratio was chosen to be an order of magnitude greater than the known noise variance. The segment length chosen for each example is 192, and the decimation rate was specified to be unity. The analysis window is a Kaiser window with beta set to 8.0.

Shown in Figure 21a is the deconvolution of case I performed with the conditions just described. The SNR of the deconvolved data is 58.7 dB without any postfiltering, an improvement of more than 29 dB compared to the synthetic data. Figures 21b and 21c are the deconvolved data after the application of a 3 point and a 5 point postfilter, respectively. A recursive median filter as described earlier was used. The resulting SNR after the 3 point postfilter was 72.2 dB, a 42 dB improvement; the SNR after the 5 point postfilter was about 74 dB, a 44 dB improvement. The three results represent enormous improvements over the base level of about 30 dB. The center bed has been virtually restored to its correct shape and magnitude and the additive noise has not been amplified excessively. Noise and ripples due to the response of the method to the discontinuity are present, but not to an objectionable level. Note that since an overlap-addition procedure is used, the noise is not symmetric about the discontinuity in the results.

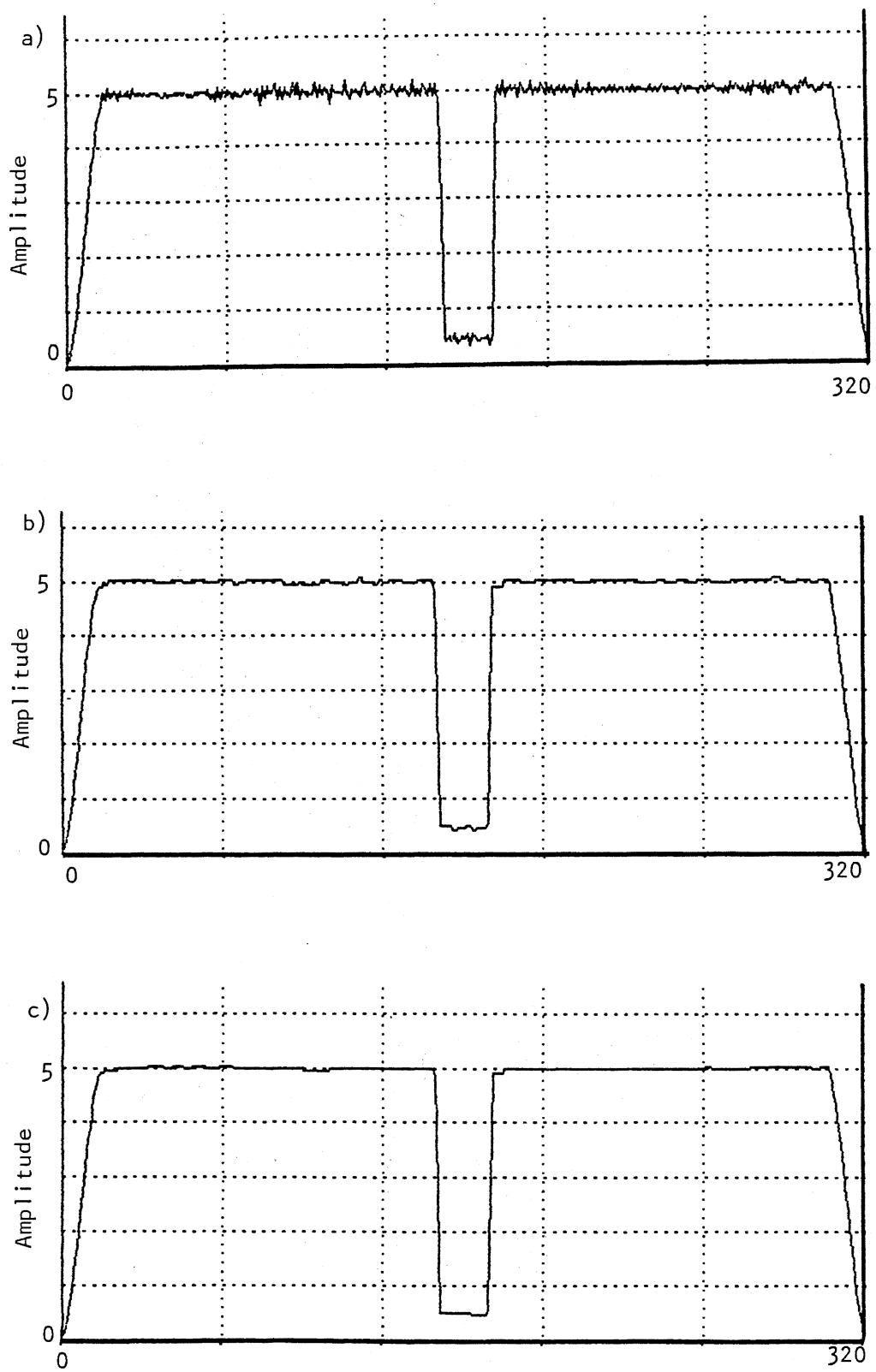

Figure 21. Deconvolution of Case I With Wiener Filtering. a) Without Postfiltering, b) With 3-Point Postfilter, c) With 5-Point Postfilter

Figure 22a illustrates the deconvolution of case II under the same conditions as before. This result is not quite as good as before due to the center bed presenting a more severe discontinuity to be restored. This decrease in performance is characterized by increased ripple present in the amplified additive noise of the result. The SNR of this example is about 49 dB which is still a significant improvement of about 28 dB over the synthetic data. Given in Figures 22b and 22c are the results of applying the same postfilters as before to the result. Postfiltering results in an SNR of about 57 dB for the 3 point operation and an SNR of about 61 dB for the 5 point operation. The overall improvements are about 36 dB and 40 dB, respectively. It should be clear by now that a significant improvement in performance may be achieved if the amplified noise is approximately white so that it may be substantially removed by postfiltering. With both case I and case II, the results are virtually identical to the original ideal data. The restoration with Wiener filtering followed by a properly chosen postfilter is nearly complete.

To provide evidence that Wiener filtering does not introduce extraneous features in the deconvolved data (other than the ripples which may be associated with the method's natural response to discontinuities), the deconvolved real data is given in Figure 23. The Wiener parameter, K, was estimated for this example by trial and error to provide a relatively smooth result. This is not a very elegant method of noise estimation; although, a "typical" value of K for real induction log data has been found to be about 0.005. Study of model estimation is a topic for further research. Examination of Figure 23 shows that the results appear reasonable given the real data in Figure 15. Each feature in the deconvolved data seems to have a close correspondence to a feature in the real

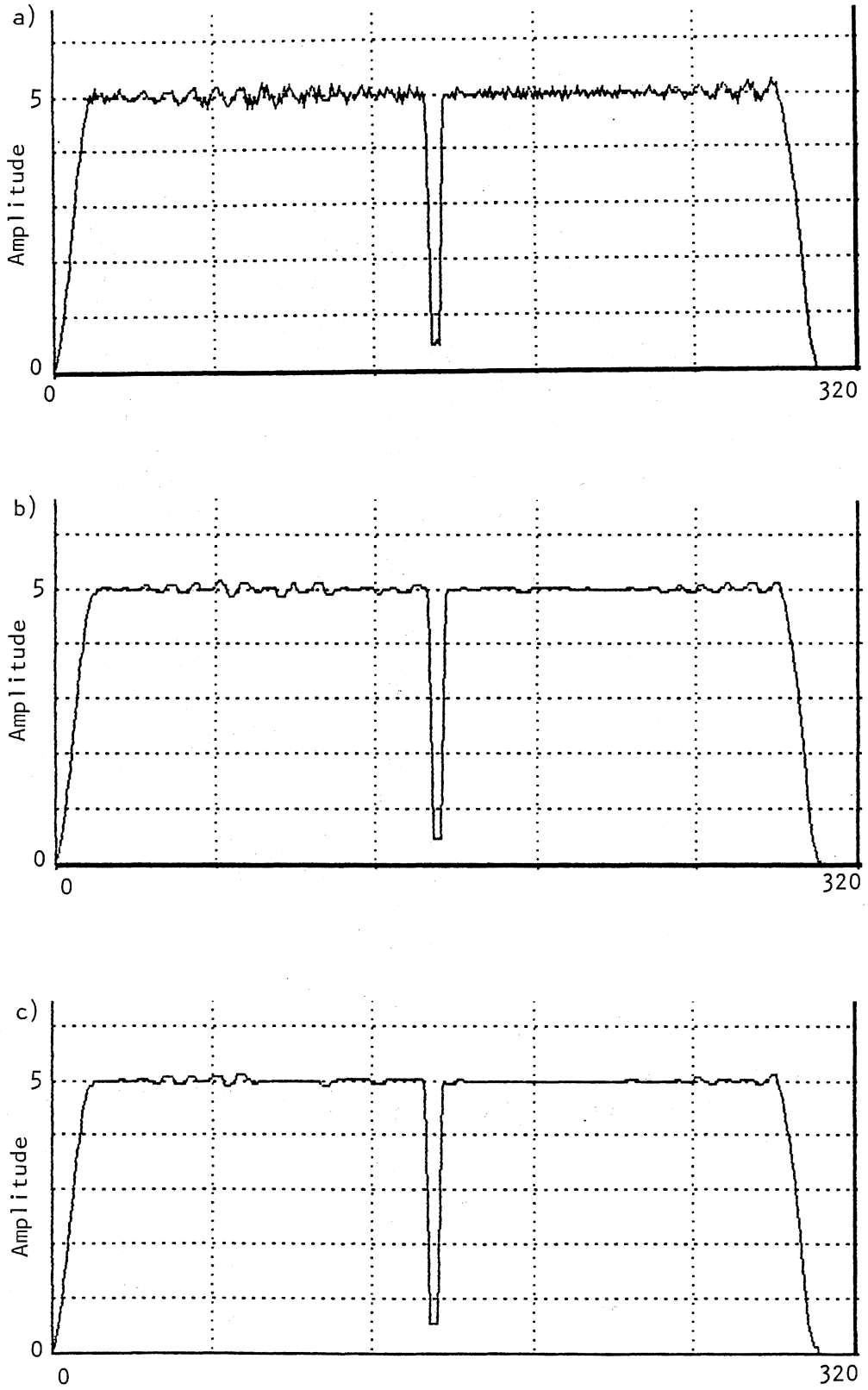

Figure 22. Deconvolution of Case II With Wiener Filtering. a) Without Postfiltering, b) With 3-Point Postfilter, c) With 5-Point Postfilter

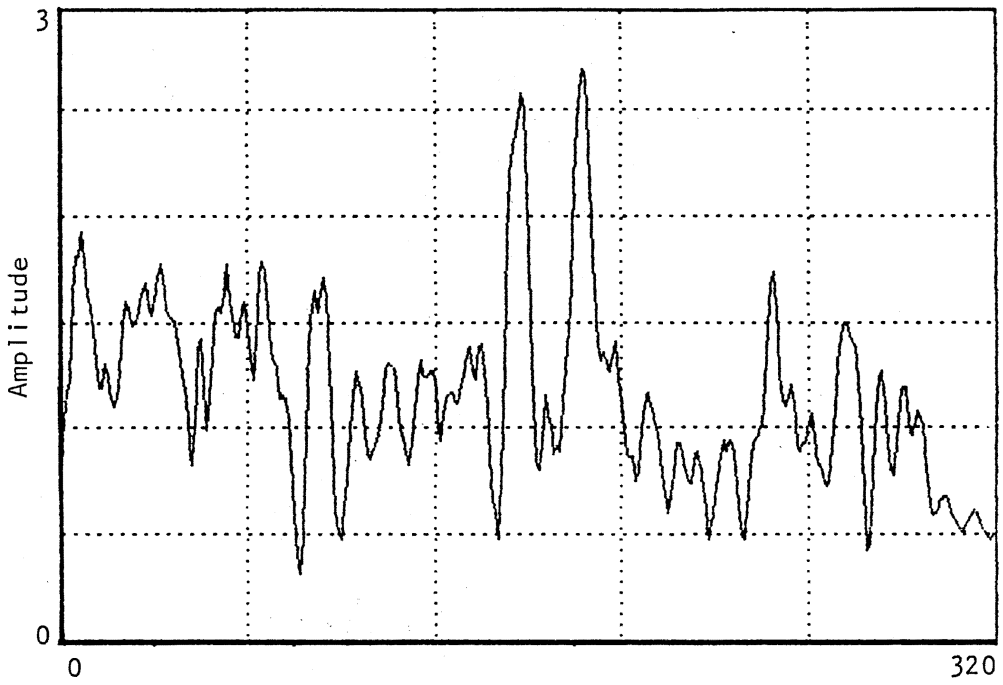

Figure 23. Deconvolution of Real Data With Wiener Filtering

data. Since only the apparent conductivity data is available, there is no method available for confirming that the answer is correct.

Shown in Figure 24a is the result of adaptively deconvolving the synthetic data with skin effect of Figure 14. WOAC was implemented with Wiener filtering and the suite of five vertical responses described above. Due to the range of data values, only three of the five responses were actually used to perform the deconvolution. The SNR of the result was calculated to be about 40 dB without postfiltering and approximately 49 dB and 55 dB after postfiltering with the 3 and 5 point postfilters, respectively. The results are shown in Figures 24b and 24c. The SNR of the original convolved data including skin effect and additive noise was slightly more than 19 dB. Thus, deconvolution and postfiltering resulted in improvements of about 21 dB, 30 dB, and 36 dB. Deconvolution was also performed nonadaptively resulting in a SNR of only about 18 dB, actually less than the convolved data. The decrease was due to large magnitude errors which were emphasized by the deconvolution. This example demonstrates well the advantages available if WOAC is applied adaptively. Since a partial correction is applied for both the data magnitude and data smoothness, a large increase in SNR is possible.

Constrained Least Squares Filtering

Constrained least squares filtering was implemented with WOAC in almost the same manner as Wiener filtering. The segment length was chosen to be 192 and the decimation rate was unity. The variance of the additive noise was assumed known as before. Constrained least squares filtering was applied to the same data as presented previously with Wiener filtering.

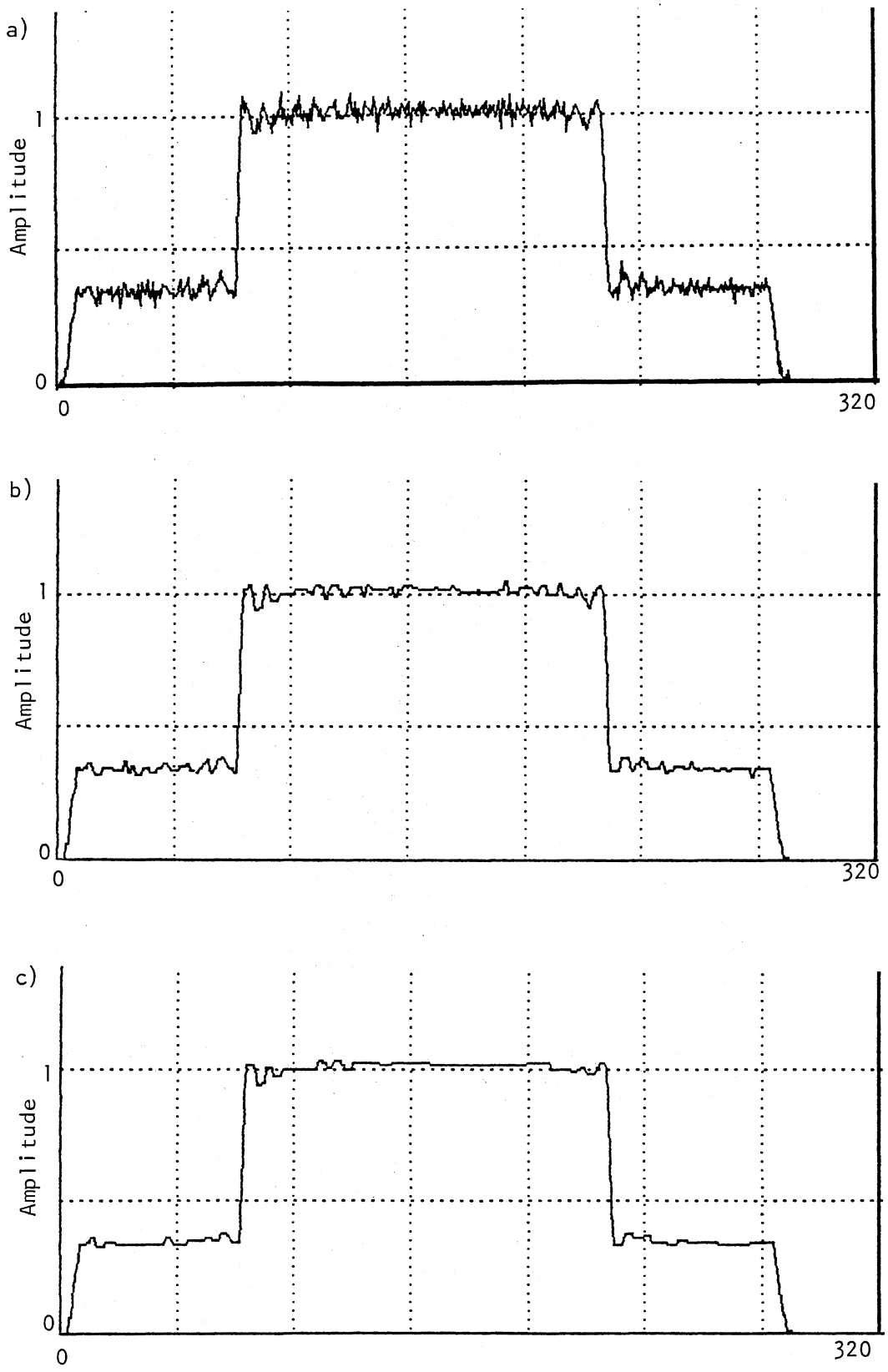

Figure 24. Adaptive Deconvolution With Wiener Filtering. a) Without Postfiltering, b) With 3-Point Postfilter, c) With 5-Point Postfilter

Case I was deconvolved to produce the result given in Figure 25. The SNR was calculated to be approximately 63 dB, an improvement of about 34 dB and an increase of about 4 dB over the corresponding SNR obtained with Wiener filtering. This is due in part to the smoothness constraint imposed on the result by the method and also on modeling errors. Additive noise is amplified to a smaller extent than with Wiener filtering. After postfiltering with the two recursive median filters, the SNR after each operation became approximately 65 dB and 67 dB, corresponding to improvements of about 35 dB and 37 dB compared to the synthetic data. These results are shown in Figures 25b and 25c, respectively. As before, the results are very good and virtually identical to the ideal data.

Figure 26a is the result of deconvolving case II using constrained least squares. Since the discontinuity was worse than in case I, the results should be expected to be poorer. This is confirmed by a calculated SNR of about 53 dB. After postfiltering, the results become as shown in Figures 26b and 26c. The SNR after the 3 point filter is about 54 dB and about 55 dB after the 5 point filter, an improvement of slightly more than 33 dB in each case. As with case I, the improvement due to postfiltering is small compared to the same operation following the application of Wiener filtering. The results of these first two examples seem to indicate that a better first result may be obtained with constrained least squares filtering and no postfilter; however, a better ultimate result may be obtained with Wiener filtering and the proper postfilter. This may be highly dependent upon the accuracy of the noise estimate.

Illustrated in Figure 27 is the deconvolved real data generated with constrained least squares. The same comments as were made earlier for Wiener filtering are applicable here. No spurious features seem to be

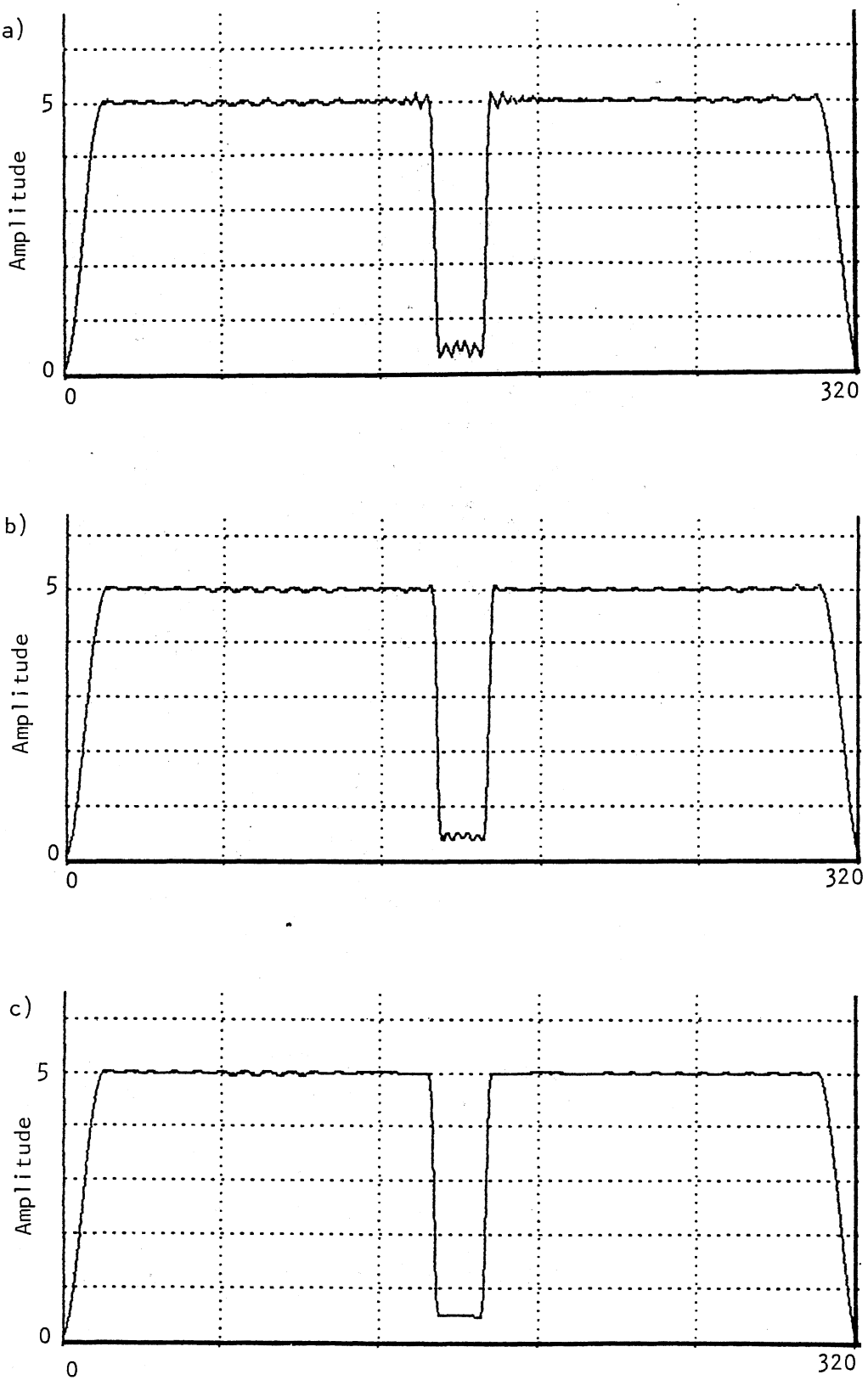

Figure 25. Deconvolution of Case I With Constrained Least Squares Filtering. a) Without Postfiltering, b) With 3-Point Postfilter, c) With 5-Point Postfilter

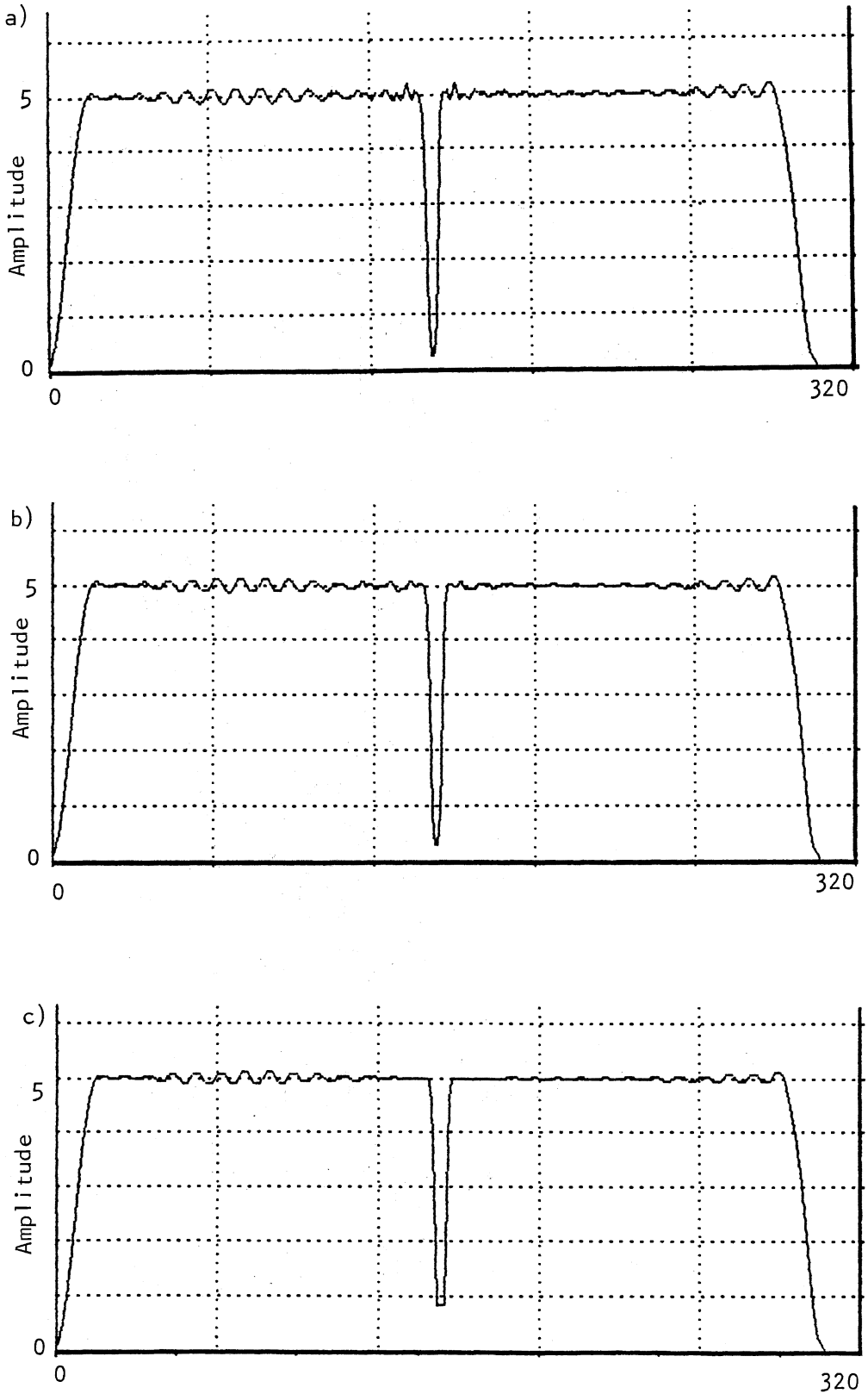

Figure 26. Deconvolution of Case II With Constrained Least Squares Filtering. a) Without Postfiltering, b) With 3-Point Postfilter, c) With 5-Point Postfilter

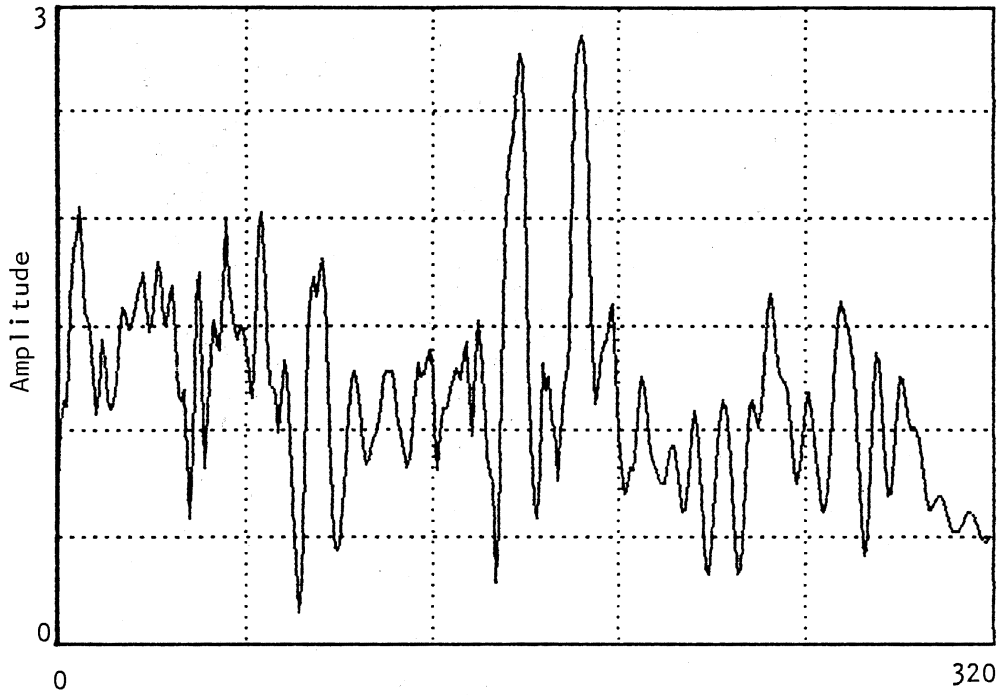

Figure 27. Deconvolution of Real Data With Constrained Least Squares Filtering

present, helping to confirm the performance of the WOAC procedure.

Given in Figure 28a is the result of adaptively deconvolving the synthetic data with skin effect using constrained least squares. The SNR before postfiltering was found to be about 51 dB, and was also about 51 dB after each postfilter indicating that there was very little amplified noise present in the data. This represents an improvement of about 32 dB compared to the synthetic data. These results, given in Figures 28b and 28c, are very much like those obtained from Wiener filtering. Again, the initial result with constrained least squares filtering is better than the Wiener filtered result, but the ultimate results are similar with Wiener filtering being slightly better.

Kalman Filtering

Kalman filtering was implemented to perform deconvolution with WOAC. The Kalman filtering algorithm was implemented as described earlier with the unknown statistical parameters generally estimated from the data to be deconvolved. The filter length was 31 and the segment length was again selected to be 192. The noise covariance was approximated as 0.01 mmho squared.

Deconvolution of case I with Kalman filtering produced the result shown in Figure 29a. The SNR was found to be slightly greater than 56 dB prior to postfiltering. After applying the two postfilters the SNR increased to slightly more than 58 dB and 60 dB, respectively. These represent increases of about 27 dB, 29 dB, and 31 dB when compared with the original synthetic data. The results are shown in Figures 29b and 29c. The restoration was not quite as complete as with the two previous methods.

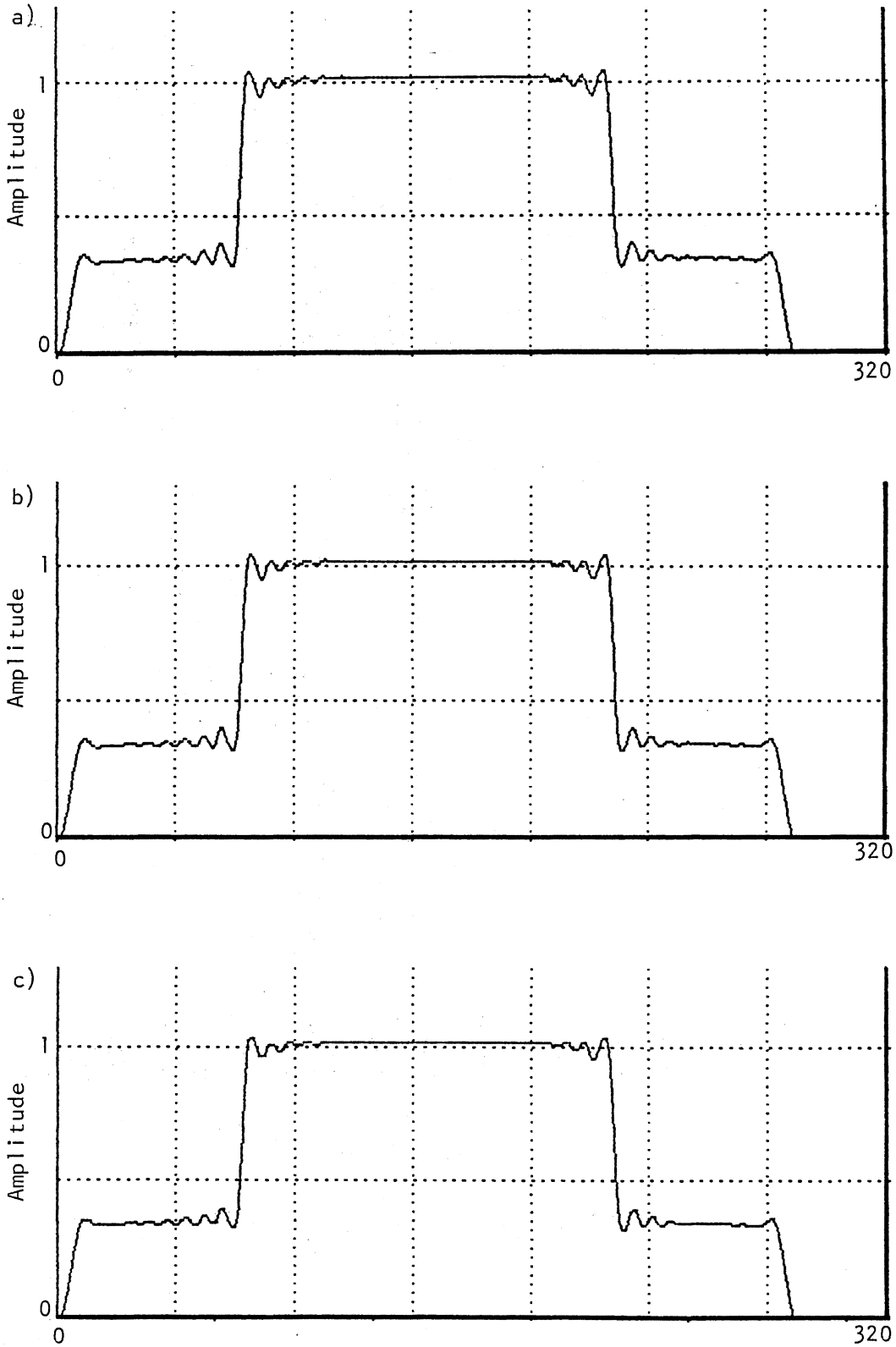

Figure 28. Adaptive Deconvolution With Constrained Least Squares Filtering. a) Without Postfiltering, b) With 3-Point Postfilter, c) With 5-Point Postfilter

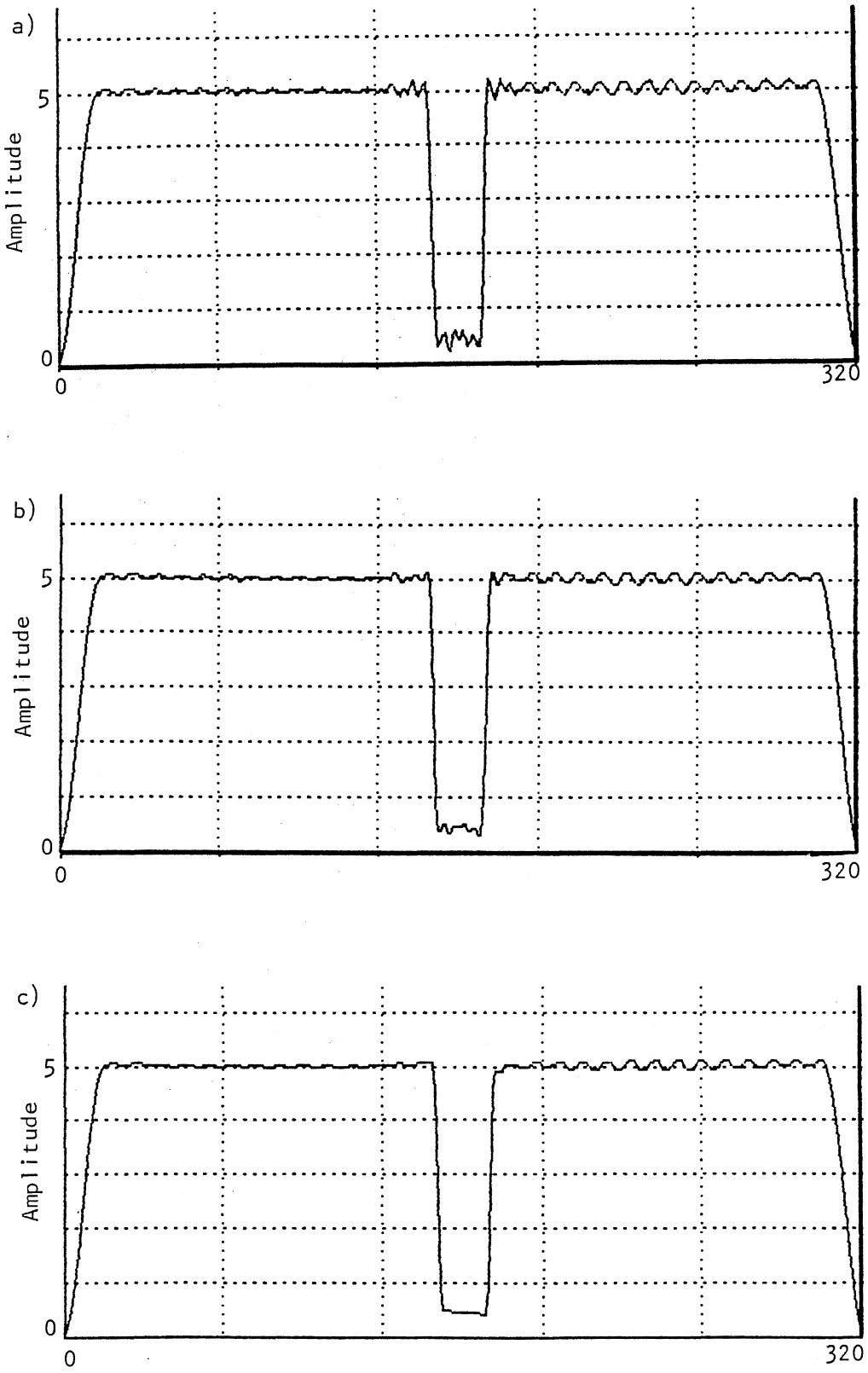

Figure 29. Deconvolution of Case I With Kalman Filtering. a) Without Postfiltering, b) With 3-Point Postfilter, c) With 5-Point Postfilter

Given in Figure 30a is the result of deconvolving case II with WOAC and Kalman filtering. The SNR was calculated to be about 45 dB before postfiltering and approximately 46 dB and 47 dB after postfiltering. These represent an increase of about 26 dB for the three simulations. The results are shown in Figures 30b and 30c. Again, the restoration was not quite as complete as with constrained least squares filtering or Wiener filtering.

Theoretically, the results from Kalman filtering should be better than those obtained with the other methods presented here. Kalman filtering does not perform as well as might be expected due to certain limiting assumptions made about the model. In particular, the conductivity process is modeled as a white noise process which is convenient but is certainly not correct. A second limitation is the shortness of the segment length and corresponding lag imposed on the process due to the relative complexity of the algorithm. An increased lag will produce a better estimate in terms of mean-square error [32]. Kalman filtering was not applied to the other two sets of data due to its reduced performance and increased computation time.

L_1 Filtering

Figure 31a shows the results produced by applying the L_1 filtering algorithm described earlier to the data of case I. The filter length was 31 points and the segment length was chosen to be 128. The SNR for this example was found to be about 47 dB prior to postfiltering to remove noise. After the application of the 3 point and 5 point postfilters, the SNR for case I increased to approximately 57 dB and 64 dB, respectively. These results represent improvements of approximately 17 dB, 28 dB, and

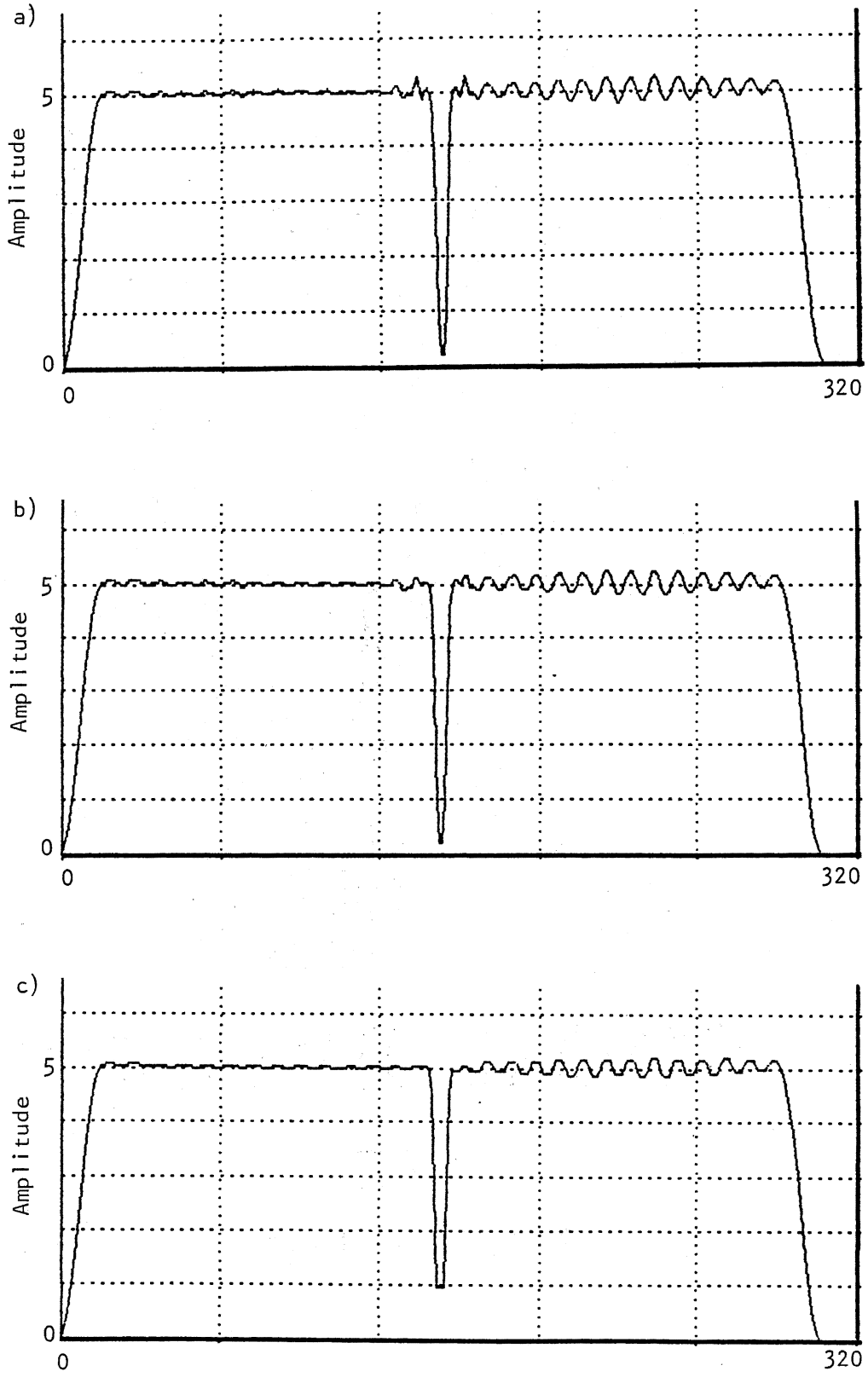

Figure 30. Deconvolution of Case II With Kalman Filtering. a) Without Postfiltering, b) With 3-Point Postfilter, c) With 5-Point Postfilter

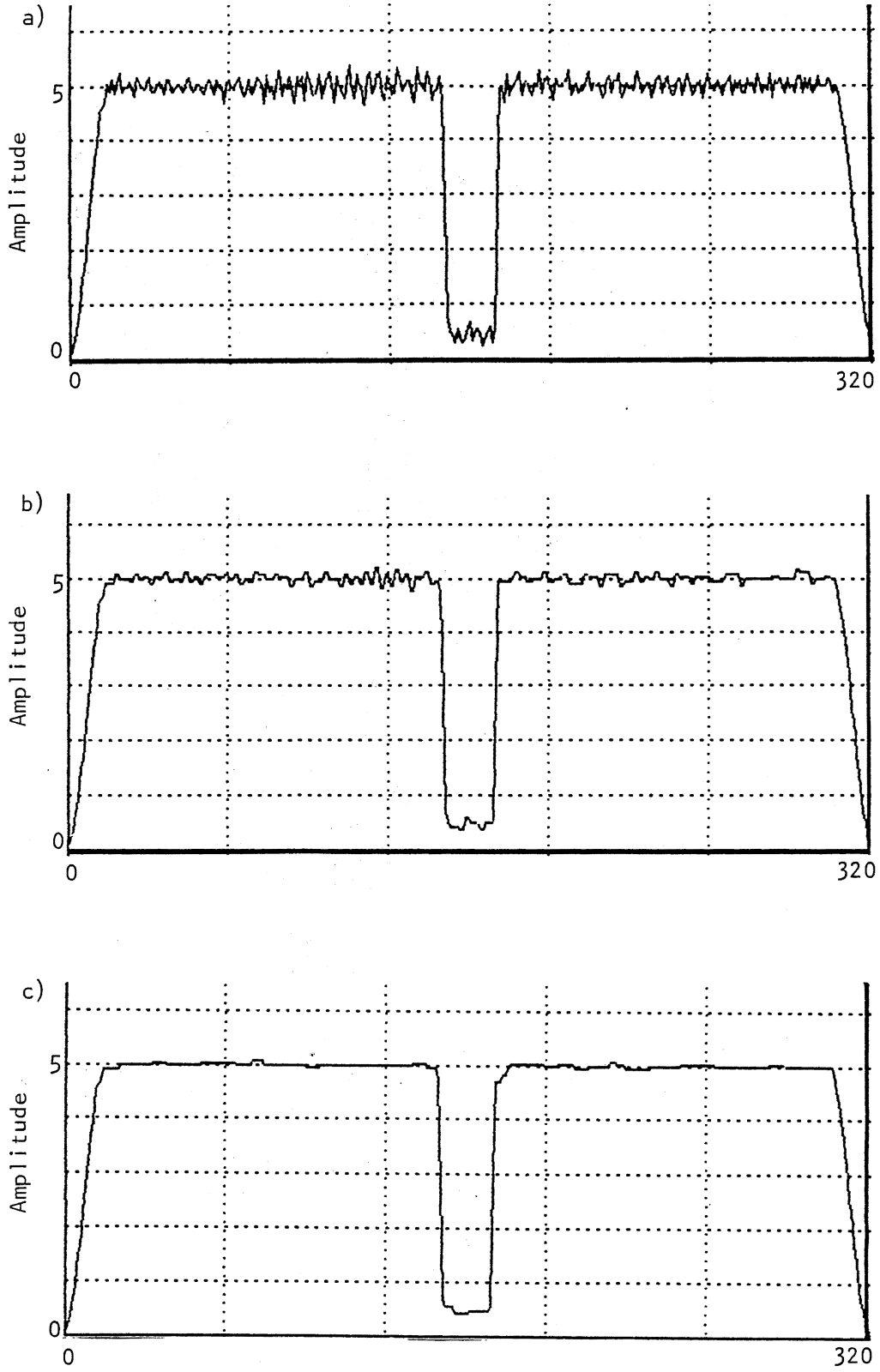

Figure 31. Deconvolution of Case I With L_1 Filtering. a) Without Postfiltering, b) With 3-Point Postfilter, c) With 5-Point Postfilter

34 dB compared to the original synthetic data. These two results are shown in Figures 31b and 31c. These results are quite comparable with those obtained with Wiener filtering and constrained least squares filtering.

Given in Figure 32a is the result of deconvolving case II using L_1 filtering and WOAC. In this case the SNR was calculated to be 44 dB before postfiltering. Figures 32b and 32c show the results obtained after postfiltering as before. The SNR increases to slightly more than 50 dB and 54 dB for the two postfilters. These results are quite good and represent improvements relative to the synthetic data of about 23 dB, 29 dB, and 34 dB. Better results may be expected if the segment length were increased equal to the segment length applied with the previous three methods. Unfortunately, L_1 requires an enormous number of computations for data of reasonable size, and 128 points were the most that could be conveniently computed at once.

Jansson's Method

Jansson's method does not perform well for deconvolving data of the type considered here. The restoration is often limited by the appearance of spurious features which appear near discontinuities. These features seem to arise from the usual overshoot which is present at discontinuities; however, the method seems to increase the problem. In fact, as Jansson's method or successive approximation deconvolution proceeds, overshoot tends to increase with the eventual result being bed splitting. In the examples presented here, iteration was not allowed to proceed to the point where spurious features became prominent. The filter length was 31 points and the segment length was 192. Shown in Figure 33a is the

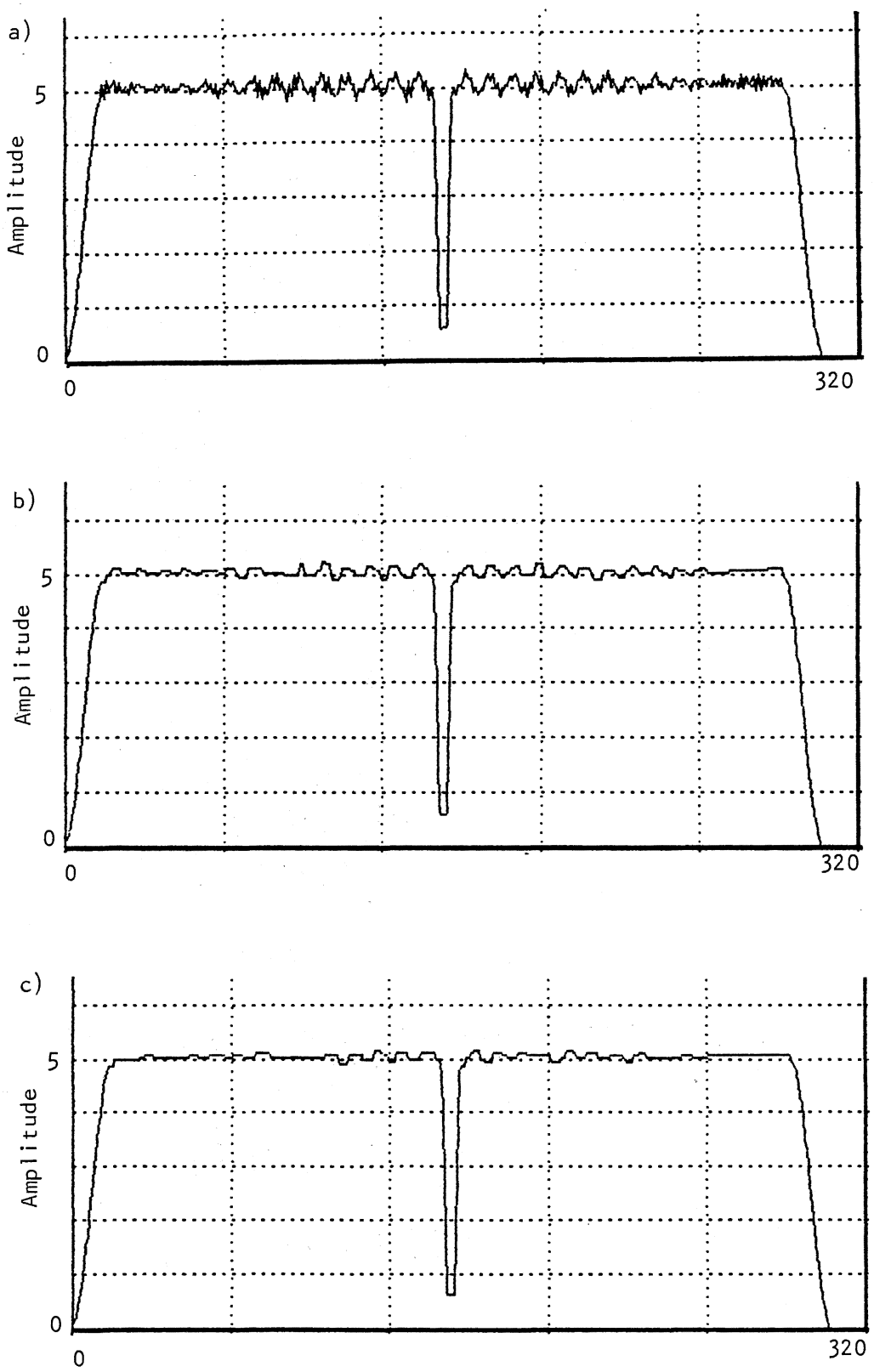

Figure 32. Deconvolution of Case II With L_1 Filtering. a) Without Postfiltering, b) With 3-Point Postfilter, c) With 5-Point Postfilter

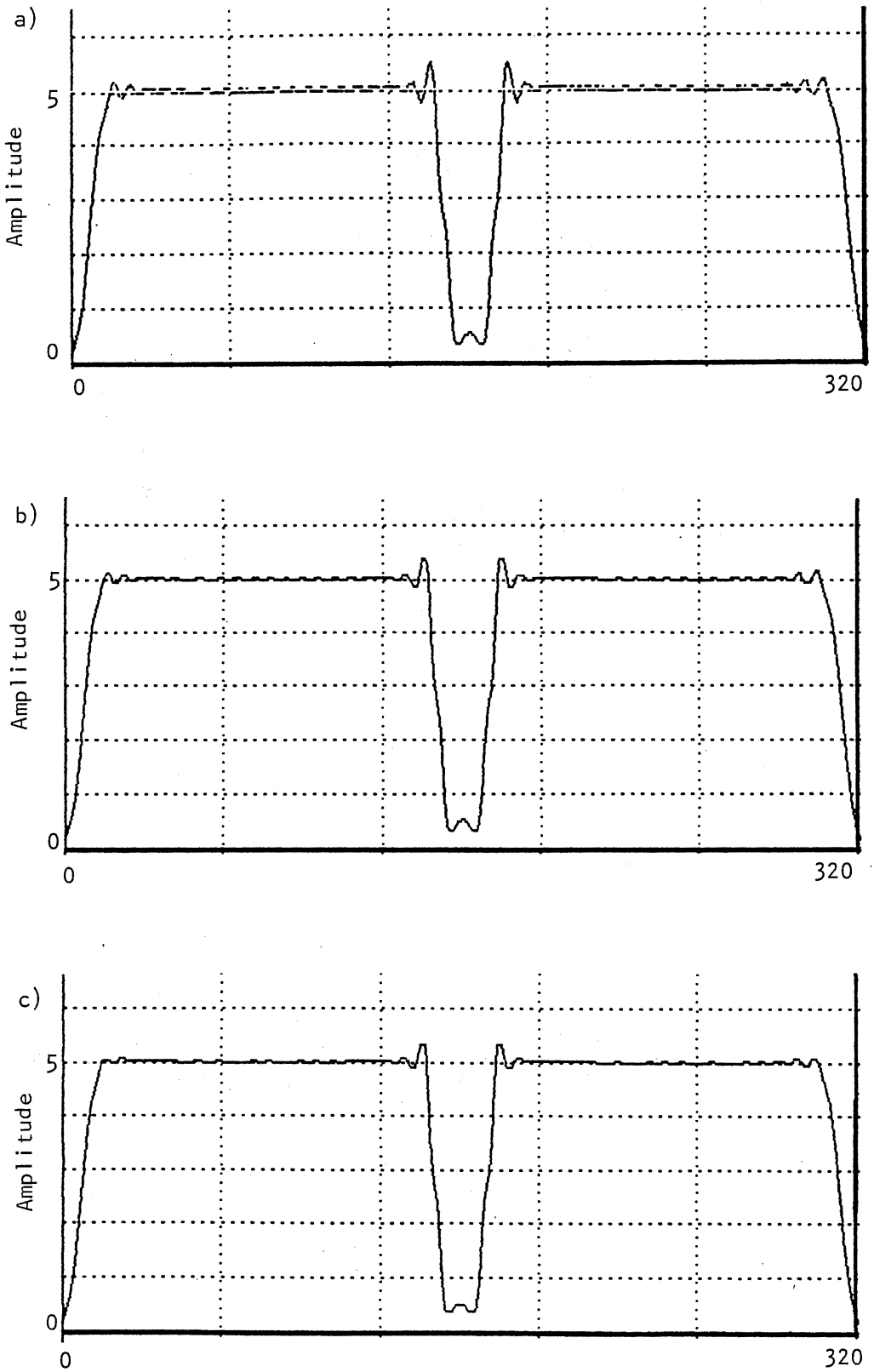

Figure 33. Deconvolution of Case I With Jansson's Method. a) Without Postfiltering, b) With 3-Point Postfilter, c) With 5-Point Postfilter

result of deconvolving case I without postfiltering. The SNR was calculated to be slightly more than 31 dB, which is only a 2 dB improvement over the synthetic data. Since the amount of noise present in the deconvolved data is very small postfiltering should not be expected to improve the result significantly. Indeed, after postfiltering the SNR is still approximately 31 dB. The results are given in Figures 33b and 33c.

Figure 34a is the result of deconvolving case II using WOAC and Jansson's method. The SNR was calculated to be about 22 dB, which is little better than the synthetic data. The improvement was again only about 2 dB. Postfiltering produces results similar to those obtained with case I. The SNR is found then to be about 23 dB after the 3 point postfilter and about 22 dB after the 5 point postfilter. These results are shown in Figures 34b and 34c. Jansson's method was not applied to the other two sets of data, since the results are not promising.

Successive Approximation

Deconvolution by successive approximation is only slightly better than Jansson's method. The implementation was identical to that of Jansson's method and the comments above regarding performance apply. Figure 35a presents the results obtained after deconvolving case I. The SNR before postfiltering was calculated to be about 33 dB. Shown in Figures 35b and 35c are the results following postfiltering which still produce an SNR of about 33 dB. The improvement was thus only approximately 3 dB.

Shown in Figure 36a is the result of deconvolving case II with successive approximation and WOAC. The SNR was found to be slightly more than 24 dB prior to postfiltering. After postfiltering, the SNR was

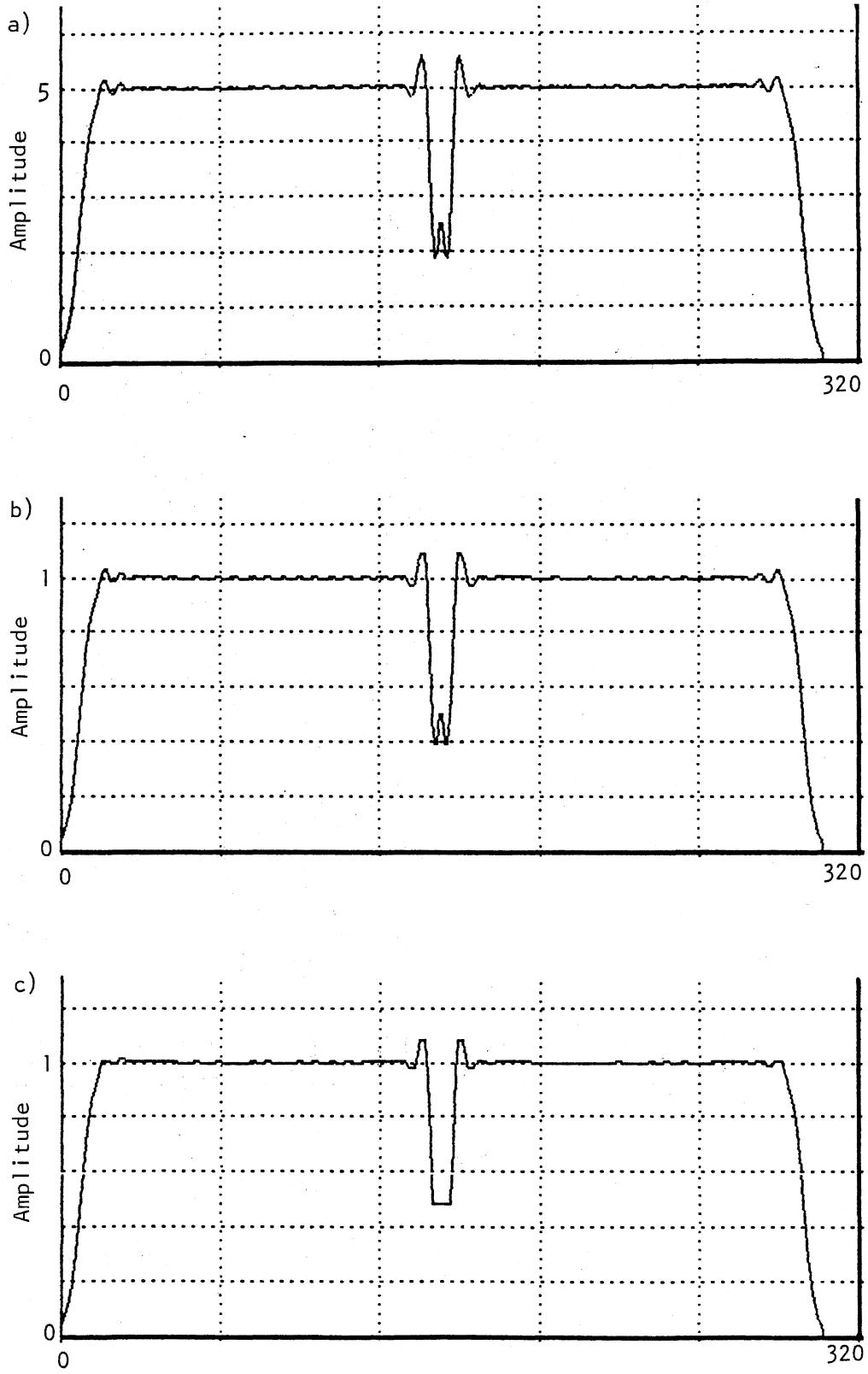

Figure 34. Deconvolution of Case II With Jansson's Method. a) Without Postfiltering, b) With 3-Point Postfilter, c) With 5-Point Postfilter

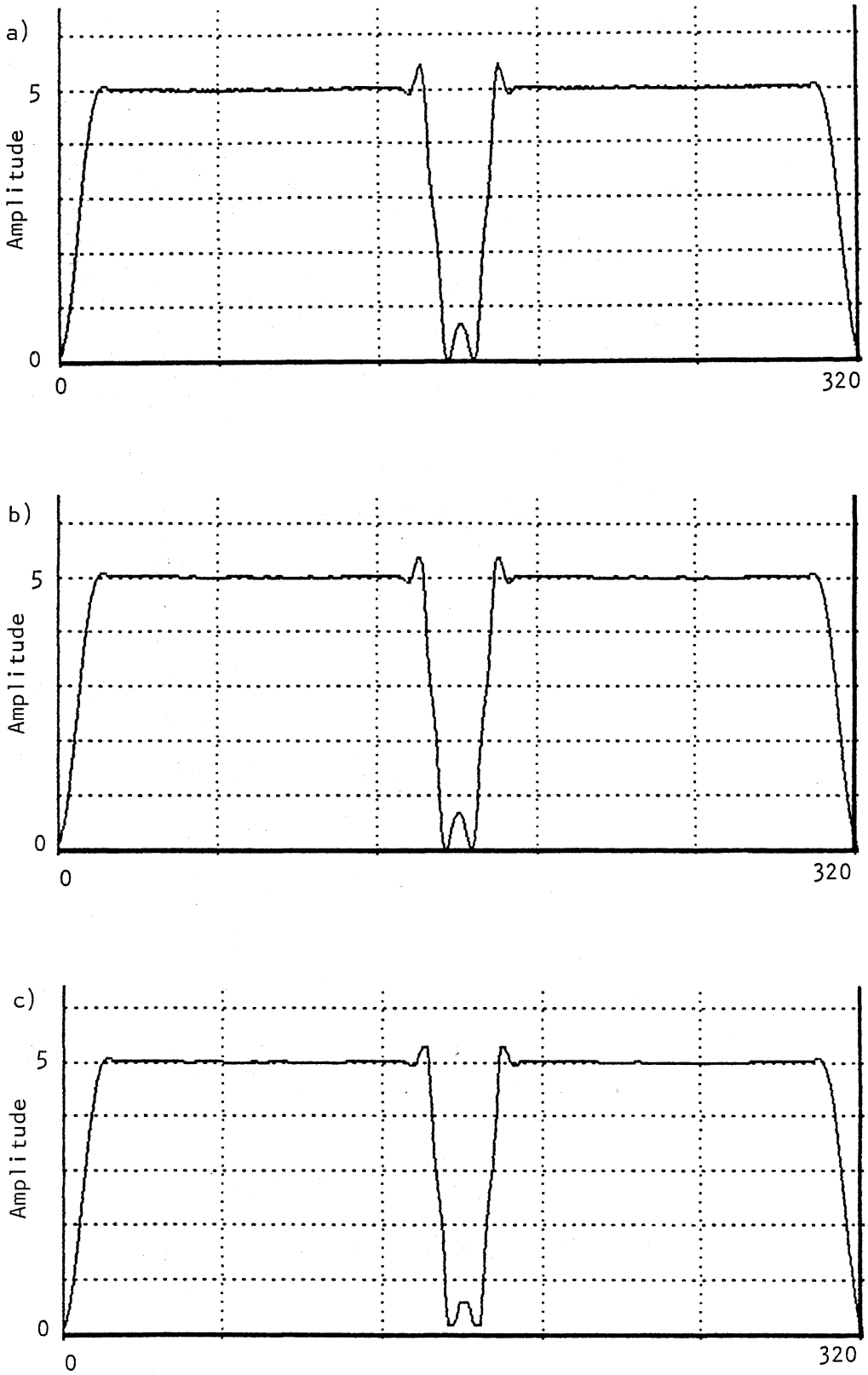

Figure 35. Deconvolution of Case I With Successive Approximation. a) Without Postfiltering, b) With 3-Point Postfilter, c) With 5-Point Postfilter

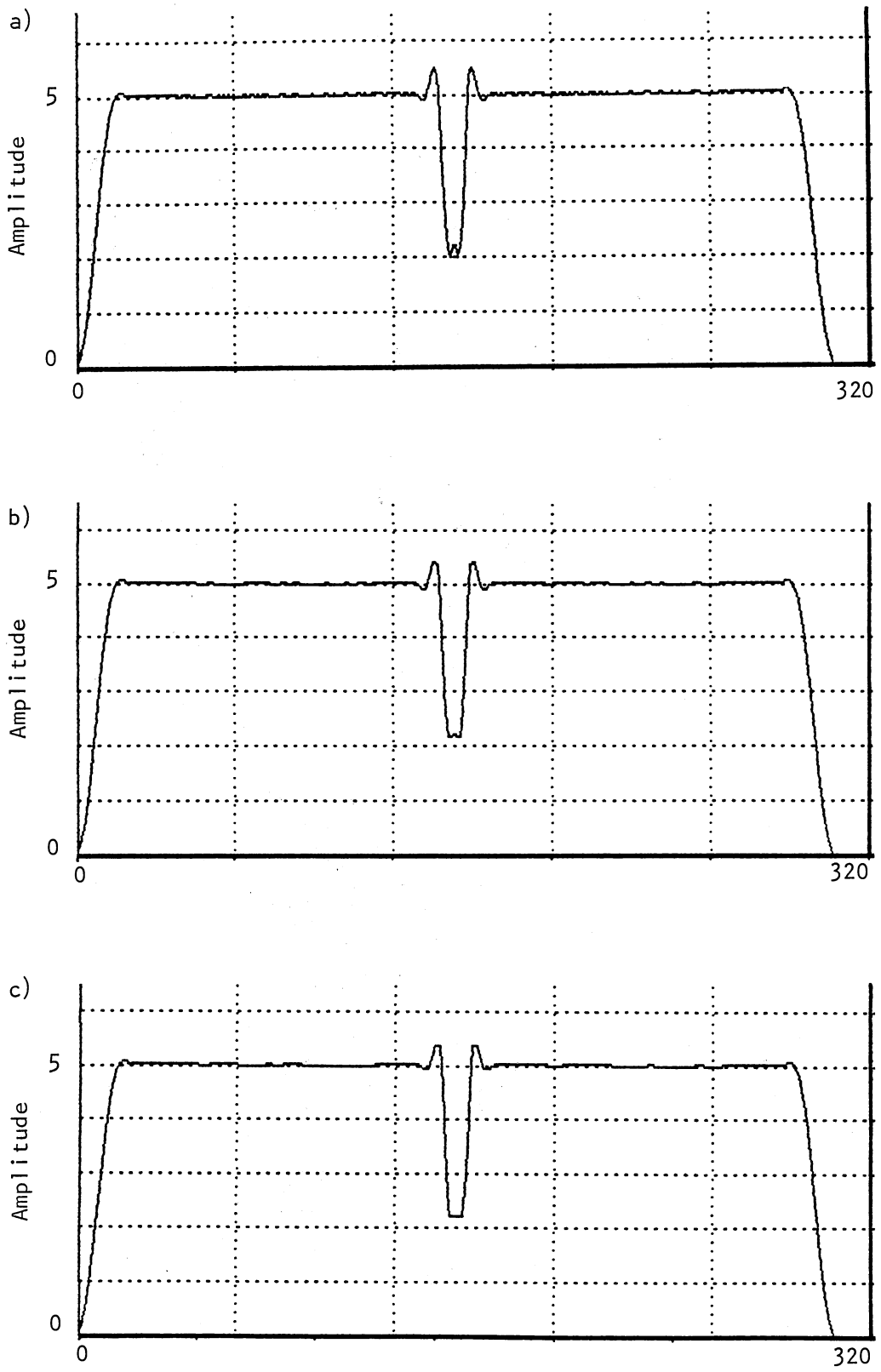

Figure 36. Deconvolution of Case II With Successive Approximation. a) Without Postfiltering, b) With 3-Point Postfilter, c) With 5-Point Postfilter

found to decrease slightly to about 24 dB for both postfilter lengths. These results are given in Figures 36b and 36c. As before, the improvement was small, amounting here to about 4 dB. Neither of the other two sets of data were deconvolved using successive approximation for the reasons stated above.

Discussion

The results outlined above are collected and summarized in Table I. Results are not included for the real data since no measure of performance could be easily calculated for comparison. Some generalizations may be drawn from these results. One point that stands out clearly is the poor performance by Jansson's method and successive approximation. Since one is similar to the other it is not surprising that they produce similar results. It is also clear that in the implementation used here, neither one is useful for performing deconvolution of induction log data with WOAC. The reason for this poor performance is not clear, although it may be due in part to the test for convergence which was used. The convergence test consisted of measuring the magnitude of the correction applied at each iteration and stopping when the correction ceased to decrease. This produced a compromise between restoration and growth of spurious features in the data. Both Jansson's method and successive approximation are likely to produce spurious features as iteration proceeds. This characteristic can result in unreliable performance. Perhaps a better method of monitoring convergence could be derived so that performance could be improved. In any event, it is very difficult to perform deconvolution using Jansson's method or successive approximation without human intervention.

TABLE I

SIGNAL TO NOISE RATIOS OF ORIGINAL AND DECONVOLVED DATA

Method	SNR (dB)			
	Case I	Case II	Real	Adaptive
Convolved Original	29.6	20.8	(a)	19.1
Wiener Filtered	58.7	49.1		39.5
with 3 pt. median	72.2	57.2		49.2
with 5 pt. median	73.6	61.0		54.5
Constrained Least Squares	62.5	52.7		50.8
with 3 pt. median	65.1	53.9		50.9
with 5 pt. median	67.2	54.5		51.4
Kalman Filtered	56.3	45.4		(b)
with 3 pt. median	58.1	46.3		
with 5 pt. median	60.7	47.2		
L1 Filtered	46.7	44.0		(b)
with 3 pt. median	47.2	50.1		
with 5 pt. median	63.8	54.3		
Jansson's Method	31.3	21.5		(b)
with 3 pt. median	31.4	22.6		
with 5 pt. median	31.5	22.2		
Successive Approximation	32.5	24.5		(b)
with 3 pt. median	32.5	24.1		
with 5 pt. median	32.8	24.1		

Notes: a. SNR could not be calculated.

b. Method not applied to data.

The remaining four methods performed relatively well with no one method definitely standing out in terms of SNR, although Wiener filtering produced the best results overall. It is possible to pick one or two methods which do offer good performance as well as ease of implementation. In particular, Wiener filtering and constrained least squares fit these criteria. Wiener filtering offers slightly easier implementation at the expense of higher noise amplification. Constrained least squares offers slightly more consistent performance at the expense of more calculations. Kalman filtering also produces results which are consistent and of good quality but the algorithm is much more complicated to implement. Theoretically, Kalman filtering should produce the best possible results; however, the statistical model for the induction log is not very good. In particular, the conductivity process is modeled as being white which is certainly not the case when short-term techniques are used, and may not be the case in general. The Kalman filtering approach thus does not produce the best results, but it does produce results that are comparable to Wiener filtering and constrained least squares filtering. L_1 filtering performs similarly to constrained least squares except that in addition to being more complicated to implement, the number of calculations required to solve even minimal problems is enormous. In an implementation on a VAX 11/750, L_1 filtering required approximately two orders of magnitude more CPU time than did Wiener filtering or constrained least squares. However, because of its nature, L_1 deconvolution would be better in cases where there is aberrant noise.

Given the results which have been presented, it is interesting to look at the way WOAC performs using some of these methods with respect to additive noise, segment length, and postfiltering. Figure 37 is a plot

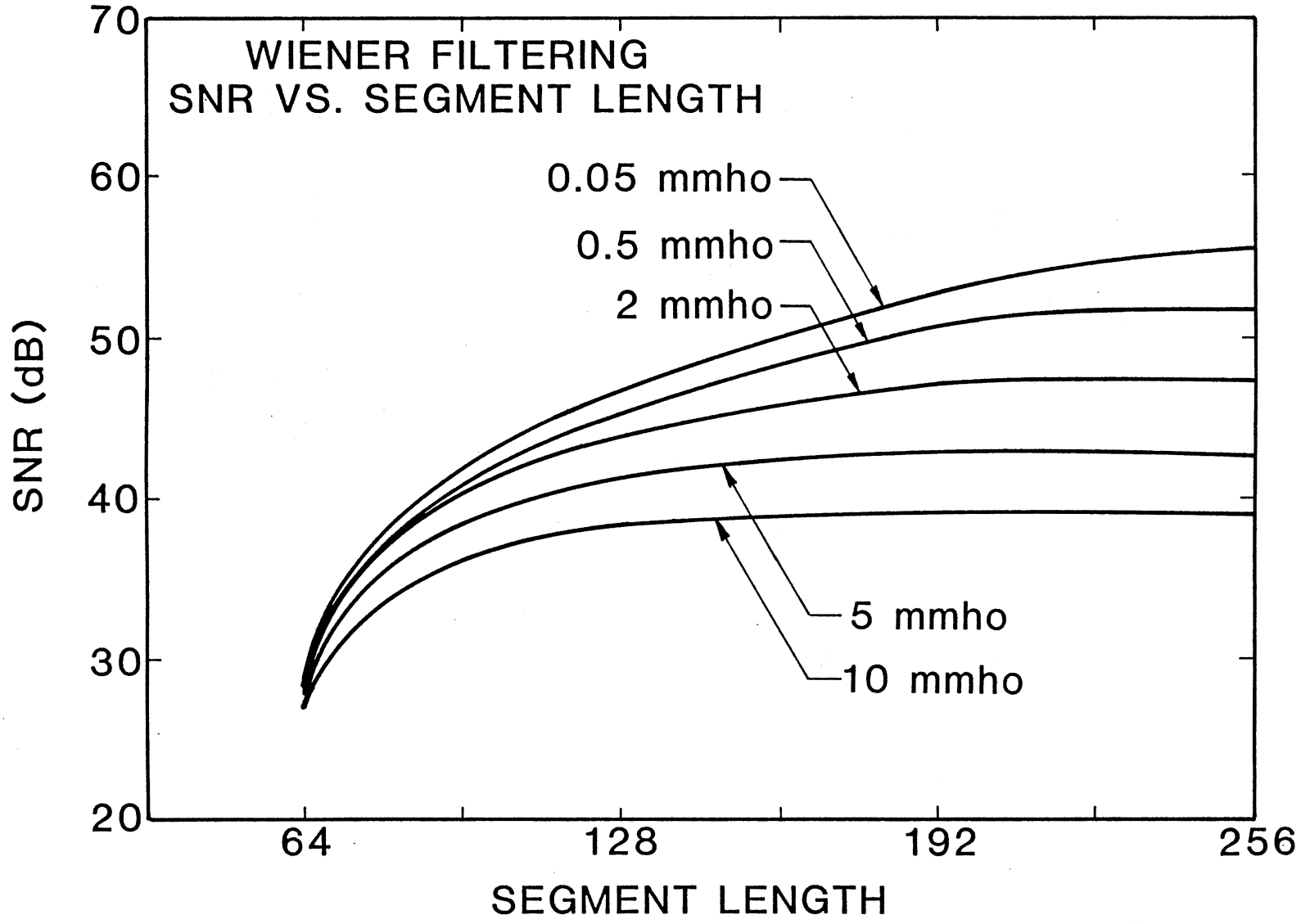

Figure 37. Wiener Filter Performance: SNR Versus Segment Length (Fixed Noise)

of Wiener filter performance as a function of segment length and additive noise in the data. The filter length was 31 and the data of case II was deconvolved. A family of curves is plotted for additive noise of 0.05 mmho, 0.5 mmho, 2.0 mmho, 5.0 mmho, and 10.0 mmho standard deviation. The curves all tend downward near the theoretical minimum segment length of approximately 64. They all tend toward constant values which are dependent upon the additive noise as the segment length is increased. Performance appears to be uniform and predictable.

Figure 38 repeats the results presented in Figure 37 except for constrained least squares filtering. Although this family of curves is similar to the one just presented there are some notable differences. Constrained least squares does not seem to perform quite as well as Wiener filtering in the presence of the larger amounts or noise. This could be due in part to poor estimation of the noise variance. However, performance is generally better when more typical amounts of noise are present in the data. For example, the SNR when additive noise standard deviation is about 2.0 mmho or less is better than that obtained with Wiener filtering. As before, the curves tend toward values that are approximately constant as segment length is increased and toward a minimum near the theoretical minimum segment length as is expected.

Figure 39 is a plot of Kalman filtering performance for a single set of data. Case II was used again and the additive noise was set to 1.0 mmho standard deviation. As with the results of the two methods just illustrated, the SNR with Kalman filtering tends upward as the segment length is increased, becoming flatter at higher segment lengths. The slope increases as the segment length is decreased toward 64. These results indicate the wide range of segment lengths which may be chosen

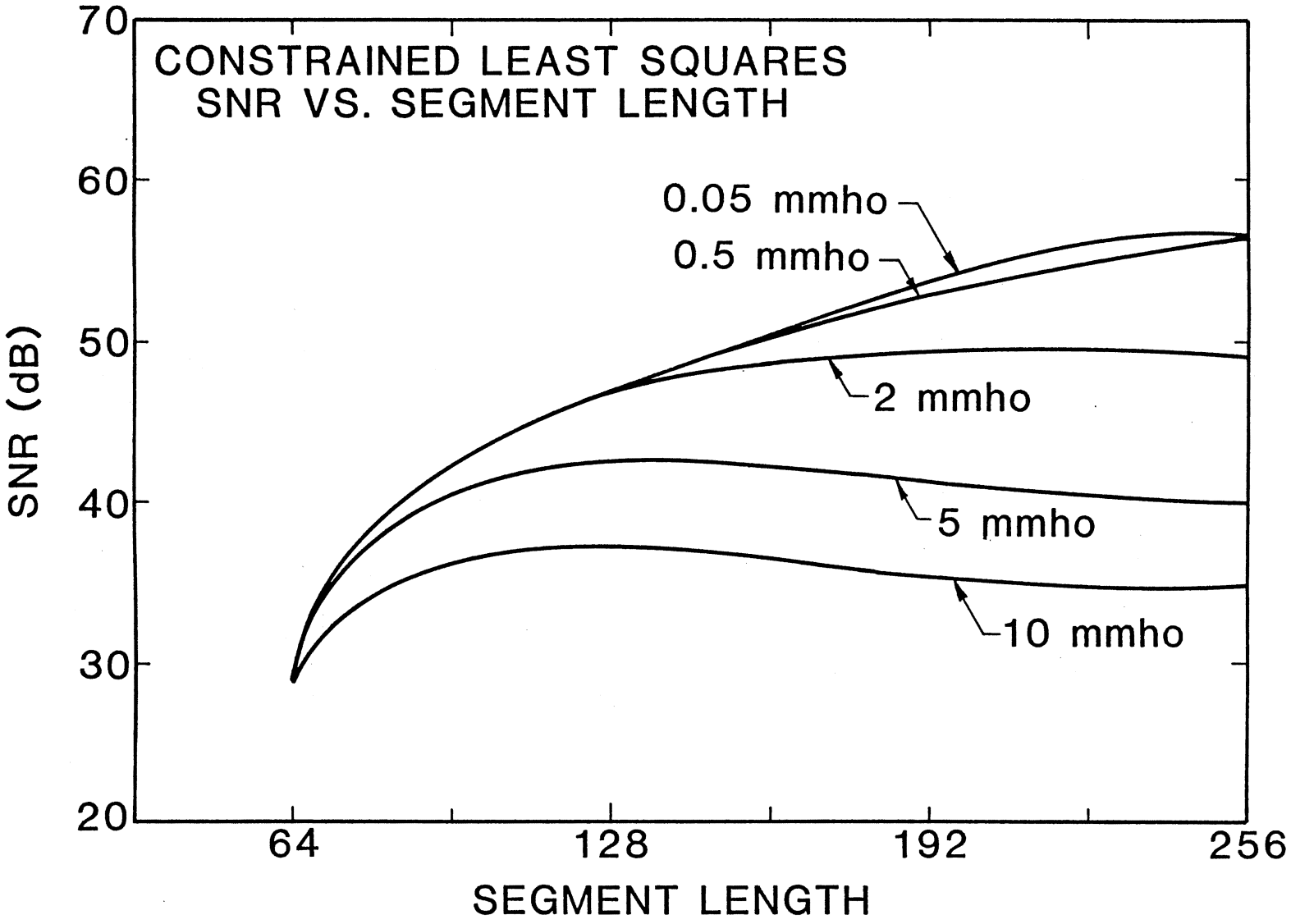

Figure 38. Constrained Least Squares Performance: SNR Versus Segment Length (Fixed Noise)

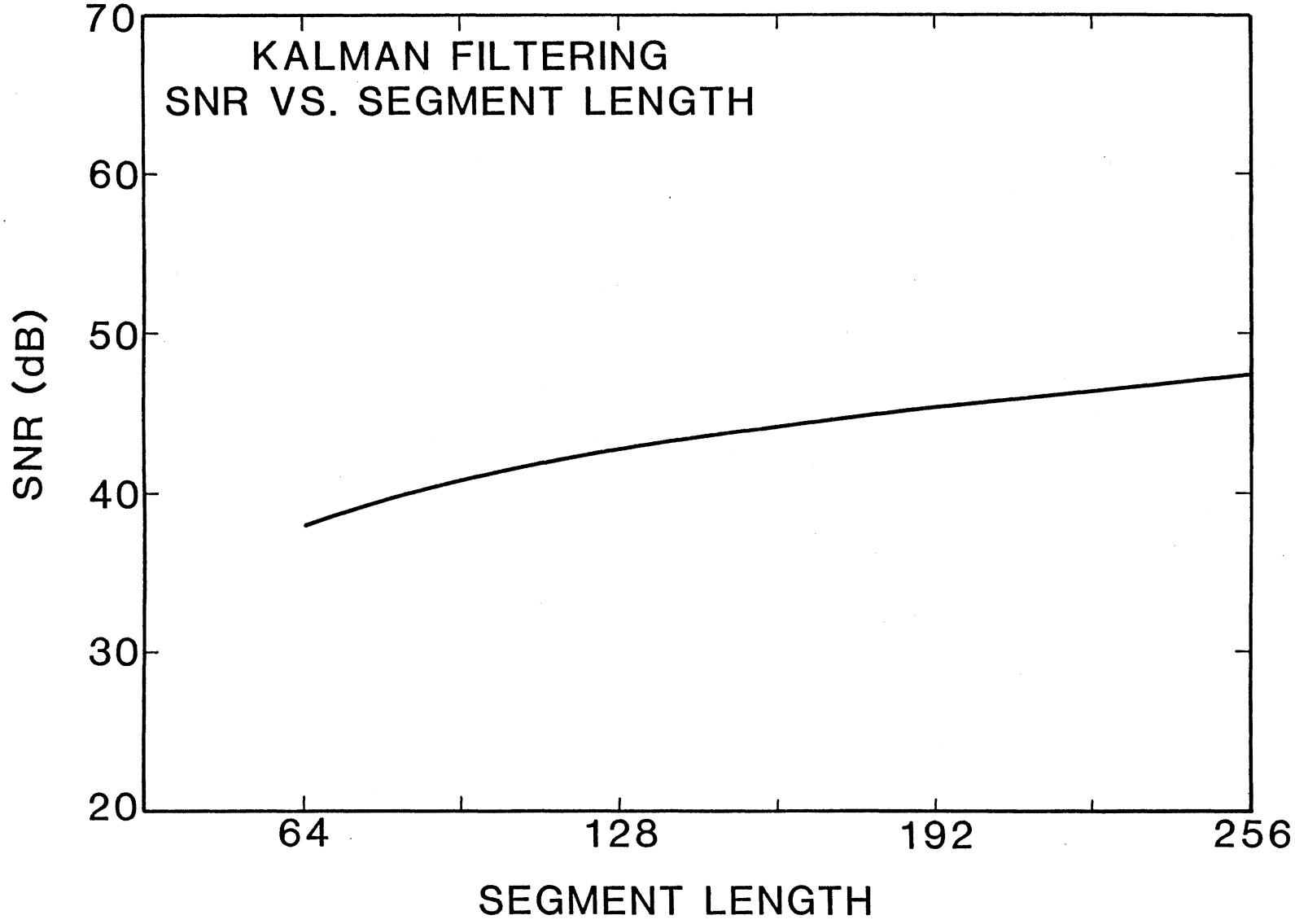

Figure 39. Kalman Filter Performance: SNR Versus Segment Length

while maintaining satisfactory performance of all three methods just described. Of course, a longer segment length will usually produce better results.

The data just presented in Figures 37-39 may be plotted as SNR for each segment length as a function of additive noise standard deviation. Figure 40 illustrates this for Wiener filtering. As before, it is clear that for segment lengths of about four times the filter length or more the performance is similar over a wide range of additive noise standard deviations. Performance decreases as segment length decreases and as additive noise increases.

Figure 41 illustrates SNR for varying segment lengths as a function of additive noise standard deviation for constrained least squares filtering. Again, the performance is similar for segment lengths greater than about four times the filter length, or 128. As expected, performance generally decreases as segment length decreases and as additive noise increases.

Figure 42 is a plot of SNR as a function of additive noise for Kalman filtering. In addition, the effects of postfiltering with a 3 point and a 5 point recursive median filter are shown. As before, it can be seen that performance decreases smoothly as additive noise increases. Postfiltering can be seen to provide a small uniform increase in SNR over the entire range of additive noise, increasing as the noise is increased. In fact, the SNR with 10.0 mmho noise standard deviation with the 5 point postfilter is almost as good as the SNR with no noise and no postfilter.

Shown in Figure 43 is a plot of SNR as a function of additive noise and postfilter for Wiener filtering. Results for segment lengths of 128 and 192 points are shown to allow easier comparison with the plots for

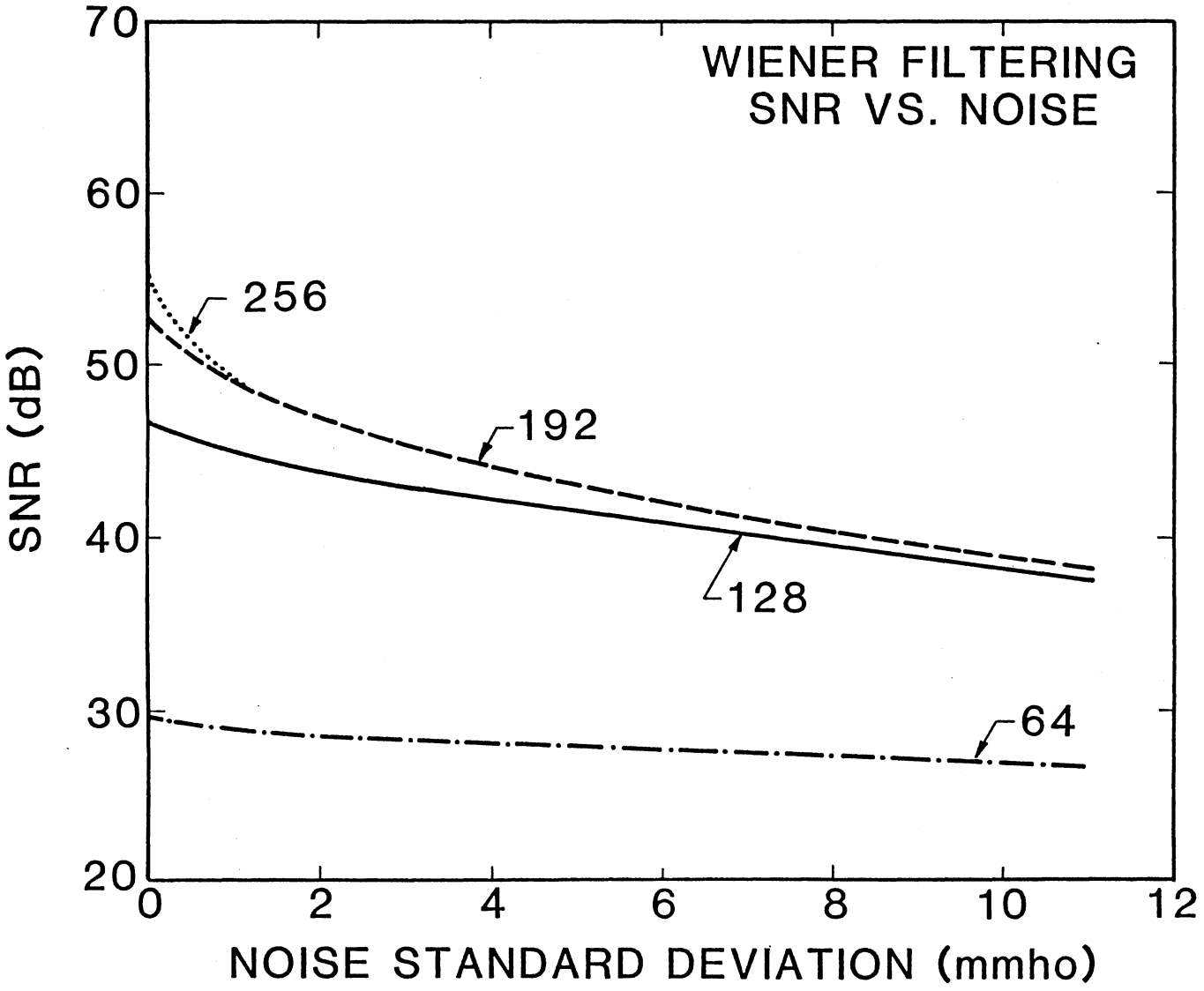

Figure 40. Wiener Filter Performance: SNR Versus Noise Standard Deviation (Fixed Segment Length)

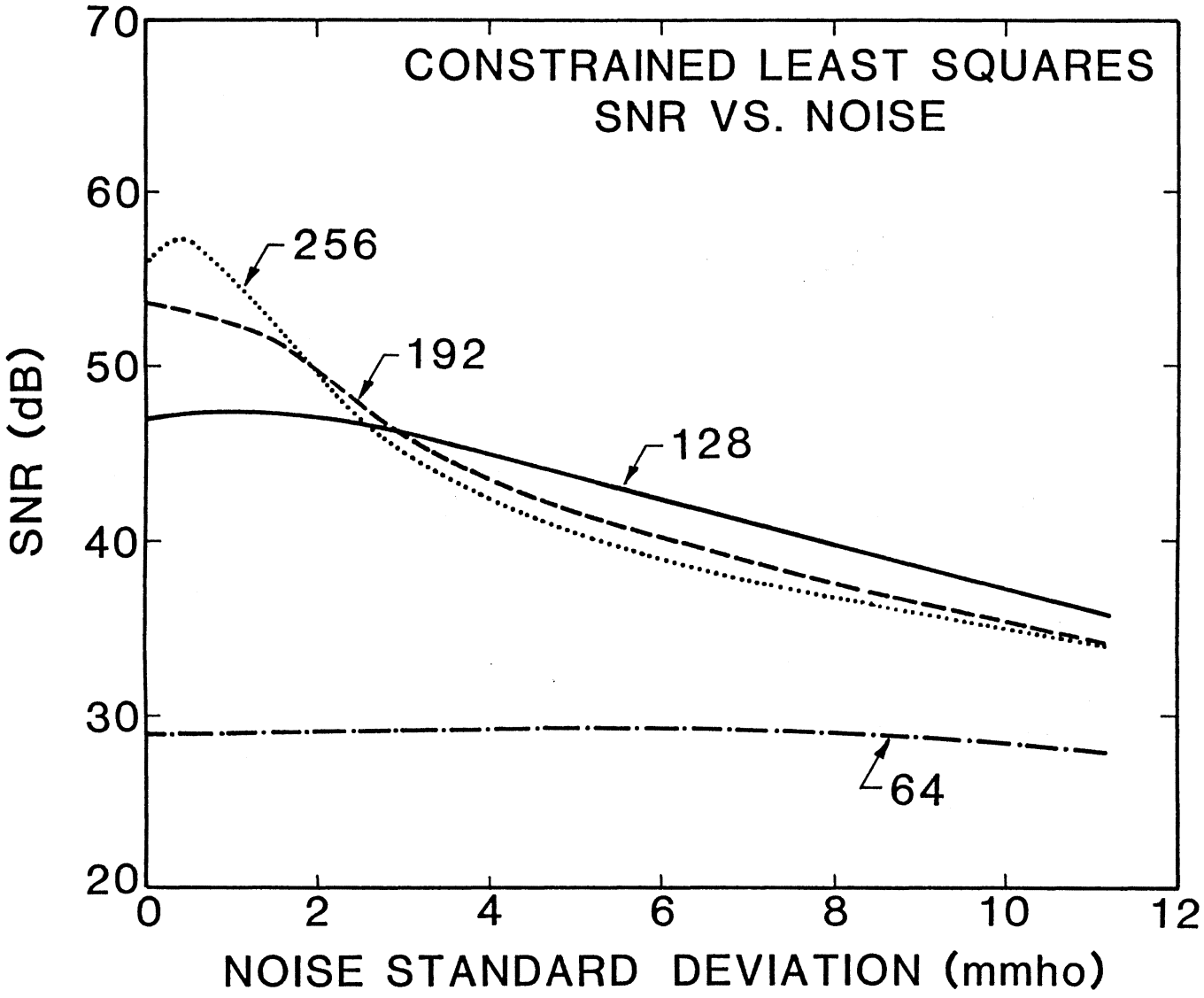

Figure 41. Constrained Least Squares Filter Performance: SNR Versus Noise Standard Deviation (Fixed Segment Length)

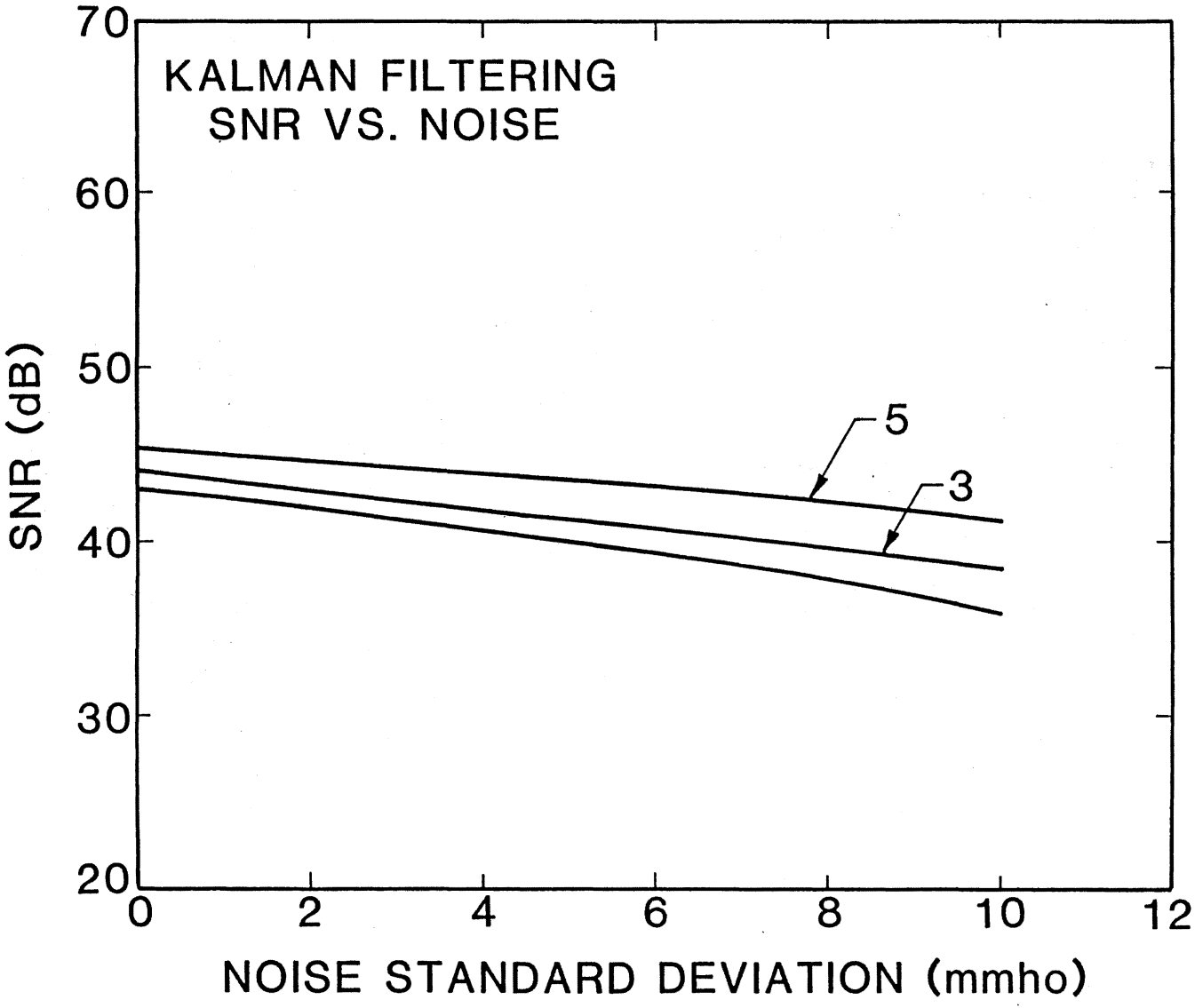

Figure 42. Kalman Filter Performance With Postfiltering: SNR Versus Noise Standard Deviation

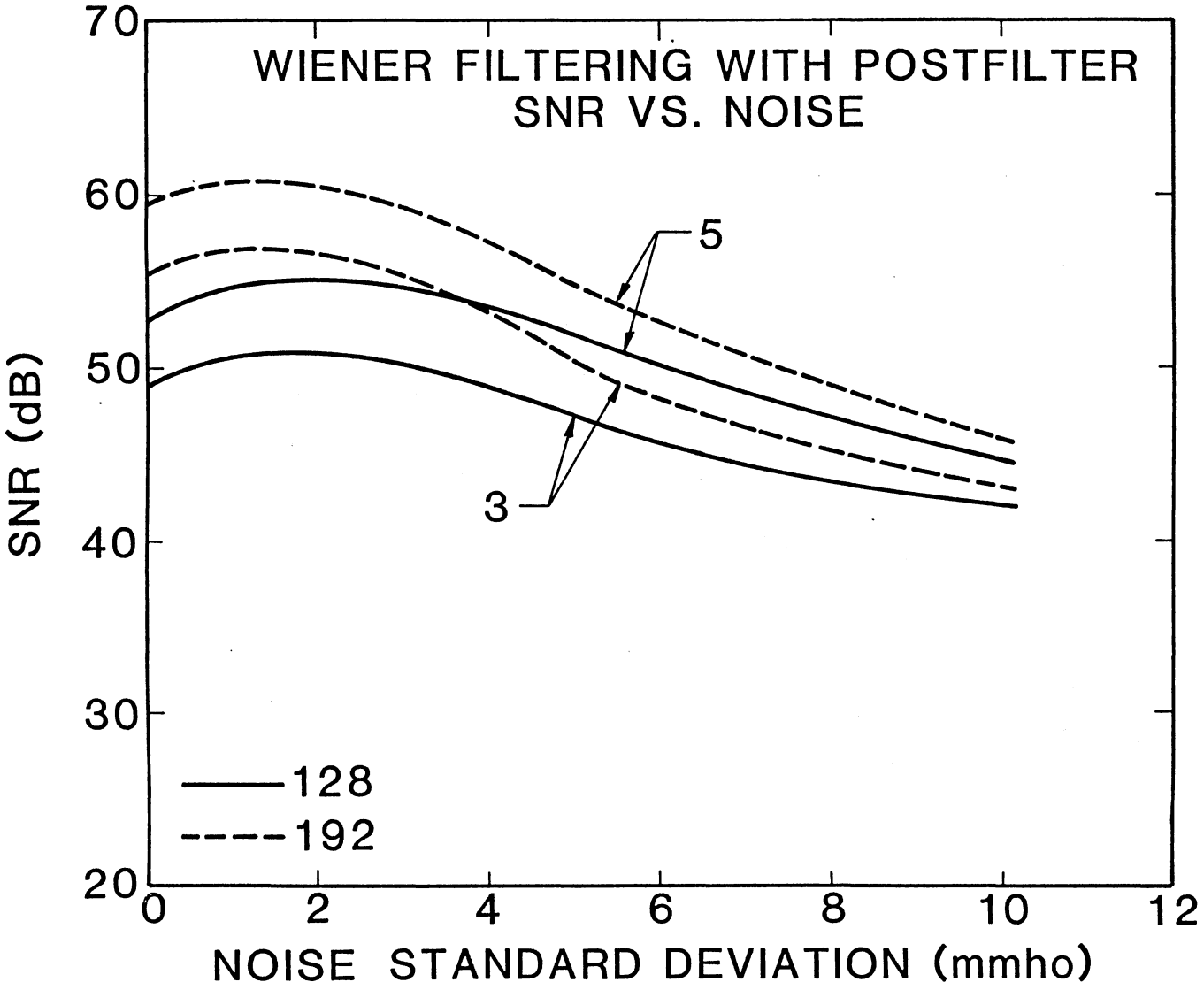

Figure 43. Wiener Filter Performance With Postfiltering: SNR Versus Noise Standard Deviation (Fixed Segment Length)

Wiener filtering presented earlier. As additive noise is increased, SNR rises slightly and then smoothly decreases. It is easy to see that postfiltering can provide a significant improvement when Wiener filtering is used as the deconvolution method since a large amount of noise is amplified. Since the results of constrained least squares filtering are usually smooth, a plot of performance as a function of postfiltering will not be shown.

Figure 44 is a plot of Kalman filter performance as a function of the estimated parameter, R, the noise covariance. The effect of postfiltering is also indicated. An estimate of the noise covariance must be made to implement Kalman filtering. Fortunately, it can be seen that this estimate may range over at least two orders of magnitude without degrading the results. As the covariance estimate becomes smaller more noise is amplified so the SNR without postfiltering begins to decrease rapidly. Postfiltering can produce a large increase in SNR, particularly if the covariance estimate is too small, thus increasing the latitude available for estimating the noise covariance.

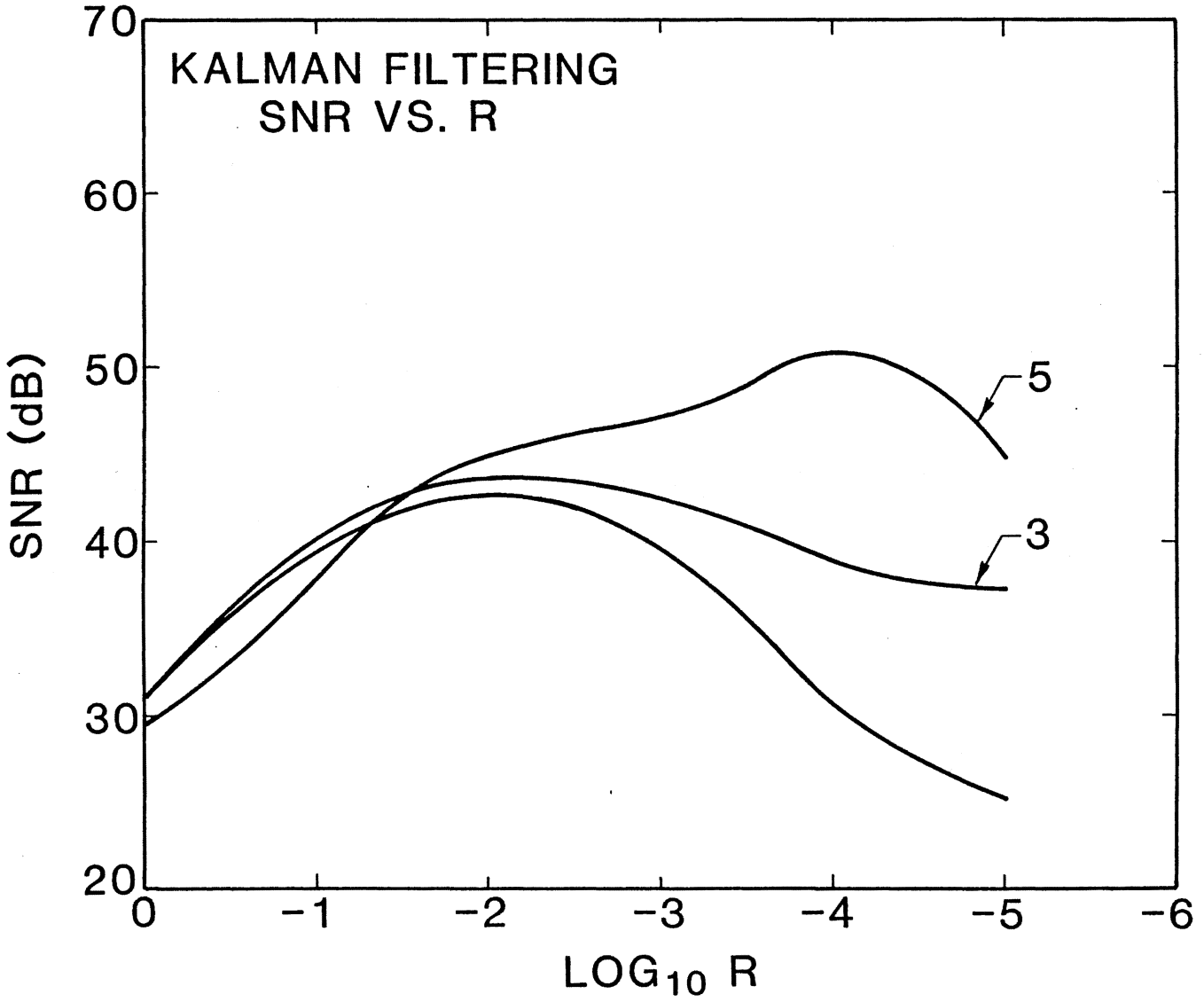

Figure 44. Kalman Filter Performance With Postfiltering: SNR Versus Noise Covariance Estimate

CHAPTER VII

SUMMARY AND CONCLUSIONS

A new procedure for deconvolution of the induction log and other similar slowly time-varying signals has been presented. The procedure which is referred to as weighted overlap-addition convolution, WOAC, uses techniques of short-term analysis and synthesis which have previously been applied primarily to filtering speech and speech-like signals. The procedure has been shown to be particularly suited to the partial correction of distortion introduced by nonlinearity in the instrument's system response by approximating a nonlinear system as a sum of segmented linear convolutions. In addition, the procedure allows the deconvolution of a very long set of data to be performed in small segments to conserve physical computer memory. The procedure is modular so that many deconvolution methods such as Wiener filtering, constrained least squares filtering, Kalman filtering, L_1 filtering, and others may be easily implemented internal to WOAC. Results using these and other methods have been presented. The procedure is well suited to operation in either the spatial or Fourier transform domain to match the filtering method selected. The procedure has been shown to be flexible in its implementation and to provide good tolerance to additive noise and discontinuities present in the data.

Examples of deconvolution of several types of data have been presented which demonstrate numerically that WOAC is stable and robust in

the presence of widely varying amounts of additive noise. The examples additionally show that the performance of the methods which have been applied with WOAC perform uniformly and predictably with the tested data. In addition, relatively large errors in the selection of parameters which describe the additive noise will not badly degrade the result. Of the several methods which were studied, Wiener filtering, constrained least squares filtering, and Kalman filtering were shown to offer particular promise.

Furthermore, the use of WOAC adaptively to deconvolve data while approximating a time-varying response has been shown to provide a significant improvement in signal to noise ratio over conventional methods. Although the ultimate accuracy of any deconvolution method depends upon the accuracy of the model used to describe the system, examples have shown that, even with rather limiting assumptions, deconvolution may be performed reliably while partially accounting for skin effect. In particular, small errors in the system model do not seem to produce large errors in the deconvolved result. It is believed that this is an important result considering past problems which have been encountered while trying to deconvolve data generated by a time-varying system response. Although the procedure does not attempt to account for all the nonlinear effects which may be present in a system or to provide an exact solution to the deconvolution problem, it does offer a new technique for performing deconvolution which may prove useful in many applications. With WOAC, it is possible that special purpose hardware may be developed for real-time or near-real-time implementation.

Suggestions for Future Research

Numerous possibilities exist for extending the ideas presented in this dissertation. Listed below are several points which could be studied in hope of providing worthwhile results which could lead to more accurate deconvolution with WOAC.

1. Although WOAC performs rather well, discontinuities produce ripples which are spread through the data in the general vicinity of the discontinuity. Several possibilities exist for reducing these ripples. The first is to perform deconvolution of the data twice, proceeding from start to end and then in the reverse direction. The two results could then be added together and averaged with the hope that the ripples could be reduced in amplitude by the averaging process. However, this would tend to spread the ripples both directions in the result.

2. Another possible means for reducing ripples present in the deconvolved data is to take advantage of the almost periodic nature of the ripples. It may be possible, at the loss of some resolution, to shift the deconvolved result a specified number of points, add it to itself, and average the result. This technique has been used in other applications to reduce overshoot due to Gibb's phenomena [47]. It is not known how much resolution would have to be lost to produce a significant reduction in the ripples.

3. The recursive median filter has been shown to reduce significantly amplified noise in the data. This is possible since the noise is random and may be selectively reduced. Recursive median filters are not commonly used in many applications and may offer more benefits if applied in a different fashion. For example, it is known that recursive median filters of different lengths may be applied to the same data to better

reduce noise. It is also possible to apply the recursive median filter from both ends of the data and average the results. Many possibilities exist here for study of this nonlinear filtering method to reduce noise without degrading the resolution of the induction log.

4. It has been shown that performance of WOAC is related to the selection of the segment length and that the segment length should usually be at least four times the filter length to achieve adequate signal to noise ratio. Optimum choice of the segment length and the decimation rate for arbitrary data has not been studied. It is possible that an optimum combination of these two parameters exists for each particular data set or that a better choice than was made here might be possible. A relationship with window selection might also exist.

5. The adaptive implementation of WOAC presented here was constructed somewhat arbitrarily primarily due to the lack of synthetic data. The choice of conductivites at which to calculate the vertical response functions to apply was made to roughly match the range of conductivities often encountered. The method of choosing which vertical response to apply during deconvolution was made by calculating an average over a short number of points in the center of each segment and using this average to select a response. A more accurate procedure could increase resolution and signal to noise ratio of the result.

6. Other techniques of adapting the filter response to the data being deconvolved may be constructed if the deconvolution method itself may be varied. For example, some deconvolution methods may perform better with specific types of data. Thus it might be possible to select which method to apply segment by segment in the same manner that the deconvolution filter is chosen. WOAC, due to its modularity, could be easily modified to provide this added feature.

7. The WOAC procedure described in this dissertation is based upon a segmented approach which is well suited to hardware implementation. A hardware design using LSI is a worthwhile project for on-line processing of data.

8. Finally, although six methods of deconvolution covering a wide range of techniques have been examined there may be still others which are well suited to application to the deconvolution problem and WOAC. One class of methods, in particular, which has not been investigated is the "entropy method." Entropy methods have been applied to image restoration [48], seismic exploration [49], and absorption spectroscopy [50].

BIBLIOGRAPHY

[1] Duesterhoeft, W. C., and R. E. Hartline. "The Effect of Coil Design on the Performance of the Induction Log." Journal of Pet. Tech. (November, 1961), pp. 1137-1150.

[2] Duesterhoeft, W. C. "Propagation Effects in Induction Logging." Geophysics, Vol. 26, No. 2 (April, 1961), pp. 192-204.

[3] Gianzero, S. "Effect of Sonde Eccentricity on Responses of Conventional Induction-Logging Tools." IEEE Trans. on Geoscience Elec., Vol. GE-16, No. 4 (October, 1978), pp. 332-339.

[4] Woodhouse, R. et al. "The Radial Response of the Induction Tool." The Log Analyst (January-February, 1975), pp. 3-9.

[5] Anderson, B., and S. K. Chang. Synthetic Induction Logs by the Finite Element Method. Ridgefield, Conn.: Schlumberger-Doll Research, 1982.

[6] Looyestijn, W. J. "Deconvolution of Petrophysical Logs: Applications and Limitations." Trans. SPWLA Twenty-Third Annual Logging Symposium. Paper W. Corpus Christi, Texas, July 6-9, 1982.

[7] Doll, H. G. "Introduction to Induction Logging and Application to Logging of Wells Drilled With Oil Base Mud." Pet. Trans. of AIME (June, 1949), pp. 148-162.

[8] Moran, J. S., and K. S. Kunz. "Basic Theory of Induction Logging and Application to Study of Two Coil Sondes." Geophysics, Vol. 27, No. 6 (December, 1962), pp. 829-858.

[9] Thadani, S. G., and H. E. Hall. "Propagated Geometrical Factors in Induction Logging." Trans., Twenty-Second SPWLA Annual Logging Symposium. Mexico City, Mexico, June 23-26, 1981.

[10] Watt, H. B. "Induction Log." Log Review 1. Houston, Texas: Dresser Industries, 1974.

[11] Duesterhoeft, W. C. "Propagation Effects on Radial Response in Induction Logging." Geophysics, Vol. 27, No. 4 (August, 1962), pp. 463-469.

[12] Stratton, J. A. Electromagnetic Theory. New York: McGraw Hill, 1941.

[13] Harned, H. S., and B. B. Owen. The Physical Chemistry of Electrolytic Solutions. Third Edition. New York: Reinhold Publishing Corp., 1958.

[14] Potter, J. E. Informal communication. Tulsa, Oklahoma, October, 1981.

[15] Dresser Atlas. Log Interpretation Fundamentals. Houston, Texas: Dresser Industries, 1975.

[16] George, C. F. et al. "Applications of Inverse Filters to Induction Log Analysis." Geophysics, Vol. 29, No. 4 (1964), pp. 93-104.

[17] Gonzalez, R. C., and P. Wintz. Digital Image Processing. Reading, Mass.: Addison-Wesley, 1977.

[18] Frieden, B. R. "Image Enhancement and Restoration." Topics in Applied Physics. Vol. 6. New York: Springer-Verlag, 1979.

[19] Jansson, P. A. et al. "Resolution Enhancement of Spectra." Journal Optical Soc. America, Vol. 60, No. 5 (May, 1970), pp. 596-599.

[20] Wertheim, G. K. "Deconvolution and Smoothing: Applications in ESCA." Journal Electron Spectroscopy and Rel. Phen., Vol. 6 (1975), pp. 239-251.

[21] Blass, W. E., and G. W. Halsey. Deconvolution of Absorption Spectra. New York: Academic Press, 1981.

[22] Webster, G. M., Ed. Deconvolution. Tulsa, Okla.: Society of Exploration Geophysicists, 1978.

[23] McAulay, R. J., and M. L. Malpass. "Speech Enhancement Using a Soft-Decision Noise Suppression Filter." IEEE Trans. on ASSP, ASSP-27, No. 2 (1979), pp. 137-145

[24] Boll, S. F. "Suppression of Acoustic Noise in Speech Using Spectral Subtraction." IEEE Trans. on ASSP, ASSP-27, No. 2 (1970), pp. 113-120.

[25] Preuss, R. D. "Autoregressive Spectral Estimation in Noise With Application to Speech Analysis." (Unpublished Ph.D. dissertation, Oklahoma State University, 1983.)

[26] Kalman, R. E. "A New Approach to Linear Filtering and Prediction Problems." Trans. ASME, Series D, Journal of Basic Engr., Vol. 82 (1960), pp. 35-45.

[27] Kalman, R. E., and R. S. Bucy. "New Results in Linear Filtering and Prediction Theory." Trans. ASME, Series D, Journal of Basic Engr., Vol. 83 (1961), pp. 95-107.

[28] Bayless, J. W., and E. O. Brigham. "Application of the Kalman Filter to Continuous Signal Restoration." Geophysics, Vol. 35, No. 1 (1970), pp. 2-23.

[29] Graupe, D. Identification of Systems. Huntington, New York: Litton Educational Co., 1976.

[30] Morf, M. et al. "Some New Algorithms for Recursive Estimation in Constant, Linear, Discrete-Time Systems." IEEE Trans. on Automatic Control, AC-19, No. 4 (August, 1974), pp. 315-323.

[31] Brown, G. B. Introduction to Random Signal Analysis and Kalman Filtering. New York: Wiley and Sons, 1983.

[32] Sage, A. P., and J. L. Melsa. Estimation Theory With Applications to Communications and Control. New York: McGraw-Hill, 1971.

[33] Ruckebusch, G. "A Kalman Filtering Approach to Natural Gamma Ray Spectroscopy in Well Logging." IEEE Trans. on Automatic Control, AC-28, No. 3 (March, 1983), pp. 372-380.

[34] Yarlagadda, R. et al. Fast Algorithms for Lp Deconvolution. Tulsa, Okla.: Cities Services Oil and Gas Corp., 1983.

[35] Charnes, A. et al. "Optimal Estimation of Executive Compensation by Linear Programming." Management Science, Vol. 1 (1955), pp. 138-151.

[36] Byrd, R. H., and D. A. Payne. Convergence of the Iteratively Reweighted Least Squares Algorithm for Robust Regression. Technical Report No. 313. Baltimore: The Johns Hopkins University, June, 1979.

[37] Huber, P. J., and R. Dutter. "Numerical Solution of Robust Regression Problems." COMPSAT 1974. Proceedings of the Symposium on Computational Statistics. (B. Bruchmann, Ed.) Wien: Physika Verlag, 1974.

[38] LaCoste, L. J. B. "Deconvolution by Successive Approximation." Geophysics, Vol. 47, No. 12 (December, 1982), pp. 1724-1730.

[39] Helms, H. D. "Fast Fourier Transform Method of Computing Difference Equations and Simulating Filters." IEEE Trans. on Audio and Electroacoustics, AU-15, No. 2 (June, 1967), pp. 85-90.

[40] Rabiner, L. R., and R. W. Schafer. Digital Processing of Speech Signals. Englewood Cliffs, N.J.: Prentice Hall, 1978.

[41] Allen, J. B. "Short Term Spectral Analysis, Synthesis, and Modification by Discrete Fourier Transform." IEEE Trans. on Audio and Electroacoustics, AU-25, No. 3 (June, 1977), pp. 235-238.

[42] Yarlagadda, R., and J. B. Allen. "Aliasing Errors in Short-Time Analysis." Signal Processing, Vol. 4 (1982), pp. 79-84.

[43] Rabiner, L. R., and J. B. Allen. "A Unified Approach to Short-Time Fourier Analysis and Synthesis." IEEE Proceedings, Vol. 65, No. 11 (November, 1977), pp. 1558-1564.

[44] Kaiser, J. F. "Nonrecursive Digital Filter Design Using the Io-Sinh Window Function." Proceedings, 1974 IEEE Int. Symp. on Circuits and Systems, New York, N.Y., April 22-25, 1974, pp. 20-23.

[45] Kaiser, J. F., and R. W. Schafer. "On the Use of the Io-Sinh Window for Spectrum Analysis." IEEE Trans. on ASSP, ASSP-28, No. 1 (February, 1980), pp. 105-107.

[46] Box, G. E. P., and M. E. Muller. "A Note on the Generation of Normal Deviates." Annals of Mathematical Statistics, Vol. 28 (1958), pp. 610-611.

[47] Gold, B., and C. M. Rader. Digital Processing of Signals. New York: McGraw-Hill, 1969.

[48] Bryan, R. K., and J. Skilling. "Deconvolution by Maximum Entropy, as Illustrated by Application to the Jet of M87." Mon. Not. R. Astr. Soc., Vol. 191 (1980), pp. 69-79.

[49] Inguva, R., and L. H. Schick. "Information Theoretic Processing of Seismic Data." Geophysical Research Letters, Vol. 8, No. 12 (1981), pp. 1199-1202.

[50] Frieden, B. R. "Restoring With Maximum Likelihood and Maximum Entropy." Journal of the Optical Society of America, Vol. 62, No. 4 (1972), pp. 511-518.

VITA

Keith Alan Teague

Candidate for the Degree of

Doctor of Philosophy

Thesis: A WEIGHTED OVERLAP-ADDITION APPROACH TO DECONVOLUTION OF THE INDUCTION LOG

Major Field: Electrical Engineering

Biographical:

Personal Data: Born in Mulberry, Arkansas, March 23, 1957, the son of Kenneth A. Teague and Caryl Meyer Teague.

Education: Graduated from Alma High School, Alma, Arkansas, in May, 1975; received the Bachelor of Science degree in Electrical Engineering from Oklahoma State University in May, 1979; received the Master of Science degree in Electrical Engineering from Oklahoma State University in May, 1980; completed requirements for the Doctor of Philosophy degree at Oklahoma State University in May, 1984.

Professional Experience: Research Engineer, Amoco Production Company, Tulsa, Oklahoma, May, 1979, to August, 1979; Graduate Research Assistant, School of Electrical and Computer Engineering, Oklahoma State University, August, 1979, to May, 1980; Research Engineer, Amoco Production Company, Tulsa, Oklahoma, May, 1980, to August, 1981; Graduate Research Associate, School of Electrical and Computer Engineering, Oklahoma State University, August, 1981, to September, 1982; Instructor, School of Electrical and Computer Engineering, Oklahoma State University, August, 1983, to May, 1984.

Awards/Affiliations: Society of Professional Well Log Analysts Graduate Fellowship, August, 1982, to June, 1984; Mobil Research and Development Corporation Educational Assistance Grant, 1981; Member Phi Kappa Phi, Eta Kappa Nu, Institute of Electrical and Electronics Engineers (Computer Society and Acoustics, Speech, and Signal Processing Group), National Society of Professional Engineers, Society of Exploration Geophysicists, and Society of Professional Well Log Analysts.